

DISSERTATION ZUR ERLANGUNG DES DOKTORGRADES DER FAKULTÄT FÜR
CHEMIE UND PHARMAZIE DER LUDWIG-MAXIMILIANS-UNIVERSITÄT MÜNCHEN

**"Calorimetric and Theoretical Determination of
Enthalpies of Formation of HEMs and Molecular
Dynamic Simulations of Composite Propellants
Ingredients"**

Camilla Evangelisti

aus
Sondalo (So), Italien
2015

Erklärung

Diese Dissertation wurde in Sinn von § 7 der Promotionsordnung von 28. November 2011 von Herr Prof. Thomas M. Klapötke betreut.

Eidesstattliche Versicherung

Diese Dissertation wurde eigenständig und ohne unerlaubte Hilfe erarbeitet.

München, ..10.6.2015

.....
Camilla Evangelisti

24.3.2015
Dissertation eingereicht am:

1. Gutachter: Prof. Dr. Thomas M. Klapötke
2. Gutachter: Prof. Dr. Konstantin Karaghiosoff

Mündliche Prüfung am: 11.5.2015
.....

Acknowledgment

Many thanks to Herr Prof. Dr. Thomas M. Klapötke for the support in all these years. At first with my work as scientific coworker, then for my master thesis and finally for my Ph.D.. He support me in the numerous scientific trip to conference, work-shop and formation seminars.

Many thanks to Herr Dr. Manfred Bohn, to supervise me at the Fraunhofer-Institut in Karlsruhe in all these years. He estimates previously my competences and support me in these years. For the nice culinary discussion and for the great wine testing.

Thanks to Prof. Karaghiosoff, for many scientific and not scientific discussion, to spread the italian vitality and happiness in our groups. For helping me and supporting me in all these years. To be my second reviewer.

Thanks to Frau Scheckenbach, the best secretary I ever met, to be present and helpful in all the moments.

Thanks to Dr. Stierstofer for the many years of teamwork, for helping in scientific problems.

Thanks to Dr. Krumm as safety supervisor and helps in botanical problems.

Thank to Dr. Michael Nardai for the great support in the last part of my Ph.D.. To deliver me life-saving pearl-scripts and resolves all possible problems with the calculations. For the great austrian sarcasm.

Thanks to my student: Matthias Thubauville, Philipp Taenzler, Rebekka Meyer, Daniel Keefer which contributes to my scientific work in these years.

Thanks to Johann Glück, that helps me in the final phase of my Ph.D. thesis, for the refinement of the calorimetric results. A special thanks to Avital Sholomovic, for the meticulous work with the calorimeter, for all the heartily discussions, to open my mind to different point of view as well for the great kosher's food lessons.

Thanks to Dr. Michael Nardai, Regina Scharf, Carolin Pfluger, and especially to Vera Hartdegen for the numerous and arduous corrections of this work.

Thanks to Vera Hartdegen for the funny and nonsense moments in this research group.

Thanks to Quirin for the scientific work together. Because he permit me to blow up in few second several grams of different compounds, obtained from hard work. To the funny and the frivolous time at the conferences together and in lab.

Thanks to Carolin, Martin, Dennis, Marcos to delivered me several compounds for calorimetric measurements.

Special thanks to Christina Hettstedt to survive in the years to my italian fervor, for the spiritual succor and for the intimate friendship.

Special thanks to Marcos Kettner, a great college and wonderful friend, which brought a smile and a looot of fun in my years in this lab.

Thanks to my previous colleagues: Dr. Anian Nieder, Dr. Alex Penger and Dr. Andy Eckart. They support me in the years.

Thanks to my today's colleagues.

Un milione di ringraziamenti a mio marito, che negli anni é stato sempre la mia colonna portante. Ha sopportato pazientemente la sua drama queen e diva nei momenti difficili e ha riso e sorriso con me.

Un mare di abbracci e ringraziamenti alla mia famiglia. Che il libro del Prof. Vacca é servito a qualcosa... Grazie per l'infinito sopporto morale e in soldi-bresaola. Grazie al mio adorato fratello, che nonostante le nostre diverse competenze lavorative, si é rivelato sempre un ottimo interlocutore con un divertente scambio di opinioni.

Un grazie a tutti i miei amici, vicini e lontani, che hanno alleviato le pene da dottorato.

Non si presta mai attenzione a ciò che é stato fatto, ma quello che resta da fare.

One never notices what has been done, one can only see what remains to be done.

Marie Curie

Contents

1	Abbreviation	9
2	Introduction	11
2.1	History	11
2.2	Definition of Energetic Materials	13
2.3	History of Bomb Calorimetry	15
2.4	Aim of this work	16
3	Theoretical Background	23
3.1	Calorimetry	23
3.2	Quantum Chemical Calculations	25
3.3	Extracting Thermodynamical Quantities Out of Composite Methods	27
4	Methods	31
4.1	Calorimetry	31
4.2	Quantum Chemical Calculation	33
4.3	Material and Purity Control	33
5	Standardization	35
5.1	Benzoic Acid	35
5.2	Nicotinic Acid	38
5.3	Polyethylene Bulbs	39
5.4	Paraffin Stripes	40
5.5	Parafilm	41
5.6	Paraffin Oil	42
6	Crucibles	43
6.1	Stainless Steel	43
6.2	Fused Quartz	44
6.3	Platinum	45
7	Dihydroxylammonium 5,5'-Bistetrazole-1,1'-diolate and Dinitro-bis-1,2,3-triazole-1,1'-diol	47

8	Common High Energy Materials	53
8.0.1	2-Methyl-1,3,5-trinitrobenzene	55
8.0.2	Cyclotrimethylenetrinitramine	56
8.0.3	1,1-Diamino-2,2-nitroethylene	57
8.0.4	2,6- <i>Bis</i> -picrylamino-3,5-dinitropyridine	59
8.0.5	4,4'-Diamino-3,3'- <i>bis</i> furazan	61
8.0.6	4,5- <i>Bis</i> (1 <i>H</i> -tetrazol-5-yl)-2 <i>H</i> -1,2,3-triazole	62
8.0.7	<i>Bis</i> (1 <i>H</i> -tetrazol-5-yl)amine	63
9	Oxidizers	65
9.0.8	Ammonium nitrate	66
9.0.9	Ammonium perchlorate	68
9.0.10	Ammonium dinitramide	69
9.1	Carbamate's based HEDOs	71
9.1.1	2,2,2-Trinitroethyl carbamate and nitrocarbamate	71
9.2	Michael addition's compounds	73
9.2.1	4,4,4-Trinitrobutyric acid	73
9.2.2	2,2,2-Trinitroethyl-4,4,4-trinitrobutanoate	75
9.2.3	2,2,2-Trinitro-1-(2,2,2-trinitroethylamino)-1-butanone	76
10	Summary Calorimetric and Theoretical Determination of Enthalpy of Formation of HEMs	79
11	Calculations on Components of Composite Propellants	81
12	Calculation on Components of Composite Rocket Propellants: Methods	83
12.1	Computer Facility	83
13	Molecular Dynamics	85
13.1	Thermodynamic Ensembles	87
13.2	Periodic Boundary Conditions	88
14	Pre-Binder	91
14.1	Hydroxyl-terminated polybutadiene	91
14.2	Polypropylene glycol	97
14.3	Desmophen TM	102
15	Plasticizers	105
15.1	Diocetyl adipate	105
15.2	1,2,4-Butanetriol trinitrate	110

16	Mixtures of Binder Pre-polymers with Plasticizers	111
16.1	HTPB and DOA Mixture	111
16.2	PPO and DOA Mixture	116
16.3	HTPB and BTTN Mixture	121
17	Molecular Dynamic Simulations of the Interactions between with HTPB and the Organic Oxidizers TNC-NO₂ and TNE-NAP-NC	123
18	Summary Molecular Dynamics Simulations of Composite Propellants Ingredients	137
19	Curriculum Vitae	139
19.1	Papers and Conferences	142
19.1.1	Papers	142
19.1.2	Conference/Workshop	143

Chapter 1

Abbreviation

ADN= ammonium dinitramide
AN= ammonium nitrate
AP= ammonium perchlorate
BA= benzoic acid
BTA= *bis*(1*H*-tetrazol-5-yl)amine
BTT= 4,5-*bis*(1*H*-tetrazol-5-yl)-2*H*-1,2,3-triazole
BTTN= 1,2,4-butanetriol trinitrate
CED= Cohesive Energy Density
CL-20= 2,4,6,8,10,12-Hexanitro-2,4,6,8,10,12-hexaazaisowurtzitane
COMPASS= Condensed Phase Optimized Molecular Potentials for Atomistic Simulation Studies
Coulomb= Electrostatic interaction between point charges on atoms or atom groups
DABF= 4,4'-diamino-3,3'-*bis*furazan
Desmo= desmophene
DOA= dioctyl adipate
FF= Force Field
FOX-7= 1,1-diamino-2,2-nitroethylene
HEDOs= high energy density oxidizers
HMX= cyclotetramethylenetetranitramin
HNS= 1,3,5-Trinitro-2-[2-(2,4,6-trinitrophenyl)ethenyl]benzene
HTPB= hydroxyl terminated polybutadiene
HNS= MADX-1= dinitro-bis-1,2,3-triazole-1,1'-diol
NaOH= sodium hydroxide
NC= nitrocellulose
NG= nitroglycerine
NPT= constant pressure ensemble
NVT= constant volume ensemble
PETN= Pentaerythrityltetranitrat
PYX= 2,6-*bis*-picrylamino-3,5-dinitropyridine
PPO= polypropylene oxide
RDX= 1,3,5-trinitro-1,3,5-triazinan

TKX-50= dihydroxylammonium 5,5'-Bistetrazole-1,1'-diolate
TNC= 2,2,2-trinitroethyl carbamate
TNC-NO₂= 2,2,2-trinitroethyl nitrocarbamate
TNE-NAP-NC= 2,2,2-trinitroethyl(2-nitro-2-azapropyl)nitrocarbamate
TNT= 2-methyl-1,3,5-trinitrobenzene
vdW= van-der-Waals interactions
 $\Delta_f H$ = enthalpy of formation
 $\Delta_f H_{exp}^\circ(M)$ = experimental enthalpy of formation
 $\Delta_f H_{calc}^\circ(M)$ = calculated enthalpy of formation
 σ_c [%]= average deviation
 ΔU_c = energy of combustion
 $\Delta U_{c,av}$ = average energy of combustion
 E_{pot} = potential energy
 E_{vdW} = van-der-Waals energy
 E_{Coul} = electrostatic energy
 T_g = glass transition temperature

Chapter 2

Introduction

2.1 History

Since the history of war was written down in books, stone engravings or papyrus, traces of ancient explosive mixtures and fights with the use of fire were reported. One example are the Boetians in the early century. They improved the first flamethrower made of pitch, sulfur and coal, against the Athenians in Delium in 424 BC.[1] They used bellows to blow a hot jet of flame which set fire to the city walls and routed the defenders. Centuries later, the Romans used similar materials in fire bombs or fire pots. They catapulted these containers over the walls of besieged towns. But the most famous incendiary mixture of the antiquity was the "Greek Fire". It was invented by the Byzantines in 672 A.C.. It was used in naval battles with great effects, as it continued burning while floating on water. The exact formula of Greek Fire is unknown, but probably it is a mixture of sulfur, naphtha, pitch, resin, and quicklime, which ignited and burned fiercely upon contact with water.



Figure 2.1: Depiction of "Greek fire" in Madrid Skylitzes [2].

The first documentation of fireworks can be found in the 7th century in China. At that time fireworks were completely unknown in Europe up to the 17th century, when the jesuit missionary Pierre Nicolas le Chéron d'Incarville report about this method and composition of them. Whereas the origin of black-powder is not surely documented. It was probably also invented in China in the 9th century, but it also can be found in India and in the Muslim world.[3] However, with the invention of with the invention of guns and gunpowders in the 14th century in Europe, the age of explosive materials and modern warfare has begun. Between the 15th and 18th century the

improvements were concentrated on manufacturing black powder and related applications. Since the 19th century modern energetic materials were developed. Blackpowder was replaced by more effective, less expensive new energetic materials. During the 19th century, more powerful propellants (such as smokeless powder), better primers, various boosters or detonators, and new high explosives were introduced. Some important compounds of these types of explosives are: ammonium perchlorate, picric acid, nitroglycerin, 2-methyl-1,3,5-trinitrobenzene (TNT) and dynamite. In the 20th century with the two World Wars the developments accelerated. With the World War I machine gun fire, artillery barrages, firing torpedoes, laying mines, signaling and illuminating flares were introduced. Especially TNT was used. Between the World War I and the World War II 1,3,5-trinitroperhydro-1,3,5-triazine (RDX) and Pentaerythritol tetranitrate (PETN) besides several other explosives were developed (see Figure 2.2). One remarkable development between the wars was the introduction of a large amounts of mixtures of explosives, called composition (*e.g.* COMPOSITION A: RDX, wax and hexotol; COMPOSITION B: TNT, RDX). Additionally in the World War II the most important changes were: the introduction of high explosive bombs, artillery propellants, rocket propellants, high explosive artillery projectiles and antitank projectiles.

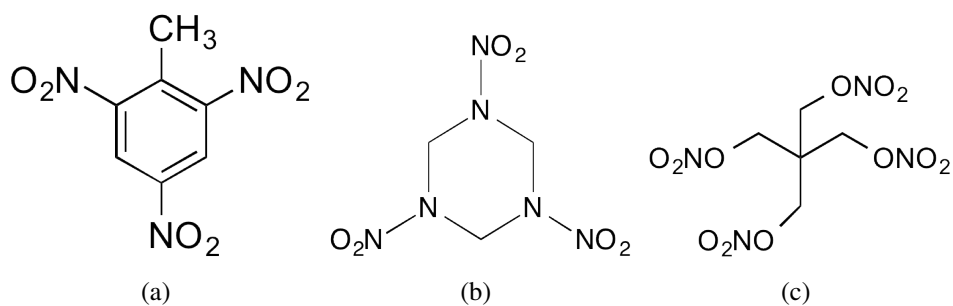


Figure 2.2: Structure of 2-methyl-1,3,5-trinitrobenzene (TNT)(a), 1,3,5-trinitroperhydro-1,3,5-triazine (RDX)(b) and pentaerythritol tetranitrate (PETN)(c).

The nuclear bombs that ended World War II did not end requirements for conventional explosives and ammunition. After the World War II in the 1950s manufacturers started to develop explosives which were less sensitive to facilitate safe and easy handling. The polymer-bonded (or plastic-bonded) explosives (PBX) show these properties, where the crystalline explosive is embedded in a rubber-like polymeric matrix. Semtex is one of the most important and known example of PBX. It was invented in 1966 by Stanislav Brebera, in Semtin a suburb of the city of Pardubice in the Czech Republic. Later the research was focussed on high thermal stability. In 1966 hexanitrostilbene (HNS) and in 1978 triaminotrinitrobenzene (TATB) fulfilled this requirement. Both explosives show excellent thermal stability and are therefore of great interest for the NAVY (fuel fires) and for hot deep oil drilling applications. In particular HNS is known as a heat- and radiation-resistant explosive which is used in heat-resistant explosives in the oil industry, with a

melting point of ca. 320 °C.[6] FOX-7 or 1,1-diamino-2,2-dinitroethene probably is one, of the last interesting insensitive compounds from the last two decades. It was first synthesized in 1998 by the FOA Defence Research Establishment, Sweden.[8] Its explosive properties seem to be extremely favorable. In the last decades environmentally friendly high energetic materials are the new trend and in this work some of them are presented.

2.2 Definition of Energetic Materials

Energetic materials can be divided in four classes: primary explosives, secondary explosives, pyrotechnics and propellants.[13] Primary explosives show a very rapid transition from combustion to detonation and have high sensitivity towards impact, friction and heat. They are used as initiators for secondary booster charges, main charges, or propellants. Secondary explosives can not be initiated simply by heat or shock, for initiation a primary explosive has to be used. The performance is usually higher than the one of the primary explosive. Pyrotechnics, in contrast to explosives, form solid as well as gaseous products. Pyrotechnics often consist of an oxidizers and a reducing agent, but they may also contain a binder, a propellant charge, colorant as well as smoke or noise generating additives.

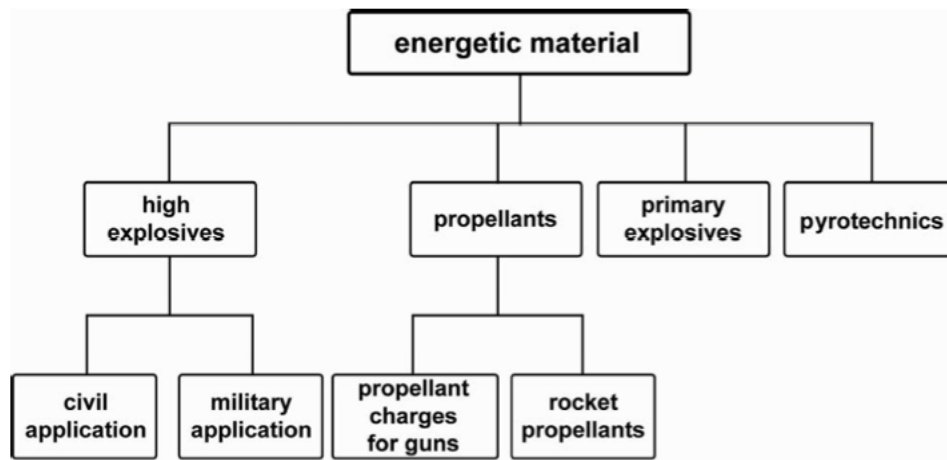


Figure 2.3: Classification of high energetics materials [13].

Propellants are explosive materials that combust rapidly and produce a large amount of hot gas. Propellants are divided into rocket propellants and gun propellant charges. The oldest known propellant charge is black-powder, a mixture of 75% KNO_3 , 10% sulfur and 15% charcoal dust. It is still used as charge for military and civilian pyrotechnic munitions. Nitrocellulose (NC) powder, an other broadly used component for propellants. It has the advantage to burn residue free. By reacting cellulose with nitric acid, nitrocellulose is formed. Using different acid concentration, NC is formed with different grades of nitration. Double and triple-base propellants contain in addition

to NC nitroglycerine (NG) and nitroguanidine. Single-base propellant charges are used in weapons from pistols to artillery weapons, instead double-base propellants are used in pistols and high performance guns of tanks.

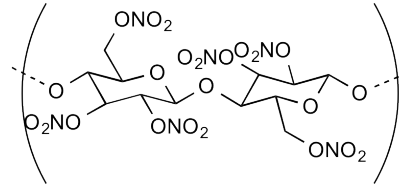


Figure 2.4: Structure of nitrocellulose, NC.

Gun propellant charges in contrast to rocket propellants may not detonate but must burn in a controlled manner. They can be also be classified into liquid-propellants and solid propellants. The advantages of liquid propellants compared to solid propellants are plenty: they less heavy, cheap to produce, less vulnerable to accidental initiation, have a high energy output per unit volume and a high storage capacity.[5] The solid rocket propellants can further be divided into double-base propellants and composite propellants. The rocket double-base propellants are based on NC/NG. Instead composite propellants are a mixture of a crystalline oxidizer (*e.g.* ammonium perchlorate, AP), a binder (*e.g.* hydroxy-terminated polybutadiene, HTPB), a plasticizer (*e.g.* glycidyl azide polymer, GAP) and usually a powdered metal fuel such as aluminum. The oxidizer provides oxygen for the appropriate combustion of the fuel in an oxygen deficient environment. In the past three decades the composite propellants have been the most commonly used class for rocket. In Table 2.1 the performance of double-base propellant are compared with the one of the composite propellant.

Table 2.1: Comparison of performances and compositions of double-base rocket propellants and composite rocket propellants.

Solid propellant	Specific impuls I_{sp} [s]	Combustion temperature T_c [K]
<i>Double-base propellants</i>		
NC (12.6% N)	200	2500
NG		
<i>Composite propellants</i>		
AP	259	4273
HTPB		
Al		
Other additive		

Ammonium perchlorate (see Figure 2.5, AP) is currently the mostly used oxidizers in solid rocket boosters. Recent research [8] is focussed on the replacement of AP, due to the toxicity of this compound.

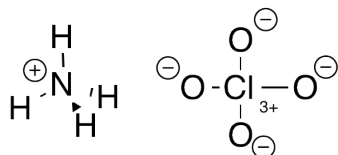


Figure 2.5: Structure of ammonium perchlorate.

Recent research demonstrated the decrease of thyroxin synthesis, if being exposed to AP, due to inhibition of iodine storage, but also other secondary effects for the human, animals and also for the environment were proved.[9] This leads to dysfunctions and affects both growth and development of humans and animals. Furthermore AP also might be toxic to a large number of maritime life forms of unknown magnitude. Additionally during the starting process of a rocket a big amount of HCl is released, which causes the formation of acid rain and ozone degradation. [10] In this work several environmentally compatible high energy dense oxidizers as possible replacements for AP were presented and investigated.

2.3 History of Bomb Calorimetry

In 1782 Lavoisier introduced the first calorimeter. [11] It was an ice-calorimeter (see Figure 2.6) and it was used to determine the produced heat of different chemical reactions as well as little animals like guinea pigs.

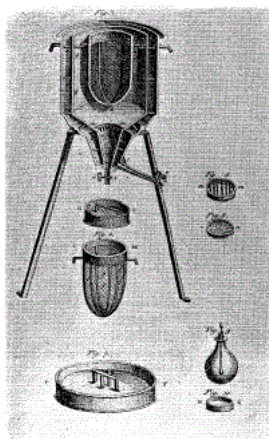


Figure 2.6: Build-up of Lavoisier's calorimeter 1782 [11].

Today many different types of calorimeters are available: differential scanning calorimeters (DSC) to measure the heat capacity of new materials and thermal decomposition, reaction calorimeters to measure the heat released or absorbed during a reaction and bomb calorimeters to measure the heat of combustion of a compound. The most used calorimetric method for energetic material, besides DSC, is the bomb calorimetry. It was developed by Pierre Berthelot around 1893. He was a pioneer in using oxygen under pressure to complete combustion.[12] He determined the heat of combustion of gases using bomb calorimetry, by mixing the gases was mixed with 20-25 bar of oxygen and then ignited. Using this method it was possible to determine the energy of combustion ΔU_c with high accuracy.

The principle of a bomb calorimeter remained almost unchanged since Berthelot's time. The construction and materials were optimized and the error minimized. The standard substances like benzoic acid show accuracies, for the combustion energy's determination, of 0.01%.

Over the years the bomb calorimetric measurements found application in different analytical fields, but the six major applications are:[13]

- (i) solid and liquid fuel testing
- (ii) waste and refuse disposal
- (iii) food and metabolic studies
- (iv) propellants and explosives testing
- (v) fundamental thermodynamic studies
- (vi) educational training

In this work, the bomb calorimetry is used for testing high energetic materials. In the past, especially in the 20th century, several studies in this field were done, mainly in the time around the first and second world war.[14][15][16] Calorimetry was an easy and quick test to measure the heat of combustion of a new synthesized compound. With the development of the computational chemistry, many properties were estimated just like the heat capacity. Nevertheless, it is still important to perform calorimetric measurements and compare it with the computational results.

2.4 Aim of this work

To predict and evaluate the performance of energetic materials, the exact estimation of the enthalpy of formation $\Delta_f H^\circ$ is fundamental. The evaluation is important to check the experimental results. Besides the predictions are helpful to plan the synthetic work and the performance of potential new energetic materials, without previous experimental parameters. For the estimation of detonation parameters (*e.g.* detonation velocity) of new compounds, 50-100 g are necessary. The synthesis for this quantity can be very expensive and time-consuming, therefore the computational approach can be of great help. For calculating the performance different codes are available (*e.g.* TIGER, CHEETAH, EXPLO5 etc.), EXPLO5 [17][18] is the used in-house program.

Two methods for the determination of the enthalpy of formation $\Delta_f H^\circ$ are known, using quantum mechanical calculation or bomb calorimetry. Rice and coworkers [19][20] were pioneers in the prediction of the enthalpy of formation of energetic materials using quantum mechanical calculations. They used B3LPY/6-31G* level of theory [21][22][12], and Gaussian03 program package.[24] In Table 2.2 a list of experimental $\Delta_f H_{exp}^\circ$ and calculated $\Delta_f H_{calc}^\circ$ enthalpies of formation of common high energy materials are listed and the good accordance is shown.

Table 2.2: List of experimental $\Delta_f H_{exp}^\circ$ and calculated $\Delta_f H_{calc}^\circ$ enthalpy of formations of common high energy materials from [20].

Compounds	$\Delta_f H_{exp}^\circ$ [kcal·mol ⁻¹]	$\Delta_f H_{calc}^\circ$ [kcal·mol ⁻¹]
RDX	18.9±1.2	20.5
PETN	-128.7±0.2	-112.1
TNT	-15.1±1.2	-16.8
FOX-7	-32.0±0.1	-25.3
HMX	24.5±0.66	30.2
HNS	16.2±2.5	8.9
CL-20	90.2±3.11	95.5

There are several methods to calculate the enthalpy of formation $\Delta_f H^\circ$. The methods named G3/G4 [25][26] are usually highly accurate but suffer from the scaling problems, normally encountered by such theories, when applied to large molecules. In this work only a couple of molecules were calculated using G3/G4, for the remaining compounds CBS-4M was used.[27] Concerning the determination of the enthalpy of formation $\Delta_f H^\circ$ of energetic materials with bomb calorimetric methods, only a few papers were published in the last years. The reasons may be the delicate subject matter and the complexity of the methods. Anyway, a couple of recent works [28][30][29] are focussed on calorimetric measurements of energetic materials. The results of these works were used as comparison with the values of this work.

In the second part of this work, the focus is on simulation of binders, plasticizers, new oxidizers and mixtures of them. These three compound species are ingredients of composite propellants mixtures. In Table 2.3 some typical ingredients of composite solid propellants are listed.

Binders, *e.g.* HTPB cured with isocyanates, form a polyurethane network which has the function to bind the oxidizing agent and other ingredients in a solid but elastic matrix. The binders are generally viscoelastic cross-linked elastomers. The plasticizers are added to improve processing (manufacturing at low viscosity) mechanical and physical properties (decreasing of the glass transition temperature T_g). The fillers influence the processing, burning behavior, mechanical properties and shock sensitivity.

Table 2.3: List of typical ingredients of composite solid propellants.

Type	Percent	Acronym	Type chemicals
Oxidizer	20-70	AP	Ammonium perchlorate
		AN	Ammonium nitrate
		ADN	Ammonium dinitramine
Metal fuel	0-30	Al	Aluminium
Binder	5-18	HTPB	Hydroxyl-terminated polybutadiene
		CTPB	Carboxyl-terminated polybutadiene
		PBAN	Polybutadiene acrylonitrile acrylic acid
		PPO	Polypropylene oxide
Plasticizer	0-7	DOA	Dioctyl adipate
		GAP-A	Azido-terminated glycidyl azide polymer

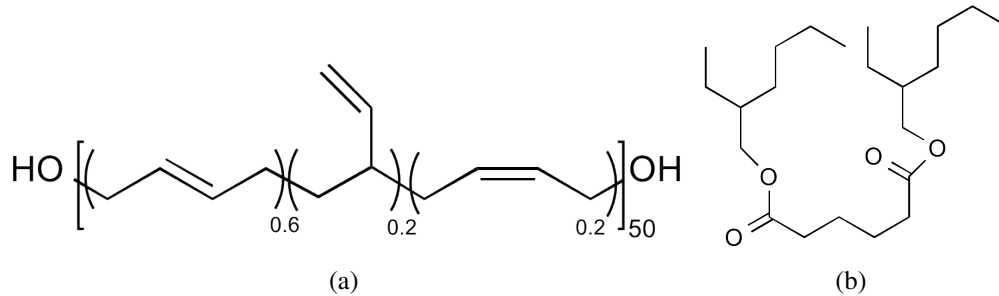


Figure 2.7: Structure of pre-binder hydroxyl-terminated polybutadiene (a) and plasticizer dioctyl adipate (b).

In recent works using computational methods, common binders as hydroxyl-terminated polybutadiene (HTPB) with common used oxidizers (*e.g.* AP), plasticizers or fuels were investigated. [31][32][33] The simulations can be helpful to compare experimental results of the glass transition temperature for blend systems or single molecules alone. The glass transition T_g is defined as the reversible transition in amorphous materials from a hard and relatively brittle state into a molten or rubber-like state. The glass transition temperature has been widely used not only for describing the position of the temperature range of a transition of particular compounds to the glassy state but also for analyzing different specific features of the amorphous compounds.

Angell [34] proposed a scala T/T_g or analyzing the specific features revealed in the temperature dependences of the viscosity of glass-forming melts. Additionally T_g are frequently used in relationships that characterize the glass-forming ability of compounds or the stability of the amorphous state during heating and T_g is also often taken to be equal to the temperature corresponding to a specific viscosity (as a rule, it is 10^{14} P).[35]

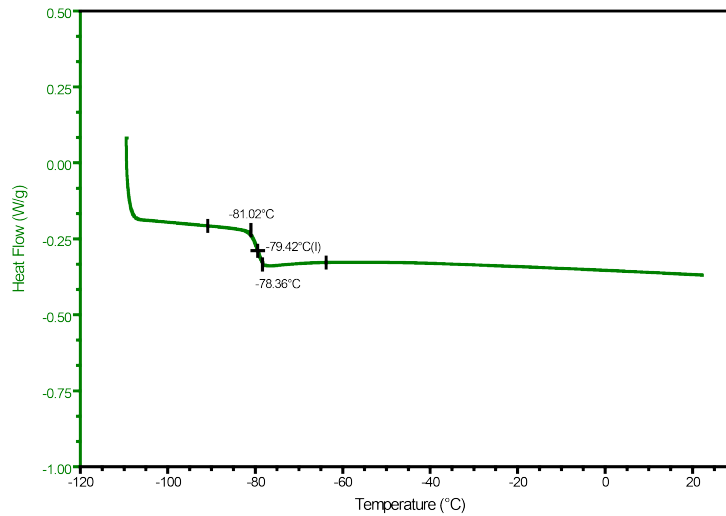


Figure 2.8: DSC graph of pre-binder hydroxyl-terminated polybutadiene (HTPB).

T_g is a fundamental property for rubber-like materials, like binders and plasticizers, due to the influence to the mechanical properties. Using differential thermal analysis (DTA) and differential scanning calorimetry (DSC), the T_g can be measured. In Figure 2.8 one example from a DSC measurements of HTPB is presented. The graph show a bend in a range between -78.36 and -81.02 °C. In this case it is a glass to liquid transition, because the HTPB was liquid. In this work few pre-binder and plasticizers were analyzed, and molecular dynamic simulations were performed. T_g was simulated and if possible compared with the literature.

Bibliography

- [1] Thucydides, *History of the Peloponnesian war*, 5th century BC.
- [2] J. Skylitzes, *Synopsis of Histories*, Militos Pub., **2000**.
- [3] *Military Explosive, TM 9-1300-214, ARMY MILITARY MANUAL*, US Army Pub., **1990**.
- [4] T. M. Klapötke, *Chemistry of High-Energy Materials*, 2nd Edition, de Gruyter, **2012**.
- [5] J. Akhavan, *Chemistry of Explosives*, RSC Pub., **2011**.
- [6] K. G. Shipp, *J. Org. Chem.* **1964**, 29, 2620.
- [7] N. V. Latypov, J. Bergman, A. Langlet, U. Wellmar, U. Bemm, *Tetrahedron Lett.* **1998**, 54, 11525-11536.
- [8] Q. J. Axthammer, T. M. Klapötke, B. Krumm, R. Moll, S. F. Rest, *Z. Anorg. Allg. Chem.* **2014**, 640, 76-83; B. Aas, M. A. Kettner, T. M. Klapötke, M. Sucèska, C. Zoller, *Eur. J. Inorg. Chem.* **2013**, 36, 6028-6036; R. Haiges, K. O. Christe, J. C. Bigler, US20140350266, **2014**.
- [9] M. S. Johnson, C. J. Salice, *Ecotoxology of Explosives*, CRC Press, **2009**.
- [10] A. Makhijani, K. R. Gurney, *Mending the Ozone Hole: Science, Technology, and Policy*, Institute for Energy and Environmental Research, **1995**.
- [11] Antoine Lavoisier, *Traité Élémentaire de chimie*, Paris, Chucet Libraire, **1798**.
- [12] P. E. M. Berthelot, *Essai de mécanique fondée sur la thermochimie*, Paris, Dunot Pub., **1897**.
- [13] Calorimeter Application, Bulletin N. 104, Parr Company Company®, **2006**.
- [14] R. Robertson, *Chemical Age*, London, **1923**.
- [15] P. Naoum, R. Aufschlager, *Zeitschrift für das Gesamte Schieß und Sprengstoffwesen* **1924**, 19, 121-123.
- [16] J. Taylor, C. R. Hall, H. Thomas, *J. Phys. Coll. Chem.* **1947**, 51, 580-592.
- [17] EXPLO5, Version 6.02, M. Sućeska, Zagreb, Croatia, **2014**.

- [18] M. Sućeska, *Propellants Explos. Pyrotech.* **1991**, *16*, 197-202.
- [19] B. M. Rice, V. P. Sharmila, J. Hare, *Combust. Flame* **1999**, *118*, 445-458.
- [20] E. F. C. Byrd, B. M. Rice, *J. Phys. Chem. A* **2006**, *110*, 1005-10133
- [21] A. D. J. Becke, *J. Chem. Phys.* **1993**, *98*, 5648-5652.
- [22] C. Lee, W. Yang, R. G. Parr, *Phys. Rev.* **1988**, *B41*, 785-789.
- [23] J. L. Chenot, *J. Chem. Phys.* **1973**, *28*, 201-207.
- [24] Gaussian 03, revision A.01, M. J. Frisch *et al.*, Gaussian, Inc., Wallingford CT, **2003**.
- [25] A. G. Baboul, L. A. Curtiss, P. C. Redfern, K. Raghavachari, *J. Chem. Phys.* **1999**, *110*, 7650-7657.
- [26] L. A. Curtiss, P. C. Redfern, K. Raghavachari, *J. Chem. Phys.* **2007**, *126*, 084108.
- [27] J. W. Ochterski, G. A. Petersson, J. A. Montgomery, *J. Chem. Phys.* **1996**, *104*, 2598-2619.
- [28] A. J. Bellamy, A. E. Contini, P. Golding, *From New Trends in Research of Energetic Materials, Proceedings of the Seminar 15th*, Pardubice, Czech Republic, Apr. 18-20, **2012**, Pt. 2, 450-459.
- [29] F. M. Betzler, T. M. Klapötke, S. Sproll, *Central European Journal of Energetic Materials* **2011**, *8*, 157-171.
- [30] S. Cudzilo, W. A. Trzcinski, R. Trebinski, P. Wolanski, *Biuletyn Wojskowej Akademii Technicznej* **1998**, *47*, 33-47.
- [31] Y. J. Cao, Y. G. Yu, R. Ye, *Appl. Therm. Eng.* **2015**, *75*, 145-153.
- [32] Q. An, W. A. Goddard, S. V. Zybin, S. N. Luo, *J. Phys. Chem. C* **2014**, *118*, 19918-19928.
- [33] L. X. Yang, L. Y. Mei, Y. H. Lan, L. Q. Liao, Y. Z. Fu, Yi-Zheng, *Adv. Mat. Res.* **2013**, 718-720.
- [34] C. A. Angell, *J. Non-Cryst. Solids* **1985**, *73*, 1-17.
- [35] O. V. Mazurin, *Glass Physics and Chemistry* **2007**, *33*, 22-36.

Chapter 3

Theoretical Background

3.1 Calorimetry

If energy is added to or subtracted from a closed system, its internal energy ΔU changes according to the first law of thermodynamics

$$\Delta U = q + w \quad (3.1)$$

with q being the heat and w being the work by which the system can be influenced. The work of expansion can be expressed by integrating the pressure p dealt to the system over the volume V

$$w_{exp} = - \int_{V_i}^{V_f} p dV \quad (3.2)$$

with the initial (V_i) and the final volume (V_f). Holding the system at constant volume, w_{exp} is equal zero. This means that if no additional work is applied to the system, ΔU is solely dependent on the heat at constant volume q_v

$$\Delta U = q_v \quad (3.3)$$

By obtaining q_v via bomb calorimetry measurements, ΔU can be determined. For that purpose a sample is burned and the energy released is transferred to the surrounding water bath, which then rises in temperature. This temperature rise ΔT is measured and put in relation to ΔU through

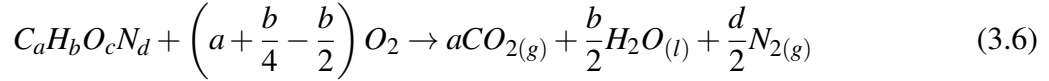
$$\Delta U = q_v = C\Delta T \quad (3.4)$$

where C is a constant being unique to the calorimeter [1] and determined via calibration with a known standard. With ΔU , the heat of combustion $\Delta_c H$ can be calculated from

$$\Delta_c H = \Delta U + \Delta n_g RT \quad (3.5)$$

where Δn_g is the molar change of the gasses participating in the combustion, R is the ideal gas constant and T is the temperature at which the combustion occurs. To determine Δn_g , the

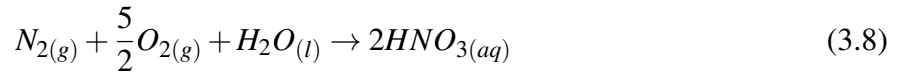
reaction equation of the specific combustion process has to be known. The sample is put under oxygen pressure, hydrogen and carbon are assumed to exist only in their highest oxidized form after combustion. Nitrogen is presumed to be released as N_2 . [2] The reaction equation notes



According to this equation, the relation for Δn_g results in

$$\Delta n_g = aCO_{2(g)} + \frac{d}{2}N_{2(g)} - \left(a + \frac{b}{4} - \frac{b}{2}\right) O_2 = \frac{1}{2} \left(d - \frac{b}{2} + c\right) \quad (3.7)$$

As the molecules investigated in this work contain up to 80 % nitrogen, the released N_2 will further react with water and form nitric acid according to the equation



The amount of nitric acid can be determined via titration with 0.1 M sodium hydroxide using bromothymol blue as indicator, which leads to a corrected ΔU_{corr}

$$\Delta U_{corr} = \Delta U - (\Delta_f H_{HNO_3}^\circ * V_{NaOH} * c_{NaOH}) \quad (3.9)$$

Here $\Delta_f H_{HNO_3}^\circ$ is the enthalpy of formation of HNO_3 (-57.7 kJ/mol), [2] c_{NaOH} is the concentration of NaOH (0.1 M) and V_{NaOH} is the volume of NaOH used in the titration. With the corrected enthalpy of combustion $\Delta_c H^\circ$ and the reaction taking place under standard conditions, the enthalpy of formation $\Delta_f H^\circ$ of the sample can be calculated according to:

$$\Delta_c H^\circ = \sum \Delta_f H^\circ(\text{products}) - \Delta_f H^\circ(\text{educts}) \quad (3.10)$$

Values for the enthalpies of formation of the reaction products according to equation 3.11 were taken from the NIST database [6] and are shown in Table 3.1. Following this, the final energy of formation notes

$$\Delta_f U^\circ(s) = \Delta_f H^\circ(s) - \Delta n_g RT \quad (3.11)$$

with the gas constant R and temperature T .

Table 3.1: Enthalpies of formation of the reaction products, $\Delta_f H^\circ$.

Compound	$\Delta_f H^\circ$ [kJ/mol]
CO ₂	-393.15
H ₂ O	-285.83
N ₂	0.0

3.2 Quantum Chemical Calculations

The thermodynamic data of a given molecule can be calculated by applying quantum chemical methods, which means solving the *Time-Independent Electronic Schrödinger Equation* (TISE)

$$\hat{H}_{el}\hat{\Psi}_{el}(r_i;R_A) = E_{el}(R)\Psi_{el}(r_i;R_A) \quad (3.12)$$

where R_A represents the nuclei coordinates and r_i symbolizes the electrons. Here, the electronic Hamiltonian \hat{H} considers the kinetic energy of the electrons as well as their interaction with the cores and each other. The *Hartree – Fock method* (HF) sets the basic algorithm for an approximate solution of the TISE.[4] Here, the trouble causing interaction between the electrons is described as an interaction of one electron with a potential field of the respective other electrons. While being remarkably successful in many cases, this description still constitutes a major approximation. For a more accurate treatment of the electron correlation, so called *Post – Hartree – Fock* methods, such as the *Møller-Plesset Perturbation Theory* (MPn) for different perturbation orders n [[5],[6]], were developed. Another factor for accuracy and computation time is the description of the wave function Ψ_{el} in equation 3.12. It is composed of different atomic-centered Gaussian functions, being called the basis set.

A method, which delivers a reasonable compromise between accuracy and computation time is the *complete basis set* CBS-4M method.[7] It splits the MP2 correlation energy $E(2)$ into a sum of pair correlation energies

$$E^{(2)} = \sum_{ij}^{occ} e_{ij}^{(2)} \quad (3.13)$$

where i and j describe HF-occupied orbitals. These pair correlation energies $e_{ij}^{(2)}$ can be expressed by the product of the coupling between i,j to virtual orbitals a,b

$$V_{ij}^{ab} = \langle ij|1/r_{ij}|ab\rangle \quad (3.14)$$

and the corresponding coefficients

$$C_{ij}^{ab} = \frac{V_{ij}^{ab}}{e_i + e_j - e_a - e_b} \quad (3.15)$$

which yields in

$$e_{ij}^{(2)} = \sum_{ab}^{N_{virt}} C_{ij}^{ab} V_{ij}^{ab} \quad (3.16)$$

This leads to the concept of the so called *Pair Natural Orbitals* (PNO) expansion for each of the pair energies

$$e_{ij}^{(2)} = \sum_a^{PNO} C_{ij}^{aa} V_{ij}^{aa} \quad (3.17)$$

An infinite number N of PNOs would constitute a complete basis set and delivers the exact pair energies. Since only a finite number of basis functions is accessible, the CBS method extrapolates the energy correction. Therefore, the PNOs are splitted into $\alpha\beta$ - and $\alpha\alpha$ -spin pairs, where the limit for infinitive N can be noted as

$$\lim_{N \rightarrow \infty} \alpha\beta e_{ij}^{(2)}(N) = \alpha\beta e_{ij}^{(2)}(CBS) + (25/512)|S|_{ij}^2(N + \delta_{ij})^{-1} \quad (3.18)$$

and

$$\lim_{N \rightarrow \infty} \alpha\alpha e_{ij}^{(2)}(N) = \alpha\alpha e_{ij}^{(2)}(CBS) + (25/512)2|S|_{ij}^2 \left[\frac{1 - |S|^2}{1 + |S|^2} \right] (N + \delta_{ij})^{-\frac{5}{3}} \quad (3.19)$$

where $|S|_{ij}$ is the absolute overlap integral of the molecular orbitals. Based on these equations, two point extrapolations with the first point $N=1$ and the second point $N=N_{ij}$ are being conducted. This leads to the second order CBS values for $\alpha\beta$ -pairs.

$$\alpha\beta e_{ij}^{(2)}(CBS) = (-25/512)|S|_{ij}^2(1 + \alpha\beta\delta_{ij})^{-1} \quad (3.20)$$

and $\alpha\alpha$ -pairs

$$\alpha\alpha e_{ij}^{(2)}(CBS) = +(-25/512)2|S|_{ij}^2 \left[\frac{1 - |S|^2}{1 + |S|^2} \right] (1 + \alpha\alpha\delta_{ij})^{-\frac{5}{3}} \quad (3.21)$$

Summing up the correction to each of the pair energies gives to the total $CBS^{(2)}$ correction

$$\Delta E^{(2)} = \sum_{i,j}^{occ} e_{ij}^{(2)}(CBS) - e_{ij}^{(2)}(N_{bf}) \quad (3.22)$$

where $e_{ij}^{(2)}(N_{bf})$ is the pair energy obtained directly from a calculation with the full set of N_{bf} basis functions. Corrections to higher order terms can be estimated using the second order correction and an interference factor.[8] Using this method, basis set truncation errors can be estimated using an extrapolation to the complete basis set limit. Because the algorithm used within this work uses calculations up to the MP4 level of theory, it is called CBS-4M.[9] M indicates improvements to several empirical corrections in contrast to the original CBS-4 method. The algorithm starts with a geometry optimization and zero point energy calculation on the unrestricted HF(UHF) level with a 3-21G* basis set.[10] The HF energy is calculated with the 6-311+G(2df) basis [11], followed by an MP2(CBS2) calculation with the 6-31G* basis.[12] At last, MP4 correlation energies are calculated using the 6-31G basis set.[13]

3.3 Extracting Thermodynamical Quantities Out of Composite Methods

Using the CBS-4M method, a quantum chemical calculation yields the enthalpy value H_{cbs} . However, this value corresponds to the gas phase. All investigated molecules in this work were solid at room temperature, so a translation of the enthalpy of solid state $\Delta_f H_s$ has to be carried out. To do so, first the enthalpy of formation of the molecule in the gaseous state $\Delta_f H_g$ is determined using

$$\Delta_f H_g = H_{cbs} - \sum_i n_i H_{cbs}(A_i) + \sum_i n_i \Delta_f H(A_i) \quad (3.23)$$

where A corresponds to the individual atoms in the molecule. The enthalpy values $H_{cbs}(A_i)$ for the specific atoms were calculated using the same level of theory as the molecule, and the values for $\Delta_f H(A_i)$ were taken from the NIST database.[6] With a known value of $\Delta_f H(g)$, the enthalpy of formation of the liquid or solid state $\Delta_f H_{(s,l)}$ can be calculated using

$$\Delta_f H_{(s,l)} = \Delta_f H(g) - \Delta_{sub/vap} H \quad (3.24)$$

Here, $\Delta_{sub} H$ and $\Delta_{vap} H$ are determined using

$$\Delta_{vap} H = \Delta S_{vap} T_b \quad (3.25)$$

$$\Delta_{sub} H = C_{sub} T_m \quad (3.26)$$

In accordance with the Trouton's rule ΔS_{vap} and C_{sub} are assumed to be constant values. It is determined that ΔS_{vap} equals $90 \text{ J}\cdot\text{mol}^{-1} \text{ K}^{-1}$ and C_{sub} $188 \text{ J}\cdot\text{mol}^{-1} \text{ K}^{-1}$, T_b being the boiling point and T_m the melting point for the compound in question.[1]

If the solid probe consists of ionic species, the CBS values were calculated separately for the respective ions. To obtain the enthalpy of formation for the salts, the lattice energy H_L has to be considered. Therefore, at first the lattice energy U_L is calculated using

$$U_L = 2I \left(\frac{\alpha}{\sqrt[3]{V_{EZ}}} + \beta \right) \quad (3.27)$$

Here, V_{EZ} is the volume of the elementary cell, I is the ionic strength and α and β are empirical parameters [14], depending on the stoichiometric composition of the corresponding ions (see table 3.2).

The lattice enthalpy ΔH_L is determined by

$$\Delta H_L = U_L + \left[p \left(\frac{n_m}{2} - 2 \right) + q \left(\frac{n_x}{2} - 2 \right) \right] RT \quad (3.28)$$

where p and q are the stoichiometric numbers of the ions in the neutral salt and the parameters n_x and n_m are dependent on the type of the molecules, whether it is monoatomic ($n_{x,m} = 3$), linear

Table 3.2: Empirical parameters Jenkins.

Salt (charge ratio)	I	$\alpha [kJ \cdot mol^{-1} nm]$	$\beta [kJ \cdot mol^{-1} nm]$
$MX(1 : 1)$	1	117.3	51.9
$M_2X(1 : 2)$	3	165.3	-29.8
$MX_2(2 : 1)$	3	133.5	60.9
$MX(2 : 2)$	4	101.6	91.5

($n_{x,m} = 5$) or non linear ($n_{x,m} = 6$). The final enthalpy of formation $\Delta_f H^\circ(C^+A^-)$ for the neutral ionic compound (composed of the ions C^+A^-) notes

$$\Delta_f H^\circ(s) = \Delta_f H^\circ(C^+A^-) = \Delta_f H(C^+) + \Delta_f H^\circ(A^-) - \Delta H_L \quad (3.29)$$

With the enthalpy of formation for the covalent or the ionic molecule, the final energy of formation for the solid state $\Delta_f U^\circ(s)$ can be determined using the equation 3.11.

Bibliography

- [1] P. Atkins, J. de Paula, *Atkins' Physical Chemistry*, Oxford University Press, 7th edition, **2002**.
- [2] F. D. Rossini, *Experimental Thermochemistry. Measurement of Heats of Reaction*, Interscience Publishers Inc., New York, 326, **1956**.
- [3] P. J. Linstrom, W. G. Mallard, Eds., NIST Standard Reference Database, National Institute of Standard and Technology, Gaithersburg MD; <http://webbook.nist.gov>. (March 2015)
- [4] A. Szabo, N. S. Ostlund, *Modern Quantum Chemistry: Introduction to Advanced Electronic Structure Theory*, Dover Publications Inc., **1996**.
- [5] M. Head-Gordon, J. A. Pople, M. J. Frisch *Chem. Phys. Lett.* **1988**, *153*, 503-506.
- [6] R.V. Parish, *Chem. Phys. Lett.* **1972**, *14*, 91.
- [7] J. W. Ochterski, G. A. Petersson, J. A. Montgomery, *J. Chem. Phys.* **1996**, *104*, 2598-2619.
- [8] G. A. Petersson, M. R. Nyden, *J. Chem. Phys.* **1981**, *75*, 3423-2425.
- [9] J. A. Montgomery, M. J. Frisch, J. W. Ochterski, G. A. Petersson, *J. Chem. Phys.* **2000**, *112*, 6532-6542.
- [10] J. S. Binkley, J. A. Pople, W. J. Hehre, *J. Am. Chem. Soc.* **1980**, *102*, 939-947.
- [11] R. Krishnan, J. S. Binkley, R. Seeger, J. A. Pople, *J. Chem. Phys.* **1980**, *72*, 650-654.
- [12] J. L. Chenot, *J. Chem. Phys.* **1973**, *28*, 201-207.
- [13] W. J. Hehre, R. Ditchfield, J. A. Pople, *J. Chem. Phys.* **1972**, *56*, 2257-2261.
- [14] H. D. B. Jenkins, D. Tudela, L. Glasser, *Inorg. Chem.* **2002**, *9*, 2364-2367.

Chapter 4

Methods

4.1 Calorimetry

Calorimeters are instruments used to measure the quantity of heat. The heat of combustion is the number of heat units liberated by a unit mass of a sample during a burning with oxygen in a defined constant volume.[1] Thus the heat of combustion results from the heat liberated by the combustion of all carbons and hydrogens (present in the sample) with oxygen to form carbon dioxide and water, including the heat liberated by the oxidation of other potentially present elements such as nitrogen.

The determination of the heat of combustion via an oxygen bomb calorimeter is carried out using a procedure in which the heat of the sample is compared to the heat (obtained from a combustion) of a similar amount of a standardizing materials like benzoic acid or paraffin oil, parafilm, etc. The measurements are performed in a high-pressure oxygen atmosphere (30 bar) within a metal pressure vessel ("bomb"). The energy released by this combustion is absorbed within the calorimeter and the resulting temperature rise within the absorbing medium is noted. The heat of combustion of the sample is calculated by multiplying the temperature rise in the calorimeter with the previously determined heat capacity of the standardizing materials.

Any bomb calorimeter requires four essential components: (see Figure 4.1)

- (i) a bomb in which the combustible charges can be burned
- (ii) a bucket for holding the bomb in a measured quantity of water, together with a stirring mechanism
- (iii) an insulating jacket to protect the bucket from thermal stresses during the combustion process
- (iv) a thermometer for measuring temperature changes within the bucket.

The bomb must be a strong, thick-walled metal vessel which can be opened for inserting the sample, removing the combustion products and cleaning. Furthermore the bomb has to be provided with valves for flushing the bomb with oxygen under pressure and for releasing residual gases at the end of a test. Electrodes to carry an ignition current to a fuse wire are also required.

The bucket should guarantee a complete immersion of the bomb with water (ca. 1900 mL),

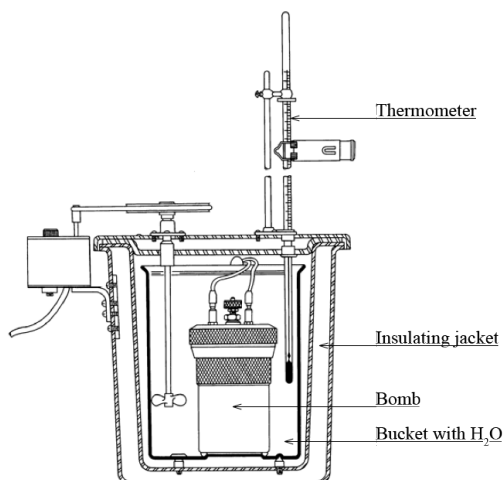


Figure 4.1: Essential components of a bomb calorimeter [1].

with a probe to read temperature and a stirrer include to promote rapid thermal equilibrium without introducing excessive heat in the form of mechanical energy.

The bucket is enclosed by a jacket which serves as a thermal shield, to protect its content from interactions (like heat transfers) with the surroundings. The purpose of the jacket is to minimize the influence of drafts, radiant energy and changes in room temperature during the measurements. The thermochemical measurements were performed on an isoperibol oxygen bomb calorimeter by Parr Instrument Company®. First the model *Parr 1356* and later *Parr 6200* was used (see Figure 4.2). The calorimeters were equipped with a static bomb.



Figure 4.2: 6200 Isoperibol oxygen bomb calorimeter.

The sample was either mixed with benzoic acid and pressed into pellets, covered with paraffin oil or wrapped in parafilm. For the pellets preparation the components, 0.1 g of substance with 0.9 g of benzoic acid, were mixed by grinding in a mortar and then pressed with a hydraulic press with a

pressure of 10 t. When paraffin oil was used, 0.1 g of substance was covered with circa 0.5 g of oil. In the case of the parafilm, 0.1 g substance was packed in 0.5 g parafilm. The mass of the prepared samples were typically 0.6-1 g. The bomb was additionally equipped with 1 mL of distilled water used to determine the values for the nitric acid correction. For the measurement the sample was placed in a crucible and ignited with a cotton thread on a platinum wire (0.05 mm in diameter and of 99.99% purity, purchased from GoodFellow) strained between the electrodes.

4.2 Quantum Chemical Calculation

All calculations were run on the Gaussian program 09, revision A. 02.[2] The computer facility is composed of 28 dual operon computers with 2.4 GHz (Opteron 2216 - HE-Dualcore, 4 virtual CPU per node) as computational nodes. Debian GNU/Linux 4.0 (64-bit) was used as operating system.

4.3 Material and Purity Control

The purity of the compounds was evaluated by analytical methods (elemental analysis, differential scanning calorimetry, NMR). All measured compounds showed a high purity without any traces of water, solvents or starting materials.

Bibliography

- [1] 6200 Calorimeter Operating Instructions, Parr Instrument Company®, **2010**.
- [2] Gaussian 09, revision A.02, M. J. Frisch *et al.*, Gaussian, Inc., Walingford CT, **2009**.

Chapter 5

Standardization

Before a material with an unknown heat of combustion can be investigated in a bomb calorimeter, the heat capacity of the calorimeter has to be determined. This determination is called standardization. In this chapter the standardization measurements for several compounds are described.

5.1 Benzoic Acid

Benzoic acid (BA) serves as intermediate in the biosynthesis of many secondary metabolites. Furthermore it is an important precursor for the industrial synthesis of many organic substances and the best known standard for bomb calorimetry.

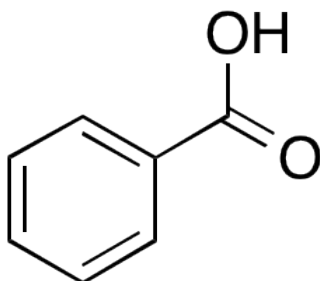


Figure 5.1: Structure of benzoic acid.

Since the 19th century benzoic acid is used as standard compound for calibration as well as combustion adding agent.[1] It is used due to its good burning behavior, low price and easy handling. All values of the calibrations with benzoic acid were compared to the NIST,[6] Standard Reference Material ® 39j 6317.8778 ± 0.7165 cal/g (26434 ± 3 J · g⁻¹) measured at 25 °C. Benzoic acid pellets from the Company Parr® were used for the calibration. For every significant change in the setup of the calorimeter, a new calibration has to be carried out. During this work, different crucibles on the base of different materials were investigated: stainless steel, fused quartz and platinum. In the following Table 5.1 the results of the calibration experiments with the stainless steel crucible are listed.

Table 5.1: Results of the calibration experiments with benzoic acid in a stainless steel crucible.

Sample	Mass [g]	ΔU_c [cal/g]	$\Delta U_{c,av}$ [cal/g]	σ_c [%]
1	1.0100	6320.61	6326.30	0.16
2	1.0085	6328.31		
3	1.0171	6338.67		
4	1.0115	6324.70		
5	1.0236	6320.27		
6	1.0087	6339.07		
7	1.0051	6312.44		

The average deviation of the results for the stainless steel crucible deviates from the NIST standard value amounts to 8.42 cal/g . This deviation is remarkable, taking the high purity of the investigated material into account. Due to these results new materials for the crucible were investigated. The second investigated crucible consisted of fused quartz. The calibration values are shown in Table 5.2.

Table 5.2: Results of the calibration experiments with benzoic acid in a quartz crucible.

Sample	Mass [g]	ΔU_c [cal/g]	$\Delta U_{c,av}$ [cal/g]	σ_c [%]
1	1.0206	6310.62	6313.38	0.09
2	0.9976	6309.04		
3	1.0095	6308.95		
4	1.0112	6305.89		
5	1.0213	6318.39		
6	1.0101	6318.79		
7	0.9935	6312.76		
8	1.0043	6322.61		

For the quartz crucible the average value for the benzoic acid fits better with the NIST reference (4.5 cal/g deviance) compared to the steel crucible. Unfortunately while using the quartz crucible several problems occurred, which will be discussed in detail later in this work. Consequently a platinum crucible was investigated as the third material (see Table 5.3).

Benzoic acid was used as adding agent for the combustion for several decades. Recently studies mentioned a possible acid-base reaction of this compound with salts or particularly acid sensitive

Table 5.3: Results of the calibration experiments with benzoic acid in a platin crucible.

Sample	Mass [g]	ΔU_c [cal/g]	$\Delta U_{c,av}$ [cal/g]	σ_c [%]
1	1.0206	6315.60	6323.69	0.14
2	1.0089	6310.57		
3	1.0493	6331.97		
4	1.0076	6326.05		
5	1.0229	6328.50		
6	1.0244	6329.46		

substance.[12] A possible alternative to benzoic acid was necessary. Hence paraffin oil, paraffin stripes and polyethylene capsules were investigated.

5.2 Nicotinic Acid

The second wellknown standard after benzoic acid is nicotinic acid.[3] The benefit of this standard is its cheap commercial availability (from the company Sigma Aldrich®). The heat of combustion ΔU_c for nicotinic acid measured at 25 °C by NIST [6], Standard Reference Material ® 39j results 5322.46 ± 0.716538 cal/g (22184 ± 3 J·g⁻¹).

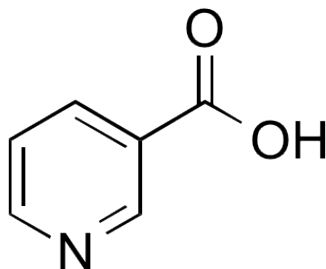


Figure 5.2: Structure of nicotinic acid.

Table 5.4: Results of the calibration experiments with nicotinic acid.

Sample	Mass [g]	ΔU_c [cal/g]	$\Delta U_{c,av}$ [cal/g]	σ_c [%]
1	0.9928	5325.93	5329.23	0.19
2	0.9984	5332.43		
3	0.9957	5328.52		
4	0.9915	5326.72		
5	0.9994	5320.41		
6	0.9964	5322.67		
7	0.9990	5330.39		
8	0.9982	5341.97		
9	0.9968	5331.01		
10	0.9978	5332.22		

The average deviation of the results, listed in Table 5.4, deviates from the NIST standard value amounts to 6.77 cal/g. As in the case of for benzoic acid, there is also the problem of a acid-base reaction with present salts. This is why the compound was not further investigated.

5.3 Polyethylene Bulbs

A possible alternative, also suggested in literature [5], are polyethylene bulbs (PE), used as sample container, or pieces of them, as burning additive. The investigated material was, purchased of NeoLab, Heidelberg, Germany.

Table 5.5: Results of the calibration experiments with polyethylene bulbs.

Sample	Mass [g]	ΔU_c [cal/g]	$\Delta U_{c,av}$ [cal/g]	σ_c [%]
1	0.8189	11095.54	11083.52	0.67
2	0.8934	11078.39		
3	0.8690	11129.49		
4	0.6145	11155.05		
5	0.6583	10915.25		
6	0.6682	10995.39		
7	0.6800	11132.58		
8	0.6866	11103.91		
9	0.6818	11175.87		
10	0.6479	11058.02		

The PE-bulbs burnt completely without any traces of grime. The literature described values is smaller than the obtained data within this work (see Table 5.5).[5] In our case the deviation is too high to use the bulbs for analytical measurements.

5.4 Paraffin Stripes

The company IKA® provides special paraffin stripes for calorimetric combustions. The stripes should help when problems occur during combustion of the sample or when the sample contains water. Comparing the values of different measurements with paraffin stripes (see Table 5.6) reveals a big deviation of 2.66%, which is why this additive was classified as unable for further measurements.

Table 5.6: Results of the calibration experiments with paraffin stripes.

Sample	Mass [g]	ΔU_c [cal/g]	$\Delta U_{c,av}$ [cal/g]	σ_c [%]
1	0.1104	12297.64	12352.98	2.66
2	0.0788	12289.88		
3	0.1259	12018.78		
4	0.0948	12805.61		

5.5 Parafilm

The investigated compounds in this work were obtained as different forms of solids. Some were crystalline, or in pellet form, others were electrostatically charged powders. These powders normally burnt inconsistent because they were scattered by contact with the crucible. To avoid this problem Parafilm® M from the *Pechiney Plastic Packaging* was investigated. The parafilm showed a good burning behavior. Calibration experiments gave good results with a average deviance of 0.37 % (see Table 5.7).

Table 5.7: Results of the calibration experiments with parafilm.

Sample	Mass [g]	ΔU_c [cal/g]	$\Delta U_{c,av}$ [cal/g]	σ_c [%]
1	0.9007	11197.54	11225.18	0.37
2	0.8878	11198.62		
3	0.6746	11188.43		
4	0.5779	11244.18		
5	0.6160	11223.82		
6	0.5881	11298.46		

Therefore parafilm was used for complicated measurements, especially for sensitive and electrostatic compounds in this work.

5.6 Paraffin Oil

The last investigated standard was paraffin oil from Sigma Aldrich® which shows the analytical specification of Ph. Eur. BP.. The oil has different advantages: it is cheap, easy to handle and has a good burning behavior. [6]

Table 5.8: Results of the calibration experiments with paraffin oil.

Sample	Mass [g]	ΔU_c [cal/g]	$\Delta U_{c,av}$ [cal/g]	σ_c [%]
1	0.6719	11071.58	11107.86	0.37
2	0.4539	11160.72		
3	0.6165	11136.60		
4	0.5829	11105.41		
5	0.6377	11064.98		

Due to the moderate deviance (0.37 %, see Table 5.8) and the advantages mentioned before, it was used as standard additive for almost all compounds presented in this work.

Chapter 6

Crucibles

6.1 Stainless Steel

The stainless steel crucibles are probably most common for bomb calorimetric measurements. Even the company Parr® mentions it as standard accessory for calorimetric measurements. In this work several measurements were performed with it, which revealed many advantages but mostly disadvantages. The costs are limited due to the cheap and easy production. Unfortunately many substances did not burn completely, without residues of grime and so the surface was covered with black deposit after a short period of time. This deposit basically consists of residues of the burning process of the compounds, carbon residues and iron oxides. As shown in Figure 6.1, on the left is a new lucent crucible and on the right the black and oxidated crucible.

The calibration measurements (with benzoic acid) using a new crucible showed a small deviation (0.16 %) which increased exponentially to the sooting of the crucible. Even the use of a used soiled substance with a good burning behavior and constant heat of combustion like TNT and RDX, the crucible considerably affected the deviation in a negative manner. This made the search for a new crucible necessary.

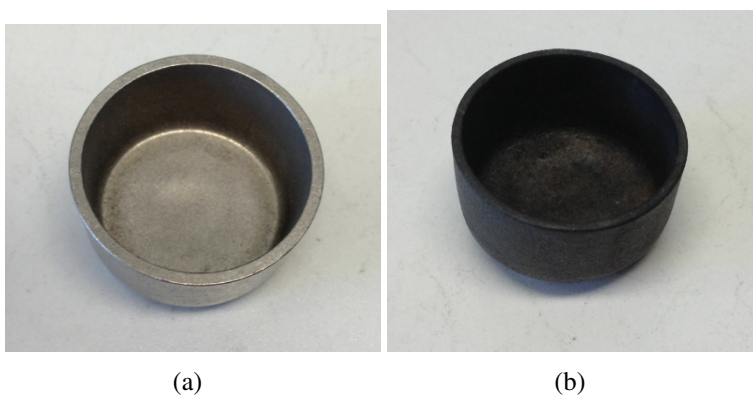


Figure 6.1: New stainless steel crucible (a) and used stainless steel crucible (b).

6.2 Fused Quartz

A crucible consisting of fused quartz was the second choice for the experiments. The calibration experiments were very positive and the deviance was also lower (0.09 %) compared to the steel crucible. Unfortunately many problems occurred. For example the fused quartz crucible from the company IKA® crushed only after 30 measurements (see Figure 6.2). The crucible had a wall thickness of only 1-2 mm.



Figure 6.2: Broken fused quartz crucible.

The second fused quartz crucible, extra produced for this works measurements in the chemistry department of the LMU, was more stable with a wall thickness of 5 mm (see Figure 6.3).



Figure 6.3: Stable fused quartz crucible.

Unfortunately after 100 measurements the surface became rough. The decomposition products of the measured high energetic materials caused little splits to the surface of the crucible. This damage influenced the burning behavior of the compounds, resulting in a higher pollution with grime compared to a smooth surface. Also the deviation increased and no more measurements were possible.

6.3 Platinum

Despite the costs, platinum proved to be the most appropriate material for the calorimetric combustion. The burning behavior of the samples enhanced using the platinum crucible and no residues or only little amounts of grime were observed. It is stable toward corrosion. The difference of platinum compared to quartz or steel, is its great heat capacity and heat of conduction. These properties allow, by the combustion a fast heating up and cooling down of the material.

The first experiments were made with a platinum container with wall thickness about 0.1 mm. By investigating high energetic materials a high amount of energy was released, which affected the stability of the crucible (see Figure 6.3).



Figure 6.4: Used platinum crucible.

A new crucible was necessary, and it was made of one ounce (28.3495231 g) of platinum. The resulting crucible has a wall thickness of 0.5 mm and is resistant to high energetic materials (see Figure 6.3).



Figure 6.5: New platinum crucible.

Bibliography

- [1] F. Stohmann, *J. Pr. Chem.* **1897**, 55, 263-284.
- [2] P. J. Linstrom, W. G. Mallard, Eds., NIST Standard Reference Database, National Institute of Standard and Technology, Gaithersburg MD; <http://webbook.nist.gov>, (**March 2015**).
- [3] S. S. Pinto, H. P. Diogo, M. E. Minas da Piedade, *J. Chem. Thermodyn.* **2003**, 35, 177-188.
- [4] Q. J. Axthammer, C. Evangelisti, T. M. Klapötke, *Characterization, bombcalorimetric measurements and quantum chemical calculations of high energetic dense oxidizers (HEDO)*, From International Annual Conference of ICT , Karlsruhe, Germany, 44th, 88/1-88/15, **2013**.
- [5] M. V. Roux, R. Notario, C. Foces-Foces, M. Temprado, F. Ros, V. N. Emel'yanenko, S. P. Verevkin, *J. Phys. Chem. A* **2011**, 115, 3167-3173.
- [6] S. Sunner, M. Mansonn, *Combustion Calorimetry: Experimental Chemical Thermodynamics*, Pergamon Press, Oxford, 72, **1979**.

Chapter 7

Dihydroxylammonium 5,5'-Bistetrazole-1,1'-diolate and Dinitro-bis-1,2,3-triazole-1,1'-diol

Dihydroxylammonium 5,5'-bistetrazole-1,1'-diolate (TKX-50) and dinitro-bis-1,2,3-triazole-1,1'-diol (MADX-1), see Figure 7.1, are two new compounds in the tetrazole and triazole N-oxide chemistry that are easy to prepare, powerful. The two compounds accomplish the requirements to replace RDX: thermal stability, low toxicity and safety of handling.[1][2][3]

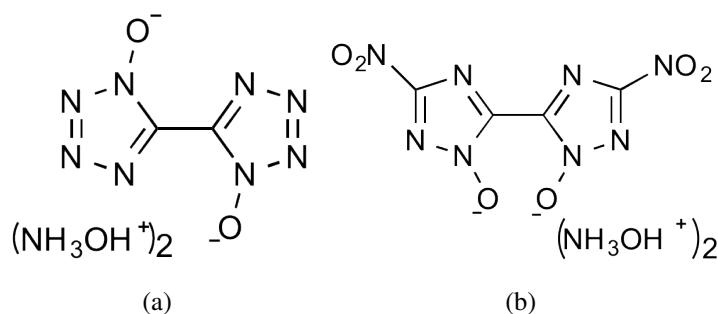


Figure 7.1: Dihydroxylammonium 5,5'-bistetrazole-1,1'-diolate (TKX-50)(a) and dinitro-bis-1,2,3-triazole-1,1'-diol (MADX-1)(b).

The thermal stabilities of TKX-50 and MADX-1 are similar with 221 °C and 217 °C respectively. Both compounds meet the military requirements for new explosives, which demand thermal stability above 200 °C. The impact sensitivity of TKX-50 is 20 J and for MADX-1 >40 J, which are much lower than the impact for RDX with 7 J. For the friction sensitivity of TKX-50 the value is similar like the one for RDX with 120 N, whereas MADX-1 is insensitive towards friction (>360 N).

For the calorimetric measurements several standard additives were investigated: paraffin oil, parafilm and polyethylene bulbs. In Table 7.1 and 7.2 the five best measurements for the two investigated compounds are reported. For TKX-50 paraffin oil seemed to be the most suitable

additive and for MADX-1 it was parafilm. In several cases a big amount of grime was observed which cannot be explained satisfying, when considering the high purity of the compounds, which are confirmed by elemental analysis and NMR spectroscopy.

Table 7.1: Calorimetric measurements for dihydroxylammonium 5,5'-Bistetrazole-1,1'-diolate (TKX-50).

TKX-50 [g]	Paraffin oil [g]	0.1 M NaOH [ml]	ΔU_c [cal/g]	$\Delta U_{c,av}$ [cal/g]	σ_c [%]
0.0987	0.4438	7.50	2461.08	2458.36	1.33
0.1340	0.6032	4.0	2497.10		
0.0973	0.4567	5.2	2458.65		
0.1092	0.5162	5.5	2416.61		

The values for TKX-50 are shown in Table 7.1, seem to be quite consistent regarding to the deviation of only 1.33 %. Anyway, the reported values are the best out of several measurements. That is surprising considering the high performance of TKX-50. Much more inconsistent are the results for MADX-1, which showed a bigger deviation with 4 % (see Table 7.2).

Table 7.2: Calorimetric measurements for dinitro-bis-1,2,3-triazole-1,1'-diol (MADX-1).

MADX-1 [g]	Parafilm [g]	0.1 M NaOH [ml]	ΔU_c [cal/g]	$\Delta U_{c,av}$ [cal/g]	σ_c [%]
0.0847	0.5968	9.7	1880.21	1788.69	4
0.0762	0.5878	9.05	1740.78		
0.0968	0.5959	9.3	1833.96		
0.0905	0.5765	6	1699.79		

In the comparison between the calculated and experimentally determined $\Delta_f H^\circ(\text{M})$ [kJ/mol], the accordance is significant.

Table 7.3: Comparison of heat of formations $\Delta_f H^\circ(\text{M})$ [kJ/mol] calculated or experimental for dihydroxylammonium 5,5'-Bistetrazole-1,1'-diolate (TKX-50).

$\Delta_f H_{exp}^\circ(\text{M})$ [kJ/mol]	$\Delta_f H_{calc}^\circ(\text{M})$ [kJ/mol]
473	458

Instead for MADX-1, the deviation is bigger by 32 J.

Table 7.4: Comparison of heat of formations $\Delta_f H^\circ(\text{M})$ [kJ/mol] calculated or experimental for dinitro-bis-1,2,3-triazole-1,1'-diol (MADX-1).

$\Delta_f H^\circ_{exp}(\text{M})$ [kJ/mol]	$\Delta_f H^\circ_{calc}(\text{M})$ [kJ/mol]
249	217

For a full characterization of TKX-50, the decomposition products were analyzed after the combustion. The control of the thermal decomposition is essential for the storage and transportation of high energetic materials. Consequently studies of the thermal decomposition are necessarily to prevent accidents. Goddard *et al.* performed recently molecular dynamics studies to discover the initial decomposition steps of TKX-50 at high temperature.[4] It was found that by increasing the temperature (from 25 °C to 1025 °C) several fragment were formed, like the conjugated acid base hydroxyl amine NH_2OH and H-diolate $(\text{H}-\text{C}_2\text{O}_2\text{N}_8)^-$. Also others gaseous species were found: N_2 and N_2O . In Prof. Klaprearsch's group the decomposition products were experimentally investigated and confirmed partially the results from Goddard. After the calorimetric combustion the gases were collected in a balloon and measured in gas chamber for IR measurements. The resulting spectrum is shown in Figure 7.

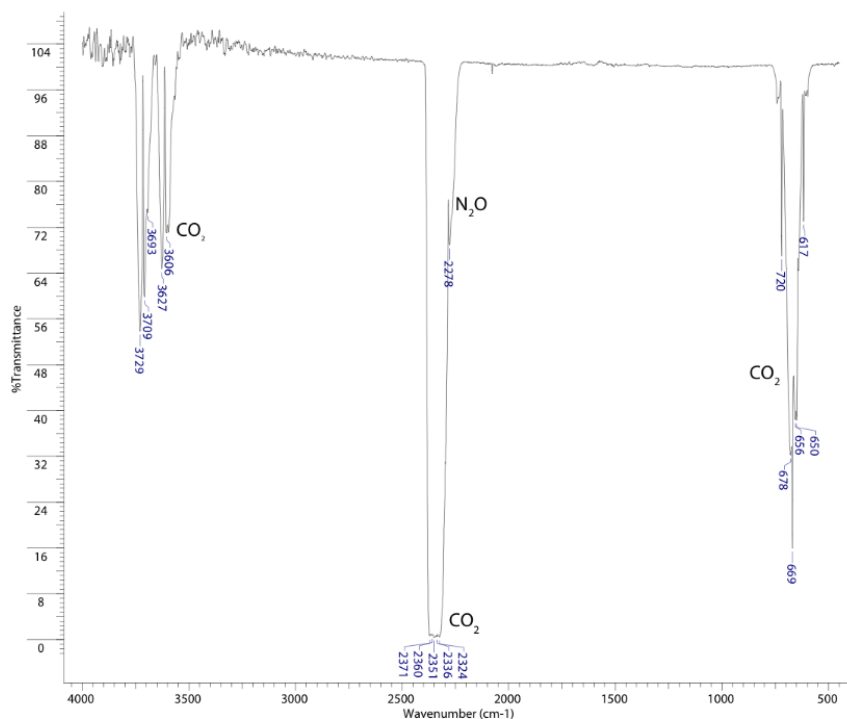


Figure 7.2: IR spectrum of the gaseous products resulting by the TKX-50 combustion.

The IR spectrum of the measured gases, shows three different band regions at $617-720\text{ cm}^{-1}$, $2278-2371\text{ cm}^{-1}$ and $3606-3729\text{ cm}^{-1}$. Some absorption bands are characteristic for CO_2 , the bands between 2324 and 2371 cm^{-1} belong to the asymmetric stretch ν_3 and the signals between 617 and 678 cm^{-1} , can be assigned to the bending stretch ν_2 of CO_2 . The third signal is an overtone bands of $\nu_3 + 2\nu_2$ between 3606 and 3729 cm^{-1} . [5] At 2278 cm^{-1} the typically the band for nitrous oxide N_2O can be detected. [4] Other molecules such as H_2O , CH_4 , CO or other oxides of nitrogen could not been found in the spectrum. The detected gases CO_2 and N_2O are environmentally friendly and the former showed the highest amount. The absence of CO -bands in the spectrum can be explained by a fully oxidation of CO to CO_2 due to the overpressure in the bomb calorimeter (30 bar). [8]

Bibliography

- [1] N. Fischer, D. Fischer, T. M. Klapötke, D. G. Piercey, J. Stierstorfer, *J. Mat. Chem.* **2012**, *22*, 20418-20422.
- [2] A. A. Dippold, T. M. Klapötke, *J. Am. Chem. Soc.* **2013**, *135*, 9931-9938.
- [3] V. Golubev, T. M. Klapötke, J. Stierstorfer, *TKX-50 and MAD-XI - A Progress Report*, 40th Intl. Pyrotechnics Seminar, Colorado Springs, CO, July 13 - 18, **2014**.
- [4] Q. An, W. Liu, W. A. Goddard, T. Chen, S. Zybin, H. Xiao, *J. Phys. Chem. C* **2014**, *118*, 27175-27181.
- [5] X. Zhang, S. P. Sander, *J. Phys. Chem. A* **2011**, *115*, 9854-9860.
- [6] P. S. Makashir, E. M. Kurian, *Propell. Explos. Pyrot.* **199**, *24*, 260-265.
- [7] P. J. Linstrom, W. G. Mallard, Eds., NIST Standard Reference Database, National Institute of Standard and Technology, Gaithersburg MD; <http://webbook.nist.gov>, (**March 2015**).
- [8] M. F. Bölter, MSc thesis, LMU Munich, Munich, **2014**.

Chapter 8

Common High Energy Materials

In this chapter several high energy materials are presented. Each compound was characterized by calorimetric measurements and quantum chemical calculations. The idea behind was at first the investigation of well know compounds like cyclotrimethylenetrinitramine (RDX), 2-methyl-1,3,5-trinitrobenzene (TNT) or 1,1-diamino-2,2-nitroethylene (FOX-7) and comparison with the literature. Then new high energetic materials were investigated as RDX or as hexanitrostilben (HNS) replacements.

RDX is the most well known nitramine explosive with excellent performance data. Unfortunately, RDX is toxic [1] and novel RDX-replacement are essential. The criteria for novel explosives are: a high density above 2.0 g cm^{-3} , a detonation velocity as good as RDX or $> 8500 \text{ m s}^{-1}$, a thermal stability above $200 \text{ }^\circ\text{C}$ and low solubility in water for eco-friendliness. Another important point is the insensitivity of the compounds towards accidental ignition by impact, friction and electrostatic discharge. These compounds are classified as insensitive high energy dense compounds. In the last decade several studies were concentrated in the development of green explosives. These explosives had to contain atoms such as C, N, O or H that produce non-toxic decomposition products. In this chapter three compounds according to these criteria are presented, the 4,4'-diamino-3,3'-bisfurazan (DABF), 4,5-bis(1*H*-tetrazol-5-yl)-2*H*-1,2,3-triazole (BTT) and bis(1*H*-tetrazol-5-yl)amine (BTA).

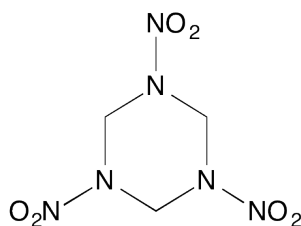


Figure 8.1: Structure of cyclotrimethylenetrinitramine, hexogen, (RDX).

HNS is a secondary explosive with a high impact sensitivity than RDX of 5 J, and a friction sensitivity of 240 N. Another advantage of HNS is the high heat resistance. It melts at $316 \text{ }^\circ\text{C}$. The compound was used in space missions and filled in seismic sources.[2] HNS was used for several

decades but the design of new materials with better performance is a new goal. In this chapter 2,6-*Bis*-picrylamino-3,5-dinitropyridine (PYX) as possible HNS-replacement is investigated.

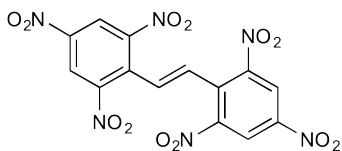


Figure 8.2: Structure of hexanitrostilben (HNS).

In addition to the calorimetric characterization the interest was pointed out to the different *N*-content in the investigated compounds the *N*-content variates, and in Table 8.1 the different amount are listed.

Table 8.1: List of investigated compound and its *N*-amount in%.

Compounds	<i>N</i> -amount %
2-Methyl-1,3,5-trinitrobenzene (TNT)	18.50
cyclotrimethylenetrinitramine (RDX)	37.84
1,1-Diamino-2,2-nitroethylene (FOX-7)	37.84
2,6- <i>Bis</i> -picrylamino-3,5-dinitropyridine (PYX)	24.80
4,4'-Diamino-3,3'- <i>bis</i> furazan (DABF)	49.99
4,5- <i>Bis</i> (1 <i>H</i> -tetrazol-5-yl)-2 <i>H</i> -1,2,3-triazole (BTT)	75.11
<i>Bis</i> (1 <i>H</i> -tetrazol-5-yl)amine (BTA)	82.34

By *N*-rich molecules was assumed a different combustion behavior as well a different amount for the nitric acid correction. In the chapter the assumptions were discussed in details.

8.0.1 2-Methyl-1,3,5-trinitrobenzene

The first analyzed compound was 2-methyl-1,3,5-trinitrobenzene (TNT), one of the most common secondary explosives (see Figure 8.0.1). Julius Willbrand prepared it first in 1863.[3] It melts at 80 °C and is well used for applications because of its low sensitivity to impact (15 J) or friction (353 N). [3]

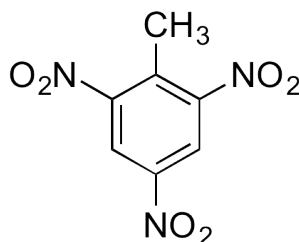


Figure 8.3: Structure of 2-methyl-1,3,5-trinitrobenzene (TNT).

During the calorimetric investigation, four samples were burnt with paraffin oil as additive as shown in Table 8.2 TNT burnt without production of grime, and the deviation for the four samples was moderate (2 %). The amount of NaOH for the nitric acid correction is small, around 6 mL, that is not surprising because of the low *N*-content in the molecule (18.5 %).

Table 8.2: Calorimetric measurements for 2-methyl-1,3,5-trinitrobenzene (TNT).

TNT [g]	Paraffin oil [g]	0.1 M NaOH [mL]	ΔU_c [cal/g]	$\Delta U_{c,av}$ [cal/g]	σ_c [%]
0.0985	0.5032	6.6	3256.12	3203.06	2
0.1063	0.5035	6.5	3273.19		
0.0995	0.5076	6.6	3129.30		
0.1081	0.4983	6.4	3153.53		

The average value for the combustion experiments $\Delta U_{c,av}$ [cal/g] was used for the calculation of the enthalpy of formation $\Delta_f H^\circ(\text{M})$ [kJ/mol]. Comparing the measured and calculated $\Delta_f H^\circ(\text{M})$ [kJ/mol], the two values show a difference of 21 kJ/mol. The literature values are between the two values, -66 kJ/mol for reference 1 [3] and -62 kJ/mol for reference 2 [5]. That imports a good accordance in our results.

Table 8.3: Comparison of heat of formations $\Delta_f H^\circ(\text{M})$ [kJ/mol] calculated or experimental for 2-methyl-1,3,5-trinitrobenzene (TNT).

$\Delta_f H_{exp}^\circ(\text{M})$ [kJ/mol]	$\Delta_f H_{calc}^\circ(\text{M})$ [kJ/mol]	[3] $\Delta_f H^\circ(\text{M})$ [kJ/mol]	[5] $\Delta_f H^\circ(\text{M})$ [kJ/mol]
-76	-57	-66	-63

8.0.2 Cyclotrimethylenetrinitramine

Cyclotrimethylenetrinitramine, hexogen, (RDX) (see Figure 8.0.2) is one of the most powerful high explosives, widely used in the second world war. Today it is still in many military devices. Georg Friedrich Henning investigated it in Berlin for the first time in 1898 for pharmaceutical purpose and in 1920 was used for military scope.[6] The sensitivity to impact is 7.4 J and to friction 120 N, and the detonation velocity 8750 m/s.[3]

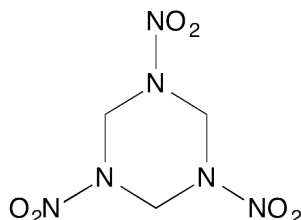


Figure 8.4: Structure of cyclotrimethylenetrinitramine, hexogen, RDX.

The substance was investigated four times using paraffin oil as additive (see Table 8.4). One value was far out of range (2384.74 cal/g) and therefore was neglected. The average deviation of the other samples was small (1 %).

Table 8.4: Calorimetric measurements for cyclotrimethylenetrinitramine (RDX).

RDX [g]	Paraffin oil [g]	0.1 M NaOH [mL]	ΔU_c [cal/g]	$\Delta U_{c,av}$ [cal/g]	σ_c [%]
0.0979	0.5197	6.95	1847.13	1824.71	1
0.1054	0.5559	6.85	1963.80		
0.1028	0.5974	5.9	2384.74		
0.1045	0.5792	7.8	1802.29		

The average value $\Delta U_{c,av}$ [cal/g] was used to obtain $\Delta_f H^\circ(\text{M})$ [kJ/mol].

Table 8.5: Comparison of heat of formations $\Delta_f H^\circ(\text{M})$ [kJ/mol] calculated or experimental for cyclotrimethylenetrinitramine (RDX).

$\Delta_f H^\circ_{exp}(\text{M})$ [kJ/mol]	$\Delta_f H^\circ_{calc}(\text{M})$ [kJ/mol]	[7] $\Delta_f H^\circ(\text{M})$ [kJ/mol]
75	87	62

Comparing the measured value with the calculated, the deviation is limited (13 kJ/mol) better than TNT. By comparing with the literature, most measurements were made mixture of RDX with other compounds, only one value was found and in this case the difference with reference value is by 12 kJ/mol. [7] Concerning the nitric acid correction, the titration with NaOH results with values a bit higher as TNT as it was expected to a higher *N*-content of 37 %.

8.0.3 1,1-Diamino-2,2-nitroethylene

1,1-Diamino-2,2-nitroethylene (FOX-7) is one of the common insensitive explosives. FOX-7 shows better performance than RDX with a detonation velocity of 8870 m/s instead of 8750 m/s.[3] The first report about this compound was from the Swedish Research Defence Agency [8], but probably Russian scientist have synthesized it first. The sensitivity data are also lower than RDX, with a impact sensitivity of 25 J and a friction sensitivity of >350 N.

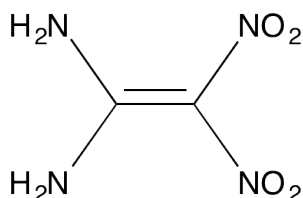


Figure 8.5: Structure of 1,1-diamino-2,2-nitroethylene, FOX-7.

For the measurements benzoic acid (BA) was used. BA is not the best additive, but in case of neutral and stable molecules as FOX-7, it doesn't react as for salts. The samples were burning good and the values showed a really low deviance by <0.1 %.

Table 8.6: Calorimetric measurements for 1,1-diamino-2,2-nitroethylene (FOX-7).

FOX-7 [g]	BA [g]	0.1 M NaOH [mL]	$\Delta U_{c,av}$ [cal/g]	ΔU_c [cal/g]	σ_c [%]
0.0985	0.8865	8.1	2153.26	2134.12	<0.1
0.1005	0.9045	7.95	2111.89		
0.0995	0.8955	8.3	2137.22		
0.0861	0.7749	7.4	2045.29		

The measured value for FOX-7 is -44 kJ/mol, whereas the calculated values variate from -84.1 to -111.2 kJ/mol. These variations were also discovered by Bellamy. [9]. For FOX-7 was possible the calculations of $\Delta_f H^\circ(M)$ [kJ/mol] with different computational methods, because of the contain amount of atoms and the elementary bond connectivity. By aromatic system like TNT and RDX, the computational time improves enormously.

The structure of FOX-7 shows unusual bond lengths and angles that may explain the huge deviations in the reported values.

The C=C bond length is 1.456 \AA , an intermediate between that of a C–C single bond (1.54 \AA) and of a normal C=C double bond (1.34 \AA). The normal C–NH₂ bond and C–NO₂ are shorter

Table 8.7: Comparison of heat of formations $\Delta_f H^\circ(\text{M})$ [kJ/mol] calculated or experimental for 1,1-diamino-2,2-nitroethylene (FOX-7).

Methods	Values
$\Delta_f H_{exp}^\circ(\text{M})$ [kJ/mol]	-44
CBS-4M $\Delta_f H^\circ(\text{M})$ [kJ/mol]	-84
CBS-QB3 $\Delta_f H^\circ(\text{M})$ [kJ/mol]	-111
G3 $\Delta_f H^\circ(\text{M})$ [kJ/mol]	-88
G4 $\Delta_f H^\circ(\text{M})$ [kJ/mol]	-94
[9] $\Delta_f H^\circ(\text{M})$ [kJ/mol]	-53 to -134

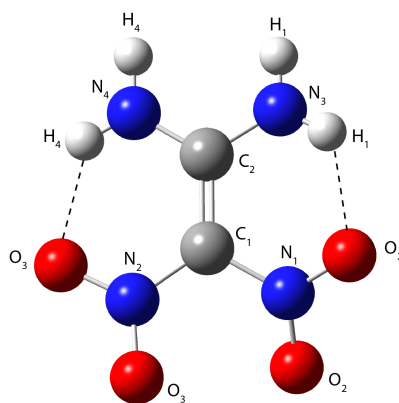


Figure 8.6: Calculated structure of FOX-7.

(respectively 1.31 Å/1.32 Å and 1.42 Å/1.39 Å), because of the electron-donating amino groups on C1 and the electron-withdrawing nitro groups on C2. The structure is essentially planar, with a average C–C torsion angle of 4.8° and two strong hydrogen bonds exist between NH and NO on both side of the molecule.

8.0.4 2,6-Bis-picrylamino-3,5-dinitropyridine

2,6-Bis-picrylamino-3,5-dinitropyridine (PYX) depicted in Figure 8.0.4 was used as obtained from the commercial supplier Dynathec®. This compound was synthesized for the first time in Los Alamos National Laboratory, U.S.A. in 1980. The advantage of PYX is the high thermal stability. It decomposes at 360 °C, that ensure safer production, increase the shelf life of a munitions and low vulnerability to accidental initiations. Another is the replacement of RDX with high energy dense materials having a higher decomposition temperature. The heteroaromatic nitro system like in PYX, has the advantage to deliver higher performance compared to analogous aromatic system. The picryl groups increase the energetic of the parent compounds and the nitro groups in aromatic ring increase both density and thermal stability. The amino groups in the aromatic ring increases the insensitivity of the compound towards mechanical stimuli. The sensitivity data are low, with a impact sensitivity of >10 J and to friction 360 N. Because of the high thermal stability PYX is useful for booster explosive charges.[10]

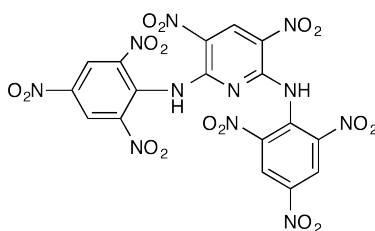


Figure 8.7: 2,6-Bis-picrylamino-3,5-dinitropyridine (PYX).

Three samples of this compound were burnt without production of grime. Other samples, which were not burning so good, are not reported. The deviation is 1 % and the amount of NaOH is surprisingly different for the first sample by 3.5 mL, comparing with the second and third samples, both by 7 mL. Instead the combustion values ΔU_c [cal/g] are in the same range.

Table 8.8: Calorimetric measurements for 2,6-Bis-picrylamino-3,5-dinitropyridine (PYX).

PYX [g]	Paraffin oil [g]	0.1 M NaOH [mL]	ΔU_c [cal/g]	$\Delta U_{c,av}$ [cal/g]	σ_c [%]
0.0912	0.5878	3.5	2786.58	2798.47	1
0.0877	0.6081	7.9	2776.90		
0.0878	0.6037	7.5	2831.92		

Comparing the experimental and calculated $\Delta_f H^\circ(M)$ [kJ/mol], the two results were fitting not so good. That is a bit unexpected considering the high level of purity of the commercial compound, as the elemental analysis and NMR confirmed.

Table 8.9: Comparison of heat of formations $\Delta_f H^\circ(\text{M})$ [kJ/mol] calculated or experimental for 2,6-bis-picrylamino-3,5-dinitropyridine (PYX).

$\Delta_f H_{exp}^\circ(\text{M})$ [kJ/mol]	$\Delta_f H_{calc}^\circ(\text{M})$ [kJ/mol]
75	95

One possible explanation is that the computational method CBS-4M is not such accurate by big amount of aromatic cyclic present in the molecule. The aromatic character implicate several vdW interactions and weak interactions that can be better considered by more accurate computational method.

8.0.5 4,4'-Diamino-3,3'-bisfuran

Aminofurazan can be used as precursor for biologically active compounds or for the synthesis of energetic materials. The 4,4'-diamino-3,3'-bisfuran (DABF) was synthesized according to literature.[11] The advantages of this compound are multiple: it is insensitive, with a impact sensitivity $> 40\text{J}$ and to friction $> 360\text{N}$; it has a high thermal stability with a decomposition temperature of $304\text{ }^\circ\text{C}$ and an higher $\Delta_f H^\circ(\text{M})$ [kJ/mol] than other furazans. The compound has two N-O-bonds, that contain active oxygen and improve the performance.

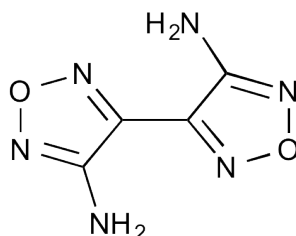


Figure 8.8: 4,4'-Diamino-3,3'-bisfuran (DABF).

Four samples were investigated using paraffin oil as additive. The combustion was without production of grime and the deviation was low ($< 1\%$). The *N*-content of the compound was around 50% , twice that PYX by 25% , nevertheless the amount of NaOH for the acid correction was similar.

Table 8.10: Calorimetric measurements for 4,4'-diamino-3,3'-bisfuran (DABF).

DABF [g]	Paraffin oil [g]	0.1 M NaOH [mL]	ΔU_c [cal/g]	$\Delta U_{c,av}$ [cal/g]	σ_c [%]
0.0963	0.5092	7.15	3182.91	3278.26	< 1
0.5152	0.5152	7.7	3319.36		
0.5075	0.5075	7.35	3354.68		
0.4967	0.4967	7.5	3256.07		

By a comparison between the measurements and the calculations show a deviation of 35 kJ/mol . That can not be in detail explain, especially by a low deviation of the combustion values. No literature values were found.

Table 8.11: Comparison of heat of formations $\Delta_f H^\circ(\text{M})$ [kJ/mol] calculated or experimental for 4,4'-diamino-3,3'-bisfuran (DABF).

$\Delta_f H_{exp}^\circ(\text{M})$ [kJ/mol]	$\Delta_f H_{calc}^\circ(\text{M})$ [kJ/mol]
371	336

8.0.6 4,5-Bis(1H-tetrazol-5-yl)-2H-1,2,3-triazole

4,5-Bis(1H-tetrazol-5-yl)-2H-1,2,3-triazole (BTT) was synthesized according to the literature [12] [13] High nitrogen compounds, like BTT, are of great interest because by the decomposition products mainly produced non-toxic nitrogen gas. The compound can be used for clean-burning gas generants, explosives and smokeless pyrotechnic ingredients. As new green compounds, high-nitrogen energetic substances containing tetrazoles attached to heterocyclic backbone were synthesized. An other propriety of the compound is the insensitiveness to impact (40 J) and to friction (>360 N).

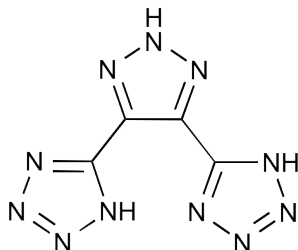


Figure 8.9: 4,5-Bis(1H-tetrazol-5-yl)-2H-1,2,3-triazole (BTT).

In Table 8.12 are shown the results of the measurements, and only two were used for the evaluation. The third deviated too much.

Table 8.12: Calorimetric measurements for 4,5-bis(1H-tetrazol-5-yl)-2H-1,2,3-triazole (BTT).

BTT [g]	Paraffin oil [g]	0.1 M NaOH [mL]	ΔU_c [cal/g]	$\Delta U_{c,av}$ [cal/g]	σ_c [%]
0.0795	0.6010	9.2	3033.02	3037.12	<1
0.0787	0.5901	9.3	3041.24		
0.0732	0.5894	9.0	3100.18		

Remarkable is the higher amount of NaOH used for the titration as for other N-rich compounds. In this case the used volume was around 9 mL, usually remains by 7 mL. Until now it is not possible to explain if the higher amounts is connected with the higher amount of N in the molecule (75%) or if it is a causality.

Table 8.13: Comparison of heat of formations $\Delta_f H^\circ(\text{M})$ [kJ/mol] calculated or experimental for 4,5-bis(1H-tetrazol-5-yl)-2H-1,2,3-triazole (BTT).

$\Delta_f H_{exp}^\circ(\text{M})$ [kJ/mol]	$\Delta_f H_{calc}^\circ(\text{M})$ [kJ/mol]
782	793

The comparison between calculated and experimental values show a good agreement, also in this case no literature values were found for comparison.

8.0.7 Bis(1H-tetrazol-5-yl)amine

Bis(1H-tetrazol-5-yl)amine (BTA) was characterized in our group [14] and it is an interesting green energetic material with high nitrogen content (82%) and low carbon content. The applications are as ingredients in low-smoke producing pyrotechnic compositions, gas generators, propellants and especially as RDX-replacements. BTA shows a high thermal stability with a decomposition temperature of 263 °C. It is insensitive to impact (<100 J) and to friction (<360 N).

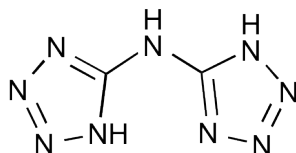


Figure 8.10: Bis(1H-tetrazol-5-yl)amine (BTA).

The compound was burning good, despite that the deviance is higher than one of the other N-rich compounds. One reason can be the hygroscopic character of BTA. The compound was put in the 60 °C oven to dry, and can be that during the measurements gain water again. That can be observed by the increasing values by ΔU_c [cal/g]. Also in this case the amount of NaOH for the acid correction is around 9 mL, as for BTT. This could be also explained by the big amount of N in the molecule.

Table 8.14: Calorimetric measurements for Bis(1H-tetrazol-5-yl)amine (BTA).

BTA [g]	Paraffin oil [g]	0.1 M NaOH [mL]	ΔU_c [cal/g]	$\Delta U_{c,av}$ [cal/g]	σ_c [%]
0.0798	0.5993	9.05	2434.24	2495.88	2
0.0829	0.6032	8.5	2457.89		
0.0813	0.6047	9.1	2481.50		
0.0904	0.6065	9.6	2578.37		
0.0862	0.6081	9.4	2527.40		

Nevertheless, the accordance between calculated and experimental $\Delta_f H^\circ(\text{M})$ [kJ/mol] values are unexpected good.

Table 8.15: Comparison of heat of formations $\Delta_f H^\circ(\text{M})$ [kJ/mol] calculated or experimental for Bis(1H-tetrazol-5-yl)amine (BTA).

$\Delta_f H^\circ_{exp}(\text{M})$ [kJ/mol]	$\Delta_f H^\circ_{calc}(\text{M})$ [kJ/mol]
591	588

Bibliography

- [1] L. M. Sweeney, C. P. Gut Jr., M. L. Gargas, G. Reddy, L. R. Williams, M. S. Johnson, *Regulatory Toxicology and Pharmacology* **2012**, 62, 107-114.
- [2] J. R. Bates, W. W. Lauderdale, H. Kernaghan, *ALSEP Termination Report*, NASA Reference Publication 1036, **1979**.
- [3] J. Wilbrand, *Liebigs Ann. Chem.* **1863**, 128, 178-179.
- [4] J. Köhler, R. Meyer, A. Homburg, *Explosivstoffe*, Wiley-VCH Verlag GmbH & Co. KGaA, 244, **2008**.
- [5] P. E. Rouse, *J. Chem. Eng. Data* **1976**, 21, 16-20.
- [6] E. W. Bachmann., *US Patent 2798870*, **1957**, 798, 870.
- [7] M. K. Seymour, H. L. Herman, *Encyclopedia of explosives and related items*, 9, PATR 2770, R123, **1980**.
- [8] N. V. Latypov, J. Bergman, A. Langlet, U. Wellmar, U. Bemm, *Tetrahedron Lett.* **1998**, 54, 11525-11536.
- [9] A. J. Bellamy, *FOX-7 (1,1-Diamino-2,2-dinitroethene)*, High Energy Density Materials, Springer Berlin Heidelberg, 125, 1-33, **2007**.
- [10] H. S. Jadhav, M. B. Talawar, R. Sivabalan, D. D. Dhavale, S. N. Asthana, V. N. Krishnamurthy, *Indian J. Heterocycl. Chem.* **2006**, 15, 383-386.
- [11] A. B. Sheremetev, E. V. Mantseva, *Mendeleev Commun.* **1996**, 6, 246-247.
- [12] W. P. Norris, A. Henry, A. Ronald, *J. Org. Chem.* **1964**, 29, 3650-660.
- [13] H. Tanaka, T. Toda, *WO20070133323 A1*, **2007**.
- [14] T. M. Klapötke, P. Mayer, J. Stierstofer, J. J. Weigand, *J. Mat. Chem.* **2009**, 18, 5248-5258.

Chapter 9

Oxidizers

Oxidizers are compounds that contains oxidizing elements, in which the fuel component of the explosive burns. By synthesizing new HEDOs some requirements are demands:

- (i) high density ($> 2 \text{ g/cm}^3$)
- (ii) high oxygen balance $\Omega_{CO}\%$ (higher as AP)
- (iii) melting point higher than 150°C
- (iv) low vapor pressure
- (v) decomposition point higher than 200°C
- (vi) easy and cheap synthesis
- (vii) compatibility with binder (ex. HTPB)
- (viii) low sensitivity (higher stress compatibility as PETN)
- (ix) positiv $\Delta_f H^\circ(\text{M})$

The oxygen balance is essentially $\Omega_{CO}\%$ for oxidizers. It show how many oxygen (in %) is realized in CO_2 , CO , H_2O , N_2 by the conversion of an explosive. By a positive value, oxygen is discharged and for a negative value oxygen is in deficiency. The formula for the completely combustion of the compound in CO_2 , H_2O , N_2 is:

$$\Omega_{CO_2} = \left(O - 2C - \frac{H}{2} \right) \cdot \frac{1600}{M} \quad (9.1)$$

Instead for the completely combustion of the compound in CO , H_2O , N_2 the formula is:

$$\Omega_{CO} = \left(O - C - \frac{H}{2} \right) \cdot \frac{1600}{M} \quad (9.2)$$

M is the molecular mass for the energetic materials and O, C and H correspond to the amount of each atoms in the compound. The next chapter is focussed on the estimation of the energy of formation $\Delta_f H^\circ(\text{M})$, using calorimetric measurements and calculations, for different oxidizers. In the first part of the chapter three well know compounds are presented like ammonium nitrate, ammonium perchlorate and ammonium dinitramide. In the second part new synthesized compounds were characterized.

9.0.8 Ammonium nitrate

Ammonium nitrate (AN) is used in agriculture as fertilizer but also as explosive mixtures in mining.[13] In the past several accidents happened in ammonium nitrate factories (Tessenderlo/Belgium 1942, Texas city/U.S.A. 1947, Toulouse/France 2001). Ammonium nitrate changes in several crystalline phases, depending to the temperature and pressure. The sensitivity to impact is 49 J and to friction 353 N and the detonation is depending from the crystal phase. The oxygen balance is the matter of choice for oxidizers, in the case of AN the value is $\Omega_{CO} = \Omega_{CO_2} = +20\%$.[3]

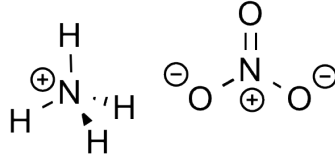


Figure 9.1: Structure of ammonium nitrate (AN).

In Table 9.1 are listed the combustion ΔU_c values, that are only in two cases useful without grime production. Because of that the average $\Delta U_{c,av}$ and the $\Delta_f H^\circ(M)$ were calculated with only two values.

Table 9.1: Calorimetric measurements for ammonium nitrate (AN).

AN [g]	BA [g]	0.1 M NaOH [mL]	$\Delta U_{c,av}$ [cal/g]	$\Delta U_{c,av}$ [cal/g]	σ_c [%]
0.1188	0.5027	6.9	357.39	342.10	6
0.1274	0.5146	6.8	326.81		

The reference report [2] -365.6 [kJ/mol] for the $\Delta_f H^\circ(M)$ an is in agreement with the calculated $\Delta_f H^\circ(M)$ values, but in the case of the measurement the value deviated .

Table 9.2: Comparison of heat of formations $\Delta_f H^\circ(M)$ [kJ/mol] calculated or experimental for ammonium nitrate (AN).

Methods	Values
$\Delta_f H_{exp}^\circ(M)$ [kJ/mol]	-160
[2] $\Delta_f H^\circ(M)$ [kJ/mol]	-365
CBS-4M $\Delta_f H^\circ(M)$ [kJ/mol]	-338
CBS-QB3 $\Delta_f H^\circ(M)$ [kJ/mol]	-350
G3 $\Delta_f H^\circ(M)$ [kJ/mol]	-332
G4 $\Delta_f H^\circ(M)$ [kJ/mol]	-335

One suggestion for the different values, was that by burning the compounds don't produce only N_2 but also several different N-oxide. For this reason a gaseous IR spectra was taken from the resulting atmosphere after the combustion (see Figure 9.0.8).

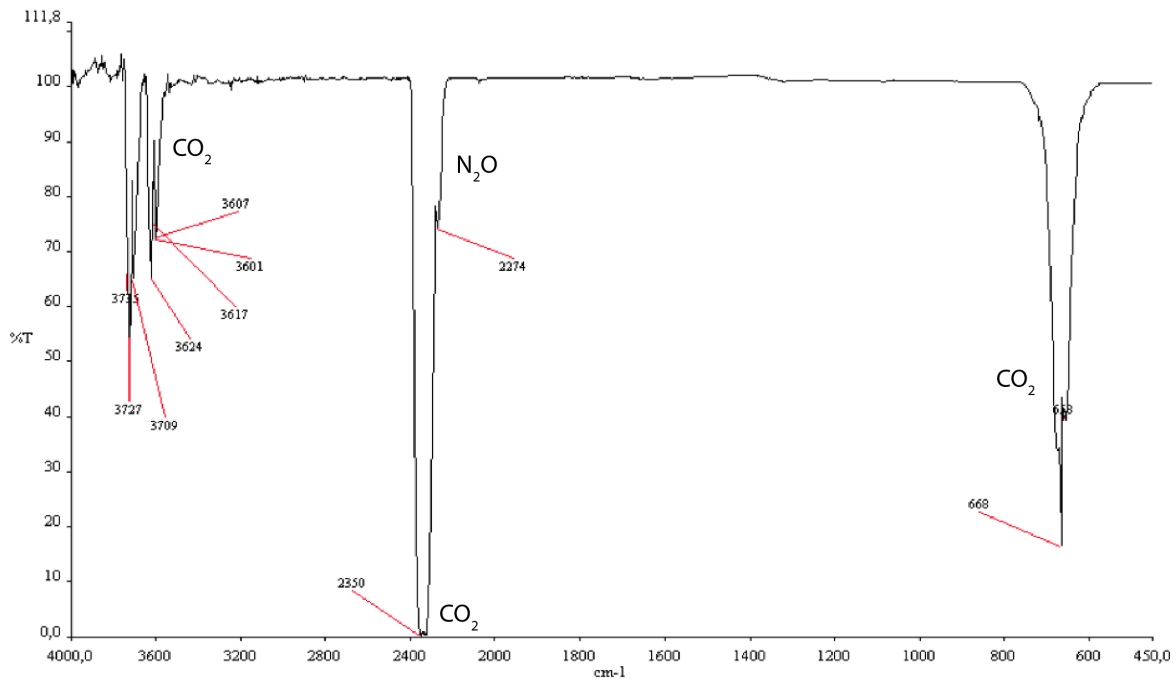


Figure 9.2: Decomposition products of ammonium nitrate (AN) detected in IR gas spectra.

As expected N_2O was detected by a vibration frequency of $\tilde{\nu} = 2274\text{ cm}^{-1}$.[4] Three other big peaks were found by $\tilde{\nu} = 3600\text{ cm}^{-1}$ (overtone bands of $\nu_3 + 2\nu_2$), $\tilde{\nu} = 2350\text{ cm}^{-1}$ (asymmetric stretch ν_3) and $\tilde{\nu} = 660\text{ cm}^{-1}$ (bending stretch ν_2 that indicate the presence of CO_2 .[5][6] Other molecules such as H_2O , CH_4 , CO or other oxides of nitrogen could not been found in the spectrum. The absence of CO -bands in the spectrum can be explained by a fully oxidation of CO to CO_2 due to the overpressure in the bomb calorimeter (30 bar). The high amount of N atoms in the molecule make problematic a successfully calorimetric investigation.

9.0.9 Ammonium perchlorate

The next investigated compound, ammonium perchlorate is the most common oxidizer. It is used in big scale for blasting as well as for military rockets.[13] There are several concerns about the HCl generated by the combustion of the AP, that contaminates the environment.[7] The produced HCl corrodes the launching platform as well pollutes the landscape. The easy production and handling of the AP is commercially convenient and consequently remains in use despite the environmental concerns. The oxygen balance is extremely high by $\Omega_{CO} = \Omega_{CO_2} = +34\%$. The sensitivity to impact is 15 J and to friction is insignificant.[3]

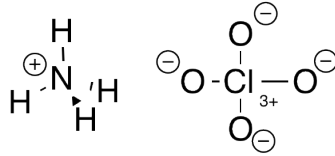


Figure 9.3: Structure of ammonium perchlorate (AP).

The compound was investigated four times and produced a big amount of residue. The measured values deviated a lot (8 %), because of the considerably production of grime.

Table 9.3: Calorimetric measurements for ammonium perchlorate (AP).

AP [g]	BA [g]	0.1 M NaOH [mL]	ΔU_c [cal/g]	$\Delta U_{c,av}$ [cal/g]	σ_c [%]
0.1037	0.9103	5.00	685.05	646.71	8
0.1034	0.9016	6.10	840.96		
0.1068	0.8962	4.65	608.37		
0.1222	0.9078	5.30	536.23		

By comparing the calculated values with the reference [8] a good agreement is shown, that is not the case between the experimental obtained $\Delta_f H^\circ(M)$. The reason is the bad combustion behavior of AP.

The compound was investigated only few times, because the HCl produced by the combustion starts to corrode the container. For further investigation a halogen resistant container is required.

Table 9.4: Comparison of heat of formations $\Delta_f H^\circ(\text{M})$ [kJ/mol] calculated or experimental for ammonium perchlorate (AP).

Methods	Values
$\Delta_f H_{exp}^\circ(\text{M})$ [kJ/mol]	+ 64
[8] $\Delta_f H^\circ(\text{M})$ [kJ/mol]	-249
CBS-4M $\Delta_f H^\circ(\text{M})$ [kJ/mol]	-237
CBS-QB3 $\Delta_f H^\circ(\text{M})$ [kJ/mol]	-234
G3 $\Delta_f H^\circ(\text{M})$ [kJ/mol]	-215
G4 $\Delta_f H^\circ(\text{M})$ [kJ/mol]	-227

9.0.10 Ammonium dinitramide

Ammonium dinitramide (ADN) was synthesized for the first time in the Soviet Union in the 1970s and was presented the scientific community after the end of cold war from Bottaro. [9] It is a powerful oxidizers with slightly higher performances that and less toxic than AP. The sensitivity to impact is 4 J and to friction 64 N. The oxygen balance is also high by $\Omega_{CO} = \Omega_{CO_2} = +25$

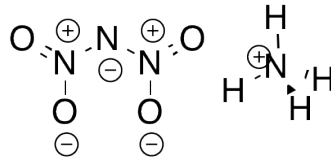


Figure 9.4: Ammonium dinitramide (ADN).

The measurements of ADN, were complicated because of the big amount of grime produced. In the Table 9.5 are show only two values, that correspond to the sample that burnt almost residue-free. The average show a variance of 3 %.

Table 9.5: Calorimetric measurements for ammonium dinitramide (ADN).

ADN [g]	Paraffin oil [g]	0.1 M NaOH [mL]	ΔU_c [cal/g]	$\Delta U_{c,av}$ [cal/g]	σ_c [%]
0.1046	0.5094	7.3	465.98	472.43	3
0.1156	0.5145	8.3	460.03		
0.1203	0.5182	5.5	491.29		

As expected the experimental values are far away from the calculated and thats results from the big amount of grime produced.

Table 9.6: Comparison of heat of formations $\Delta_f H^\circ(\text{M})$ [kJ/mol] calculated or experimental for ammonium dinitramide (ADN).

Methods	Values
$\Delta_f H_{exp}^\circ(\text{M})$ [kJ/mol]	-26
[8] $\Delta_f H^\circ(\text{M})$ [kJ/mol]	-134
CBS-4M $\Delta_f H^\circ(\text{M})$ [kJ/mol]	-84
CBS-QB3 $\Delta_f H^\circ(\text{M})$ [kJ/mol]	-105
G3 $\Delta_f H^\circ(\text{M})$ [kJ/mol]	-79
G4 $\Delta_f H^\circ(\text{M})$ [kJ/mol]	-85

Several conditions, with different amount of additive like paraffin oil, were investigated but no remarkable difference were found. Like for AN, and maybe more, a big amount of NO-oxides is produced and interferes with the combustion results.

9.1 Carbamate's based HEDOs

9.1.1 2,2,2-Trinitroethyl carbamate and nitrocarbamate

2,2,2-trinitroethyl carbamate (TNC) was briefly mentioned one time by Luk'nov and Pokhvisneva [11], but fully characterized first in our lab. The synthesis of 2,2,2-trinitroethyl nitrocarbamate (TNC-NO₂) was developed in our group.[1] TNC melts at 109 °C and is thermally stable up to a temperature of 169 °C. It shows no sensitivity to impact (>40 J), but it is sensitive to friction (64 N). By low temperature DSC measurement of TNC-NO₂ an endothermic solid phase transformation can be observed at -62 °C. On further heating, the compound melts at 109 °C and decompose at a temperature of 153 °C. The sensitivity of TNC-NO₂ are in the range of RDX and therefore sensitive to friction (10J) and impact (96 N). [12] The oxygen balance is for TNC $\Omega_{CO} = +21\%$ and for TNC-NO₂ $\Omega_{CO} = +32\%$, both in the range of ammonium nitrate.

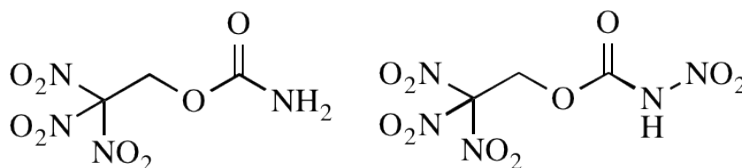


Figure 9.5: Structures of 2,2,2-trinitroethyl carbamate (TNC) and nitrocarbamate (TNC-NO₂).

The determining value for high energetic dense oxidizers (HEDO) is the specific impulse. The specific impulse I_s is used to compare the performance of solid rocket propellants and high energy dense oxidizer. The I_s is dependent on the burning temperature proportional and the molecular weight of the combustions products reciprocal. [13] The specific impulse of TNC in a mixture of 20 % of aluminum as a fuel is at 249 s. The specific impulse of TNC-NO₂ achieved at an mixture of 25 % aluminum, a specific impulse 247 s. They are therefore both in the range of the standard mixture of ammonium perchlorate.

The two compounds were mixed with benzoic acid and press in pellet with a weight approximately of 1 g. Both compounds are stable towards acid like benzoic acid and it was not necessarily in this case to use paraffin oil for the samples. In Table 9.7 and 9.8 are listed the amount of samples as well the ΔU_c [cal/g] obtained by the combustion.

Table 9.7: Calorimetric measurements for 2,2,2-trinitroethyl carbamate (TNC).

TNC [g]	BA [g]	0.1 M NaOH [mL]	ΔU_c [cal/g]	$\Delta U_{c,av}$ [cal/g]	σ_c [%]
0.0972	0.8630	6.70	1034.70	1032.49	< 1
0.1004	0.8735	7.45	1028.20		
0.0970	0.8552	6.80	1034.56		

For both compounds three measurements were possible, for TNC the deviation is extremely low ($< 1\%$) and for TNC-NO₂ is a little bit higher ($> 1\%$). The compounds were burning without any production of grime.

Table 9.8: Calorimetric measurements for 2,2,2-trinitroethyl nitrocarbamate (TNC-NO₂).

TNC-NO ₂ [g]	BA [g]	0.1 M NaOH [mL]	ΔU_c [cal/g]	$\Delta U_{c,av}$ [cal/g]	σ_c [%]
0.1440	0.8390	6.7	1255.46	1261.17	> 1
0.1494	0.8316	6.9	1277.80		
0.1531	0.8529	6.3	1250.25		

As for the other compounds the $\Delta_f H^\circ(\text{M})$ [kJ/mol] experimental was compared with the calculated. For the TNC the values are different from the calculations (53 kJ difference). That is a bit surprising considering the low deviations of the obtained ΔU_c [cal/g].

Table 9.9: Comparison of heat of formations $\Delta_f H^\circ(\text{M})$ [kJ/mol] calculated or experimental for 2,2,2-trinitroethyl carbamate (TNC).

$\Delta_f H_{exp}^\circ(\text{M})$ [kJ/mol]	$\Delta_f H_{calc}^\circ(\text{M})$ [kJ/mol]
-459	-511

In the case of TNC-NO₂ the difference are lower (28 kJ) despite the bigger deviation between the ΔU_c [cal/g]. Probably the -NO₂ added to the carbamate, increase the burning behavior of the compound and decrease the inaccuracy.

Table 9.10: Comparison of heat of formations $\Delta_f H^\circ(\text{M})$ [kJ/mol] calculated or experimental for 2,2,2-trinitroethyl nitrocarbamate (TNC-NO₂).

$\Delta_f H_{exp}^\circ(\text{M})$ [kJ/mol]	$\Delta_f H_{calc}^\circ(\text{M})$ [kJ/mol]
-330	-358

9.2 Michael addition's compounds

For the replacement of the noxious and toxic compounds, a new class of energetic substances were investigated. The compounds were synthesized using Michael addition mechanism. Through a 1,4-addition, a nucleophilic substance was linked with a α, β -non saturated carbonyl compound. [14] In this chapter, three synthesized compounds 4,4,4-trinitrobutyric acid, 2,2,2-trinitroethyl-4,4,4-trinitrobutanoate and 2,2,2-trinitro-1-(2,2,2-trinitroethylamino)-1-butanone starting from nitroform were presented and characterized.

9.2.1 4,4,4-Trinitrobutyric acid

4,4,4-Trinitrobutyric acid could be used as fuel or also a monomer which can be polymerized or copolymerized to form useful propellants plasticizers.[15] The sensitivity tests show that the compounds is almost insensitive to impact (40 J) and to friction (324 N). The oxygen balance is $\Omega_{CO} = +10\%$

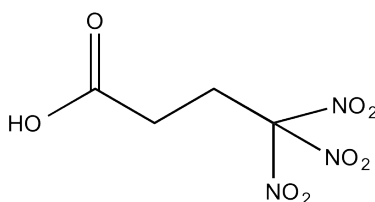


Figure 9.6: Structure of 4,4,4-Trinitrobutyric acid (TNA).

For the determination of the calorimetric combustion, four samples were burnt. In this case paraffin oil were used as additive, showing a good burning behavior. The values show an acceptable deviation of 3 %

Table 9.11: Calorimetric measurements for 4,4,4-trinitrobutyric acid (TNA).

TNA [g]	Paraffin oil [g]	0.1 M NaOH [mL]	ΔU_c [cal/g]	$\Delta U_{c,av}$ [cal/g]	σ_c [%]
0.0508	0.5120	1.3	1402.59	1467.69	3
0.0525	0.6345	1.7	1442.38		
0.0520	0.5147	1.6	1500.45		
0.0527	0.5993	1.4	1525.35		

In the literature there isn't a reported value for the calorimetry, because of that it was possible only a comparison between the calculated and the experimental values. The difference is around 36 kJ/mol.

Table 9.12: Comparison of heat of formations $\Delta_f H^\circ(\text{M})$ [kJ/mol] calculated or experimental for 4,4,4-trinitrobutyric acid (TNA).

$\Delta_f H_{exp}^\circ(\text{M})$ [kJ/mol]	$\Delta_f H_{calc}^\circ(\text{M})$ [kJ/mol]
-541	-506

Using the calculated $\Delta_f H^\circ(\text{M})$ [kJ/mol] performance parameters, the values of the specific impulse is $I_{sp,s}=252$ by a content of 15% Al.

9.2.2 2,2,2-Trinitroethyl-4,4,4-trinitrobutanoate

One more compound formed with Michael addition is 2,2,2-trinitroethyl-4,4,4-trinitrobutanoate. [15] This compound shows a high oxygen balance of $\Omega_{CO}=+20\%$ in the same range of AN and low sensitivity to impact (40 J) and middle to friction (240 N).

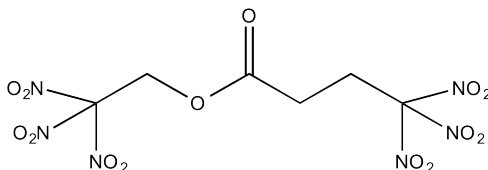


Figure 9.7: 2,2,2-Trinitroethyl-4,4,4-trinitrobutanoate (TNET).

Because of the small amount of the synthesized substance only two measurements were possible. Anyway the substance burnt without production of grime and the deviation is marginal ($< 1\%$).

Table 9.13: Calorimetric measurements for 2,2,2-trinitroethyl-4,4,4-trinitrobutanoate (TNET).

TNET [g]	Paraffin oil [g]	0.1 M NaOH [mL]	ΔU_c [cal/g]	$\Delta U_{c,av}$ [cal/g]	σ_c [%]
0.0396	0.6229	1.4	1347.67	1350.70	0.22
0.0288	0.5033	1.25	1353.73		

The deviation of the calculated value and the experimental is significant. More investigation are necessarily to explain it.

Table 9.14: Comparison of heat of formations $\Delta_f H^\circ(M)$ [kJ/mol] calculated or experimental for 2,2,2-trinitroethyl-4,4,4-trinitrobutanoate (TNET).

$\Delta_f H_{exp}^\circ(M)$ [kJ/mol]	$\Delta_f H_{calc}^\circ(M)$ [kJ/mol]
-575	-466.9

To calculate the specific impulse, the calculated value was used and results $I_{sp} s=256$ by a content of 15% Al. This compound could be a promising alternative to RDX, because the easily synthesis and the high performances (detonation velocity by 8297 m/s).

9.2.3 2,2,2-Trinitro-1-(2,2,2-trinitroethylamino)-1-butanone

The last compound in the Michael's addition topic is 2,2,2-trinitro-1-(2,2,2-trinitroethylamino)-1-butanone. [16] In this case the compound show more performance as RDX replacement as oxidizers. The sensitivity to impact is higher (10J) and to friction middle (240 N).

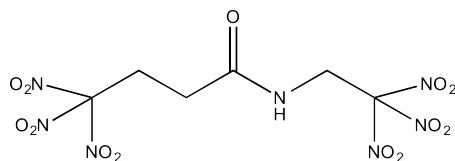


Figure 9.8: 2,2,2-Trinitro-1-(2,2,2-trinitroethylamino)-1-butanone (TNEA).

Also in this case of the slight amount of synthesized substance only two measurements were possible. The deviation is also marginal (< 1%).

Table 9.15: Calorimetric measurements for 2,2,2-trinitro-1-(2,2,2-trinitroethylamino)-1-butanone (TNEA).

TNEA [g]	Paraffin oil [g]	0.1 M NaOH [mL]	ΔU_c [cal/g]	$\Delta U_{c,av}$ [cal/g]	σ_c [%]
0.0990	0.8803	7.5	1829.87	1844.15	0.77
0.1963	0.7846	8.6	1858.43		

The experimental value and the calculated are deviating significantly and powerfully evidence can explain the difference. Also in this case more investigation and measurements are necessarily.

Table 9.16: Comparison of heat of formations $\Delta_f H^\circ(M)$ [kJ/mol] calculated or experimental for 2,2,2-trinitro-1-(2,2,2-trinitroethylamino)-1-butanone (TNEA).

$\Delta_f H_{exp}^\circ(M)$ [kJ/mol]	$\Delta_f H_{calc}^\circ(M)$ [kJ/mol]
-243	-330

To calculate the specific impulse, the calculated value was used and results I_{sp} s=260 by a content of 15% Al. This compound could be a promising alternative to RDX, because the easily synthesis and the high performances. (detonation velocity by 8345 m/s)

Bibliography

- [1] T. M. Klapötke, *Chemistry of High-Energy Materials*, 2nd edition, de Gruyter, **2012**.
- [2] J. D. Cox, D. Harrop, A. J. Head, *J. Chem. Thermodyn.* **1979**, *11*, 811-14.
- [3] J. Köhler, R. Meyer, A. Homburg, *Explosivstoffe*, Wiley-VCH Verlag GmbH & Co. KGaA, 244, **2008**.
- [4] P. S. Makashir, E. M. Kurian, *Propell. Explos. Pyrot.* **199**, *24*, 260-265.
- [5] X. Zhang, S. P. Sander, *J. Phys. Chem. A* **2011**, *115*, 9854-9860.
- [6] P. J. Linstrom, W. G. Mallard, Eds., NIST Standard Reference Database, National Institute of Standard and Technology, Gaithersburg MD; <http://webbook.nist.gov>, (**March 2015**).
- [7] M. S. Johnson, C. J. Salice, *Ecotoxicology of Explosives*, CRC Press, **2009**.
- [8] A. Smirnov, D. Lempert, T. Pivina, D. Khakimov, *Cent. Eur. J. Energ. Mat.* **2001**, *8*, 233-235.
- [9] J. C. Bottaro, R. J. Schmitt, P. E. Penwell, D. S. Ross, *Patent WO 91/19670*, **1991**.
- [10] Q. J. Axthammer, T. M. Klapötke, B. Krumm, R. Moll, S. F. Rest, *Z. Anorg. Allg. Chem.* **2014**, *640*, 76-83.
- [11] O. A. Luk'yanov, G. V. Pokhvisneva, *Russ. Chem. B.* **1992**, *41*, 1286-1288.
- [12] Q. J. Axthammer, C. Evangelisti, T. M. Klapötke, *Characterization, Bomb Calorimetric Measurement and Quantum Chemical Calculations of High Energetic Dense Oxidizers (HEDO)*, From International Annual Conference of ICT, 44th, 88/1-88/15, **2013**.
- [13] T. M. Klapötke, *Chemistry of High-Energy Materials*, de Gruyter, Berlin, 2nd Edition, **2012**.
- [14] J. P. Agrawal, R. Hodgson, *Organic chemistry of explosives*, Wiley-VCH, **2006**.
- [15] I. J. Schaffner, *US Patent 305743*, **1962**.
- [16] H. Feuer, U. Lynch-Hart, *J. Org. Chem.* **1961**, *26*, 587-589.

Chapter 10

Summary Calorimetric and Theoretical Determination of Enthalpy of Formation of HEMs

A detailed work was carried out to find the best conditions to measure energetic materials. Several additive materials were investigated and in a few cases compared with the literature. Paraffin oil and parafilm show adequate results and were chosen for the most of the calorimetric test of energetic materials. Also several crucibles were used and the platinum crucible was found as the most appropriate.

The enthalpy of formation of different energetic materials (secondary explosives and oxidizers) were determined. The calorimetric and theoretical results were compared and the eventual difference analyzed. In general a good accordance was found. The high blasting energetic materials, like TNT and RDX, show a good agreement between theory and praxis, and also compared to the literature values. On the other side, new energetic materials (TKX-50 and MADX-1) were also investigated. The burning behavior was not as good as expected, but the results were consistent.

An additional purpose of this study was the investigation of the possibility, if the *N*-content has any influence to the burning performance due to the varying *N*-content from 25 to 82% of the selected compounds. Several compounds showed a good burning behavior without huge production of grime and it do not depend on the *N*-content. For all compounds, the measured $\Delta_f H^\circ(\text{M})$ values were in the range of the calculated $\Delta_f H^\circ(\text{M})$. The volume of NaOH used for the acid correction varied with the *N*-content of the molecule, the more N the more ml NaOH were necessary. It will be interesting to consider the obtained results and evaluate more *N*-rich molecules to see if the trend found in this work corresponds.

For the oxidizers, some compounds burnt with a big formation of grime which influenced the final results. In particular AP, ADN and AN deviate a lot from the literature values. In contrast to other compounds, like the new synthesized oxidizers for example TNC, TNC-NO₂, TNA. Probably the big amount of nitro groups as well as the carbamate moiety influence the burning behavior in a positive manner.

Chapter 11

Calculations on Components of Composite Propellants

As mentioned in the introduction, the second part of this work is focussed on molecular dynamics simulations of some composite propellant ingredients: pre-binder, plasticizer and a couple of newly designed oxidizers (2,2,2-trinitroethyl nitrocarbamate TNC-NO₂, 2,2,2-trinitroethyl(2-nitro-2-azapropyl)nitrocarbamate TNE-NAP-NC). In Table 11.1 the calculated molecules are listed with atom number (N) and molar mass (M).

Table 11.1: List of simulated molecules with atom numbers (N) and molecular mass (M).

	HTPB	DesmophenTM	PPO	DOA	BTTN	TNC-NO₂	TNE-NAP-NC
N	389	282	364	68	23	21	30
M [g/mol]	2193.58	1964.11	2124.89	370.57	241.11	269.08	341.15

Hydroxyl-terminated polybutadiene (HTPB), polypropylene oxide (PPO) and DesmophenTM are pre-binders and polymer-like materials. All three polymers have medium-size and in the simulation cells they show quite linear structures. In the simulations only few units of these compounds were used, but they provide a good accordance with the experimental results. The experimental estimated glass transition temperatures T_g were compared with the results from the simulations.

The second class of calculated compounds were the plasticizers. In this category dioctyl adipate (DOA) and 1,2,4-butanetriol trinitrate (BTTN) were simulated. The plasticizers help to improve flexibility and strain, to improve physical properties of the propellant binder, to provide a secondary fuel, and to improve specific energy yield in a composite propellant formulation. Additionally with the plasticizers the T_g changes to a lower temperature range.

The third simulated class are the oxidizers. They provide the oxygen for an appropriate combustion

of the fuel in an oxygen efficient environment. The most common oxidizers is ammonium perchlorate, but for the simulations in this work newly designed oxidizers (TNC-NO₂ and TNE-NAP-NC) were taken.

Besides the pre-binders and plasticizers, the mixtures of them are of interest. The reasons are to lower the glass-to-rubber transition further and to get a propellant paste, which is usable for casting in moulds. In this work three different mixture are presented: HTPB mixed with DOA, PPO mixed with DOA and HTPB mixed with BTTN.

Chapter 12

Calculation on Components of Composite Rocket Propellants: Methods

All the calculations were performed using the Materials StudioTM program suite Version 6 of Accelrys©.[1] For the molecular dynamic (MD) calculations the potential energy force field (FF) COMPASSTM [2] from Accelrys© was used. COMPASSTM belongs to the group of so-called second generation FF, which are parameterized using experimental data and quantum mechanically calculated properties. A FF is a potential energy expression to describe the energy surface of an atomic configuration by intramolecular and intermolecular energy terms. The MD simulations were carried out using the software package Forcite in the Material StudioTM program suite. Forcite is a molecular dynamics tool that allows for example geometry optimizations, cell optimizations, energy calculations and dynamic simulations of molecules, periodic and crystalline structures. It was used for all MD calculations presented in this work. Another widely used tool is Amorphous Cell (AC) [3], that was applied to assemble the amorphous material (*e.g.* plasticizers and binders). AC is used for the construction of a system of one or more components, all contained in a user defined cell. In a following step, the cell can be optimized with Forcite, or dynamics simulations can be performed. For the crystalline systems, the Morphology tool was used to predict the external morphology habitus of a crystalline material from its internal crystal structure. The used methodology combines the Donnay-Harker rules [4] to isolate the likely growth planes, and then the Bravais-Friedel [5] rules to deduce their relative growth rates. The resulting crystal morphology and its corresponding surface attributes were used as input for further calculations (*e.g.* optimization, dynamic simulations).

12.1 Computer Facility

The computer facility is composed of a work station with Intel® Xeon® Prozessor X5650 with 2.66 GHz (12M Cache, 6 virtual CPU, 12 Threads, 288 GB RAM storage). WindowsTM 7 Professional was used as operating system.

Bibliography

- [1] Biovia© Accelrys©, Inc., San Diego, CA, USA. <http://www.accelrys.com/products/mstudio/>, (**March 2015**).
- [2] COMPASSTM, Condensed phase **O**ptimized **M**olecular **P**otentials for **A**tomistic **S**imulation **S**tudies; <http://accelrys.com/products/datasheets/compass.pdf>, (March 2015).
- [3] D. N. Theodorou, U. W. Suter, *Macromolecules* **1985**, *18*, 1485.
- [4] J.D.H. Donnay, D. Harker, *Amer. Mineralogist* **1937**, *22*, 463.
- [5] A. Bravais, *Etudes Crystallographiques*, Academie des Sciences, Paris, **1913**.

Chapter 13

Molecular Dynamics

Computer simulations allow a link between microscopic length and time and the macroscopic world of the laboratory. Especially molecular dynamics are based on the interactions between atoms and molecules and predictions of bulk properties can be obtained. Classical molecular dynamics describes the bonds with spring-constants. In classical equations of motion and the Newtonian interpretation of dynamics, the translational motion of an atom i is caused by a force \mathbf{F}_i , exerted by an external potential. The motion and the applied forces are related through Newton's second law: [1]

$$\mathbf{F}_i = m_i \vec{r}_i \quad (13.1)$$

Here m_i is the mass of particle i , \vec{r}_i is the position of it and \vec{r}_i is the acceleration. It is assumed to be independent of position, velocity and time. The force \mathbf{F}_i acting on the atoms i with the mass m_i is taken as the first derivate of the potential energy E_{pot} with respect to the particle position r_i :

$$\mathbf{F}_i = -\frac{\partial}{\partial \mathbf{r}_i} E_{pot} \quad (13.2)$$

The total potential energy E_{pot} , calculated with the force field COMPASSTM is composed by several energy terms: [2]

$$E_{pot} = E_b + E_\theta + E_\Phi + E_\chi + E'_{bb} + E_{b\theta} + E_{b\Phi} + E'_{\theta\theta} + E'_{\theta\theta\Phi} + E_{Coul} + E_{vdW} \quad (13.3)$$

These potential functions can be divided in two categories, the valence terms and non-bonded interaction terms. The valence terms include E_b , E_θ , E_Φ and E_χ for bond (b), angle (θ), torsion (Φ) and out-of-plane angle (χ) coordinates. The second class of valence terms E'_{bb} , $E_{b\theta}$, $E_{b\Phi}$ and $E'_{\theta\theta}$ and $E'_{\theta\theta\Phi}$ are for the cross-coupling between the internal coordinates in the molecules. They are important for predicting vibration frequencies and structural variations associated with conformational changes. The non-bonded terms E_{Coul} and E_{vdW} are used for interactions between pairs of atoms separated by three or more connected atoms, and of course used for pairwise interaction between atoms that belong to different molecules. The term E_{vdW} considers van-der-Waals (vdW) interactions and the term E_{Coul} the electrostatic interactions. All these energetic contributions are

detailed shown in the Equation 13.4, where intra (E_{intra} , bonded terms) and intermolecular parts (E_{inter} , non-bonded terms) are split.

$$E_{intra} = \left\{ \begin{array}{l} \text{stretch} \\ \text{bend} \\ \text{torsion} \\ \text{planar} \\ \text{cross} \end{array} \left| \begin{array}{l} \sum_b [b_2(r-r_0)^2 + b_3(r-r_0)^3 + b_4(r-r_0)^4] \\ \sum_\theta [h_2(\theta-\theta_0)^2 + h_3(\theta-\theta_0)^3 + h_4(\theta-\theta_0)^4] \\ \sum_\phi [v_1(1-\cos\phi) + v_2(1-\cos 2\phi) + v_3(1-\cos 3\phi)] \\ \sum_\chi [\kappa_\chi \chi^2] \\ \sum_b \sum_{b'} [F_{b,b'}(b-b_0)(b'-b'_0)] \\ \sum_\theta \sum_{\theta'} [F_{\theta,\theta'}(\theta-\theta_0)(\theta'-\theta'_0)] \\ \sum_b \sum_\theta [[F_{b,\theta}(b-b_0) + F_{b',\theta}(b'-b'_0)](\theta-\theta_0)] \\ \sum_b \sum_\phi [(b-b_0)(v_1 \cos\phi + v_2 \cos 2\phi + v_3 \cos 3\phi)] \\ \sum_\theta \sum_\phi [(\theta-\theta_0)(v_1 \cos\phi + v_2 \cos 2\phi + v_3 \cos 3\phi)] \\ \sum_\phi \sum_\theta \sum_{\theta'} [F_{\phi,\theta,\theta'} \cos\phi(\theta-\theta_0)(\theta'-\theta'_0)] \end{array} \right. \right. \quad (13.4)$$

$$E_{inter} = \left\{ \begin{array}{l} \text{van-der-Waals} \\ \text{Coulomb} \end{array} \left| \begin{array}{l} \sum_i \sum_{j<i} \left(\frac{A_{ij}}{r_{ij}^9} - \frac{B_{ij}}{r_{ij}^6} \right) \\ \sum_i \sum_{j<i} \frac{q_i q_j}{\epsilon \epsilon_0 r_{ij}} \end{array} \right. \right.$$

COMPASSTM force field applies 9-6 Lennard-Jones potentials for the van-der-Waals interactions.

$$A_{ij} = 2 * \epsilon_{ij} * (r_{ij}^0)^9 \quad B_{ij} = 3 * \epsilon_{ij} * (r_{ij}^0)^6 \quad (13.5)$$

The LJ-9-6 parameters (ϵ and r^0) are given for equal atom pairs. The interactions between different functional groups and molecules are approximated by mixing rules and described in COMPASSTM using Waldman-Hagler type. Between atoms i and j within different groups, r_{ij} and ϵ_{ij} have the form: [3]

$$r_{ij}^0 = \left(\frac{(r_i^0)^6 + (r_j^0)^6}{2} \right)^{1/6} \quad \epsilon_{ij}^0 = 2 * \sqrt{\epsilon_i * \epsilon_j} \left(\frac{(r_i^0)^3 + (r_j^0)^3}{(r_i^0)^6 + (r_j^0)^6} \right) \quad (13.6)$$

where r_i^0 and ϵ_i denote the minimum parameters of the LJ-potential of at m i interacting with atom i . Instead r_{ij}^0 and ϵ_{ij} are the minimum parameter of atom i interacting with atom j .

The electrostatic interaction is represented using atomic partial charges. The bond increment charges δ_{ij} were used to make the charge parameters transferable. The bond increment charges δ_{ij} represents the charge separation between two valence-bonded atoms i and j . For atom i , the total partial charge is:

$$q_i = \sum_j \delta_{ij} \quad (13.7)$$

13.1 Thermodynamic Ensembles

Two types of thermodynamic ensembles have been applied to get the thermodynamical equilibrium states of the molecules with respect to their conformation and their orientation to each other in some defined cells. One was the constant temperature, constant volume ensemble (NVT) and the other the constant temperature, constant pressure ensemble (NPT). The distribution of particle speed as a function of the temperature is given by the Maxwell-Boltzmann equation 13.8, that hold for the NVT ensemble. The latter formula can be used to determine the initial conditions of a simulation system by sampling randomly assigned vector components to the particle from this Gaussian distribution, as well as to determine the initial kinetic energy.

$$p(v)dv = \left(\frac{m}{2\pi k_B T} \right)^{3/2} e^{-\frac{mv^2}{2k_B T}} 4\pi v^2 dv \quad (13.8)$$

Additionally in the NPT simulations, the pressure was controlled using a method developed by Berendsen [4], whereas the temperature control method used was developed by Andersen [3] (the same as for NVT). Applying Andersen thermostat, the velocities of the particles are distributed new after a preset time interval τ_A according to the Maxwell-Boltzmann distribution at the desired temperature. A reasonable choice of τ_A according to ref [7] is shown in equation 13.9 with the thermal conductivity κ_{th} of the system and a dimensionless constant that is mostly set to unity:

$$\tau_A = r_A \cdot \frac{3}{2} k_B \cdot \frac{\rho^{1/3} N^{2/3}}{\kappa_{th}} \quad (13.9)$$

where r_A is a dimensionless constant, κ_{th} is the thermal conductivity, k_B is the Boltzmann constant, and ρ is the number density of particles. This method has a significant drawback: the dynamic properties of the system are systematically influenced by the randomization of velocities.

The NPT ensemble reflects a common laboratory experiment best. Bulk properties are produced well. It describes a system that allows energy and volume exchange with its environment. In a respective MD simulation, the volume V has to be allowed to fluctuate in some way: The Andersen barostat, which is also described in [6], adds the system volume as a free parameter to the equations of motion. The Berendsen method couples the system to a pressure bath to maintain the pressure at a certain target value. The strength of coupling is determined by both the compressibility of the system (using a user-defined variable γ) and a relaxation time constant (a user-defined variable τ). At each step, the x,y and z coordinates of each atom are scaled by the factor:

$$\mu = \left(1 + \frac{\Delta t}{\tau} \gamma [p_{instant} - p_0] \right)^{1/3} \quad (13.10)$$

where Δt is the time step, $p_{instant}$ is the instant mean pressure, and p_0 is the target pressure.

13.2 Periodic Boundary Conditions

In molecular dynamics simulations the periodic boundary conditions are applied to overcome the limited number of molecules in the calculated system. Therefore, periodic box boundaries without any interaction to particles are applied in almost all molecular dynamics studies found in literature.[7] This approach has two implications:

- A particle that crosses a border is shifted to the opposite boundary of the box, while its momentum remains unchanged. Hence, an pseudo-infinitely large space is created, which can be imagined in two ways: The particle may never leave the box, or the particle may be formally exchanged by its so called periodic image that enters the box in lieu of the leaving particle.

- The second effect of such a box to be considered is that particles are allowed to interact with those beyond the boundaries: For example, if a particle is located at the far right side of the box (in an arbitrary Cartesian coordinate system), its interaction radius extends beyond the border and reaches back again in the box at the left side. These two modifications have to be implemented in a simulation program explicitly and indeed reduce the effect of finite boxes.[3]

Bibliography

- [1] M. P. Allen, *Computational Soft Matter: From Synthetic Polymers to Proteins*, John von Neumann Institute for Computing, Jülich, 23, 1-28, **2004**.
- [2] (a) H. Sun, *J. Phys. Chem. B* **1998**, *102*, 7338-7364; (b) H. Sun, P. Ren, J. R. Fried; *Comp. Theor. Polym. S.* **1998**, *108*, 229-246.
- [3] Michael Matthias Nardai, Ph.D. Thesis, Universität Wien, **2014**.
- [4] H. J. C. Berendsen, J. P. M. Postma, W. F. van Gunsteren, A. DiNola, J. R. Haak, *J. Chem. Phys.* **1984**, *81*, 3684-3690.
- [5] T. A. Andrea, W. C. Swope, H. C. Andersen, *J. Chem. Phys.* **1983**, *79*, 4576-4584.
- [6] G. J. Martyna, D. J. Tobias, M. L. Klein, *J. Chem. Phys.* **1994**, *101*, 4177-4189.
- [7] M. P. Allen, D. J. Tildesley, *Computer Simulation of Liquids*, Oxford University Press, USA, 24-27, **1989**.

Chapter 14

Pre-Binder

14.1 Hydroxyl-terminated polybutadiene

Hydroxyl-terminated polybutadiene (HTPB) is a binder often used for solid rocket propellant mixtures. Together with isocyanates it forms a polyurethane elastomers (in short named HTPB-binder), in which the oxidizer (*e.g.* AP) and the fuel (Al) and some other components are held together. HTPB-binders have excellent physical properties; low glass rubber transition temperature, high tensile and tear strength and good chemical resistance. It is physically and chemically compatible with the conventional oxidizers (AP, AN) and other ingredients at normal storage conditions. As it contains mostly carbon and hydrogen, during combustion, it decomposes to give a large volume of stable small molecules like carbon monoxide, carbon dioxide, and water vapor increasing the specific impulse of the rocket motor.

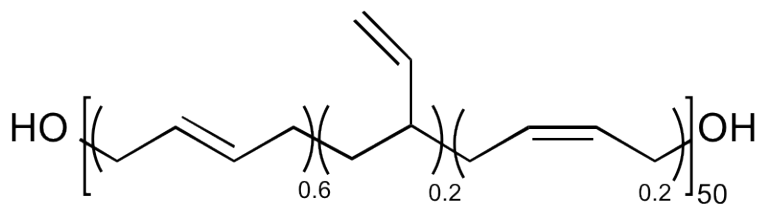


Figure 14.1: Structure of hydroxyl-terminated polybutadiene.

The NPT calculations with HTPB were performed with 3 HTPB molecules in the periodic cubic cell of 2.2 nm edge length at temperatures varying in 10 °C steps from +100 °C to -100 °C. The time period of evolution was 250 ps. The used HTPB simulate differs slightly in the ratio for trans, cis and vinyl double bond given in Figure 14.1. The complete variety of the possible random distributions of the polymer chain is also not included. In spite of this the HTPB simulate was matching well with the density property of a real HTPB.

In Figure 14.2 the arrangement of the three HTPB simulates can be seen in the cubic simulation cell.

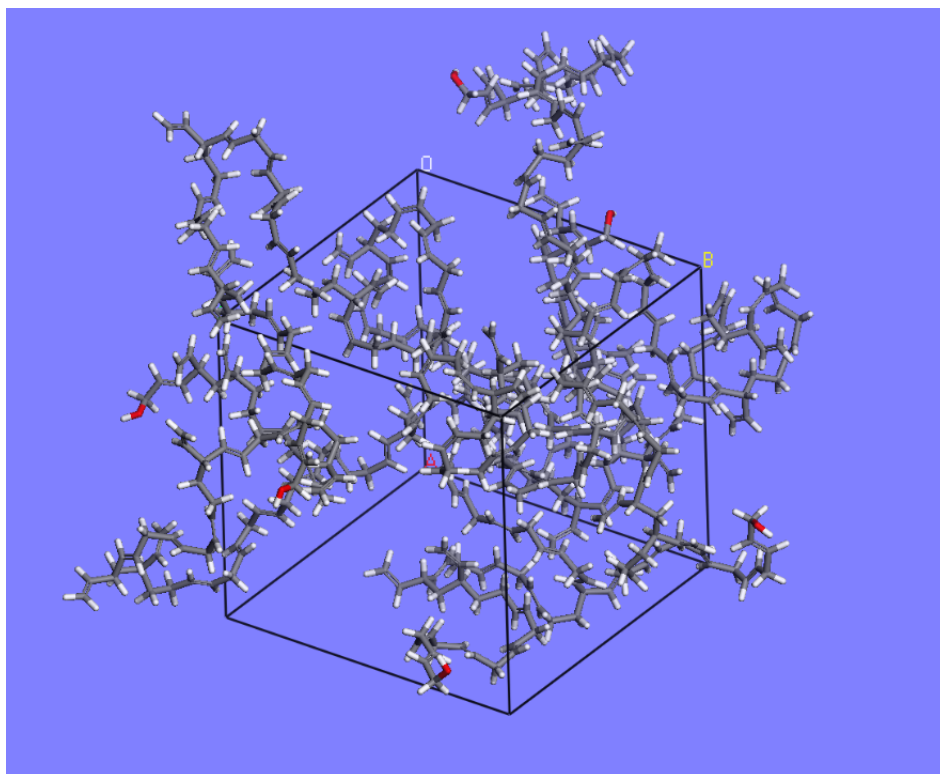


Figure 14.2: Three hydroxyl-terminated polybutadiene (HTPB) molecules in the cubic NPT simulation cell.

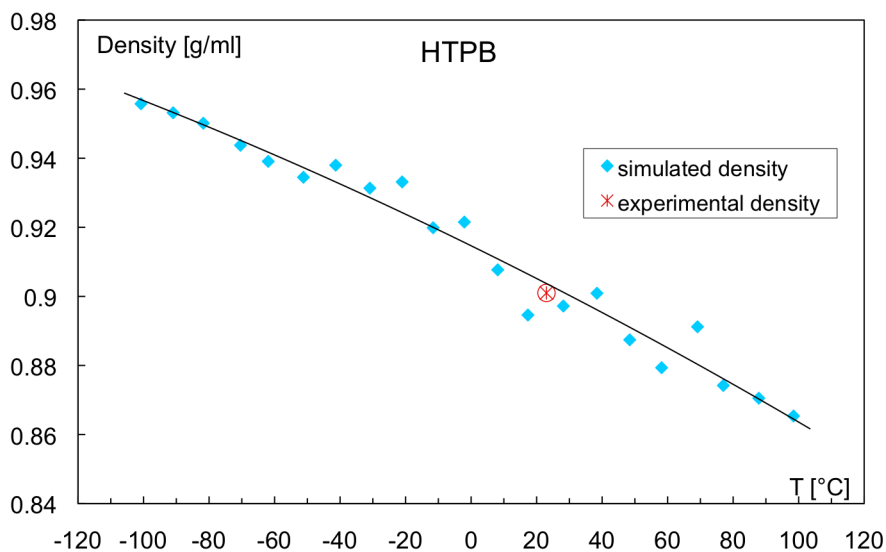


Figure 14.3: Density as function of temperature of the not cured HTPB simulate.

Figure 14.3 shows the results of the density calculations as a function of temperature. The density increases with decreasing temperature as expected and it varies in a curved way from about 0.87 g/cm^3 at $+100 \text{ }^\circ\text{C}$ to 0.96 g/cm^3 at $-100 \text{ }^\circ\text{C}$. A star dot indicates the experimental density, at

+20 °C. The agreement between calculation and experiment is very good.

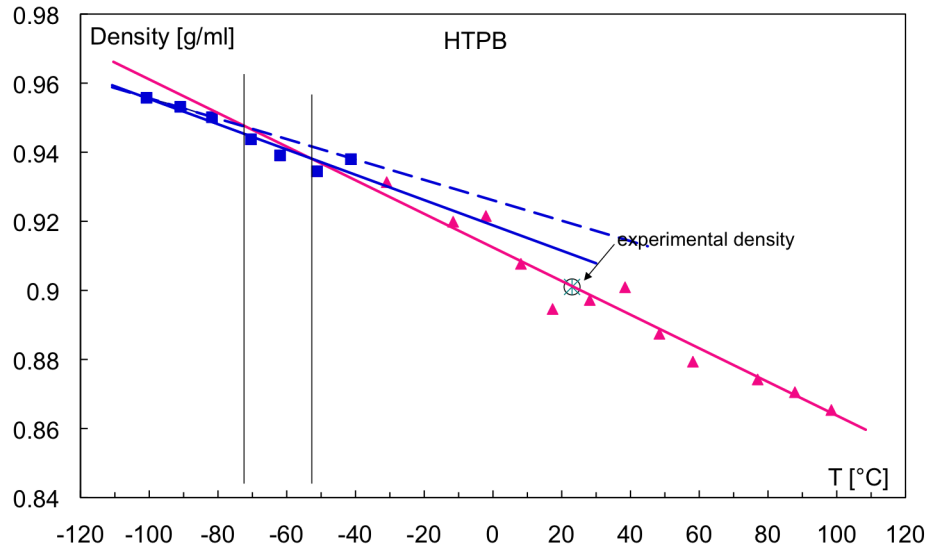


Figure 14.4: Density as function of temperature of the the not cured HTPB simulate, divided in two sections elucidating a transition.

In Figure 14.4 the data were separated into two series. The density as function of temperature for the HTPB shows a transition. At low temperatures the slope of the density line is lower than above the transition region of around $-70\text{ }^{\circ}\text{C}$ to $-50\text{ }^{\circ}\text{C}$. This corresponds with the experimental observations that HTPB and the binder HTPB-IPDI show a complicated glass-to-rubber transition. [2][3][4]

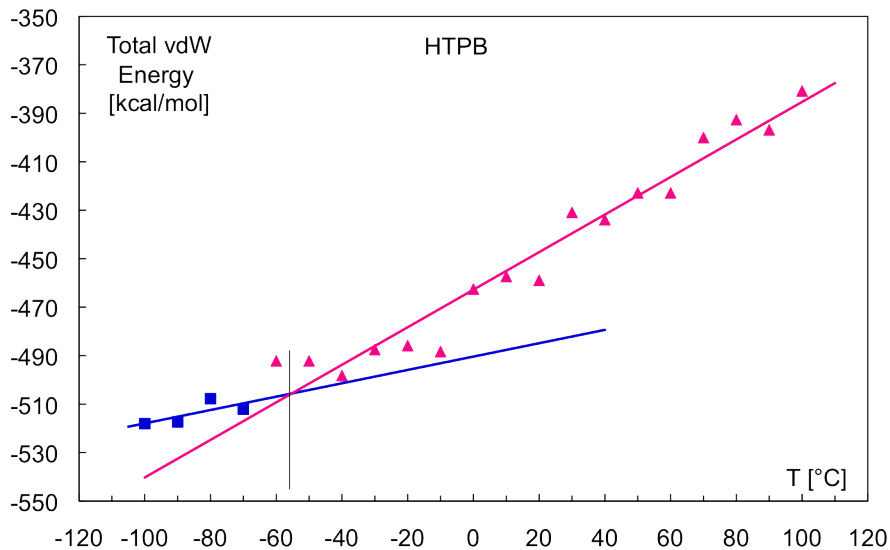


Figure 14.5: Total (intra+inter) van-der-Waals energy as function of temperature for not cured HTPB.

In Figure 14.1 to 14.8, several energy contributions as function of temperature can be seen: the total vdW energy, the inter-molecular vdW energy, the intra-molecular vdW energy and the intra-molecular electrostatic energy, respectively.

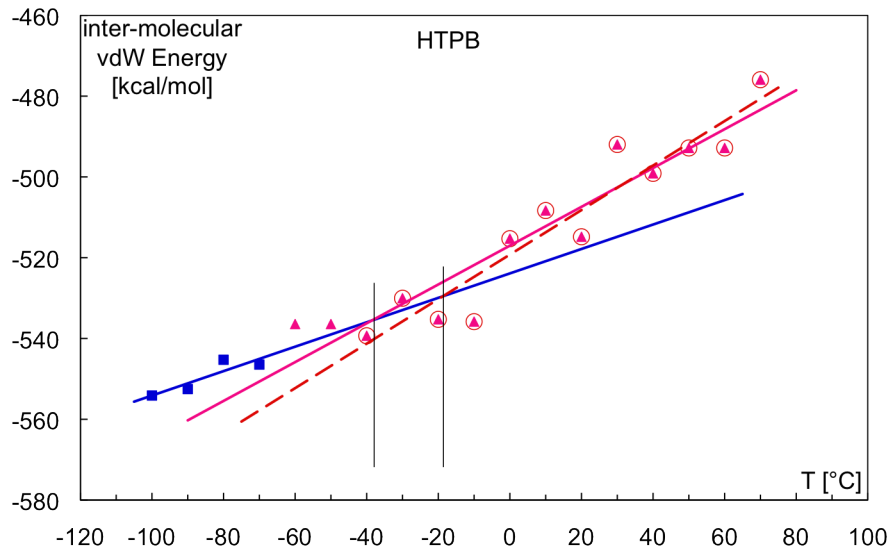


Figure 14.6: Inter-molecular van-der-Waals energy versus temperature for not cured HTPB.

Analyzing the content of these four figures on the behavior of the energetic components with the temperature some difference in the transition temperature regions can be seen. Total vdW and inter-molecular vdW changes their behavior at about $-60\text{ }^{\circ}\text{C}$, whereas the two intra-molecular energies have the change-over at about $20\text{ }^{\circ}\text{C}$ to $30\text{ }^{\circ}\text{C}$ lower temperatures. This can be interpreted as different 'freezing' temperatures for the molecular motions. The intramolecular motions are longer active than the greater chain segment parts probed by the intermolecular interactions.

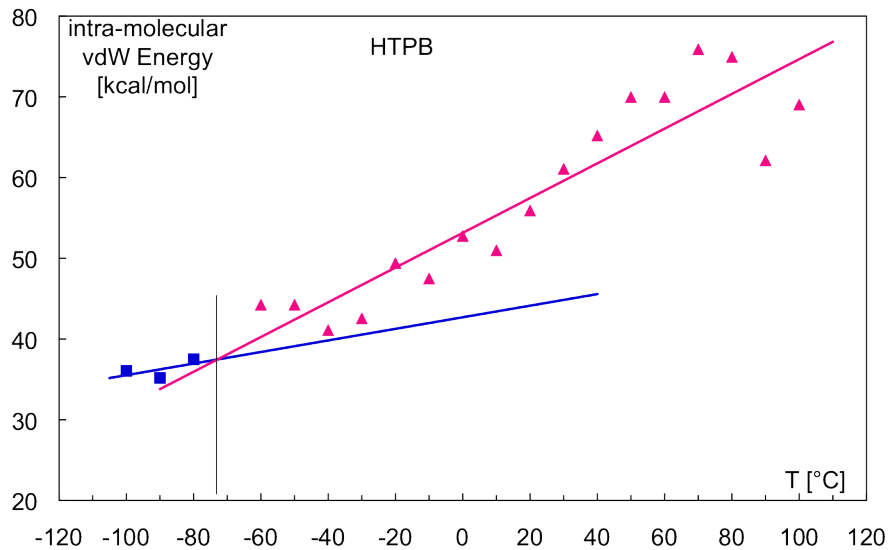


Figure 14.7: Intra-molecular van-der-Waals energy versus temperature for not cured HTPB.

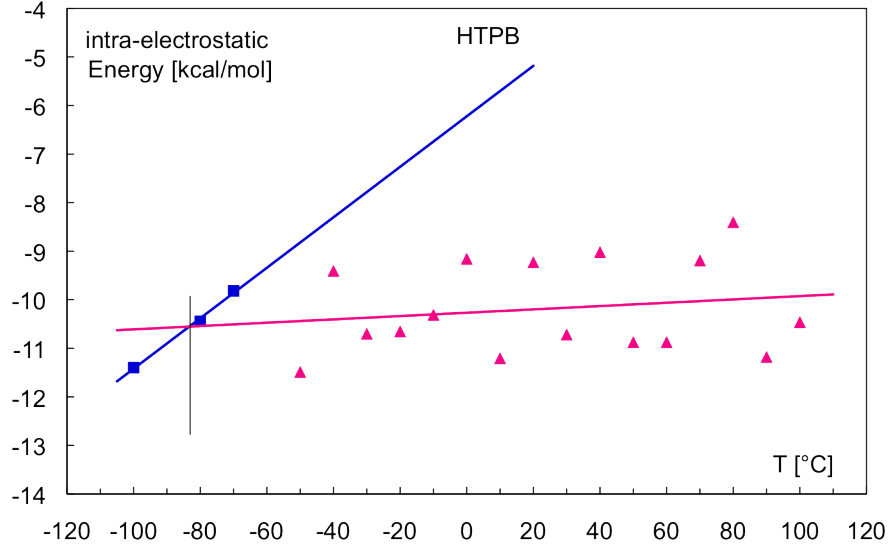


Figure 14.8: Intra-molecular electrostatic energy versus temperature for not cured HTPB.

Also important for a better understanding of the system is the analysis of the cohesive energy density (CED). CED is defined as the amount of energy needed to completely separate the molecules in a system of molecules from each other up to infinite distance between them, which means there is no longer any intermolecular interaction between them. The cohesive energy is calculated according to:

$$E_{coh} = -E_{intermol} = E_{intramol} - E_{total} \quad (14.1)$$

$E_{intermol}$ is the total intermolecular potential energy between all molecules. This quantity is obtained by the difference between the total energy of a system E_{total} and the total intramolecular energy $E_{intramol}$ in the molecules of the system. The CED is then the E_{coh} per unit volume. It corresponds to the molar energy of vaporization at given mass density:

$$\delta = \sqrt{CED} = \sqrt{\frac{E_{coh}}{V}} = \sqrt{\frac{\Delta H_{vap} - RT}{V_m}} = \sqrt{\frac{\Delta U_{vap}}{V_m}} \quad (14.2)$$

where δ is the Hildebrandt solubility parameter.[5] This parameter helps to asses if two components are miscible or not. The calculated CED values can be divided in the contributing parts of vdW interaction and Coulomb interaction. as well for the solubility parameter.

$$CED_{Total} = CED_{vdW} + CED_{Coul} \quad \delta_{Tot}^2 = \delta_{vdW}^2 + \delta_{Coul}^2 \quad (14.3)$$

The values for HTPB simulate are given in the following Table 14.1:

Table 14.1: Cohesive energy density (CED) at 25 °C values for hydroxyl-terminated polybutadiene (HTPB).

$CED_{Tot} [J/cm^3]$	$CED_{vdW} [J/cm^3]$	$CED_{Coul} [J/cm^3]$	$\delta_{Tot} [J/cm^3]^{0.5}$	$\delta_{vdW} [J/cm^3]^{0.5}$	$\delta_{Coul} [J/cm^3]^{0.5}$
282.8	274.2	8.55	16.8	16.6	2.9

Observing the CED values, the main contribution is given from the CED_{vdW} with a value of $274.2 J/cm^3$. The CED_{Coul} contributes only with a little portion ($8.55 J/cm^3$). The same trend is observed for the solubility parameter δ with a major vdW contribution (by $16.6 (J/cm^3)^{0.5}$) and again a little portion of Coulomb ($2.9 (J/cm^3)^{0.5}$). These tendencies are explained concerning the molecular structure of HTPBs, with mainly strong vdW-interaction between the p -electron of the double bonds. For other binders with polar groups these values will change according to the molecular structures.

14.2 Polypropylene glycol

Polypropylene glycol (PPG) or polypropylene oxide (PPO) is a material used in several fields: for lithium-batteries [6], in many formulations of polyurethanes, and also as binder in rocket propellants mixtures. The polymer is liquid at room temperature and its solubility in water decreases rapidly with increasing molar mass.

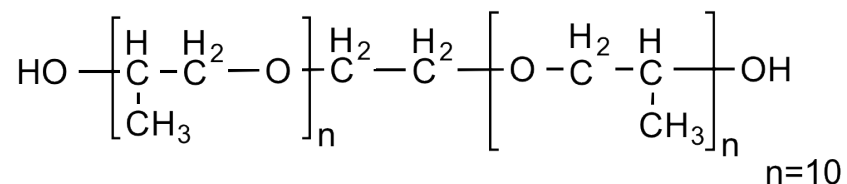


Figure 14.9: Structure of polypropylene oxide.

The hydroxyl terminated binder polypropylene oxide (PPO) is analyzed in the similar way as HTPB. In the cell three units of PPO are presented as shown in Figure 14.10, and about 800 atoms are calculated. For this system the temperature was varied in 10 °C steps from +100 °C to -160 °C for the density, and to -100 °C for the energy evaluations. The time period of evolution was 250 ps.

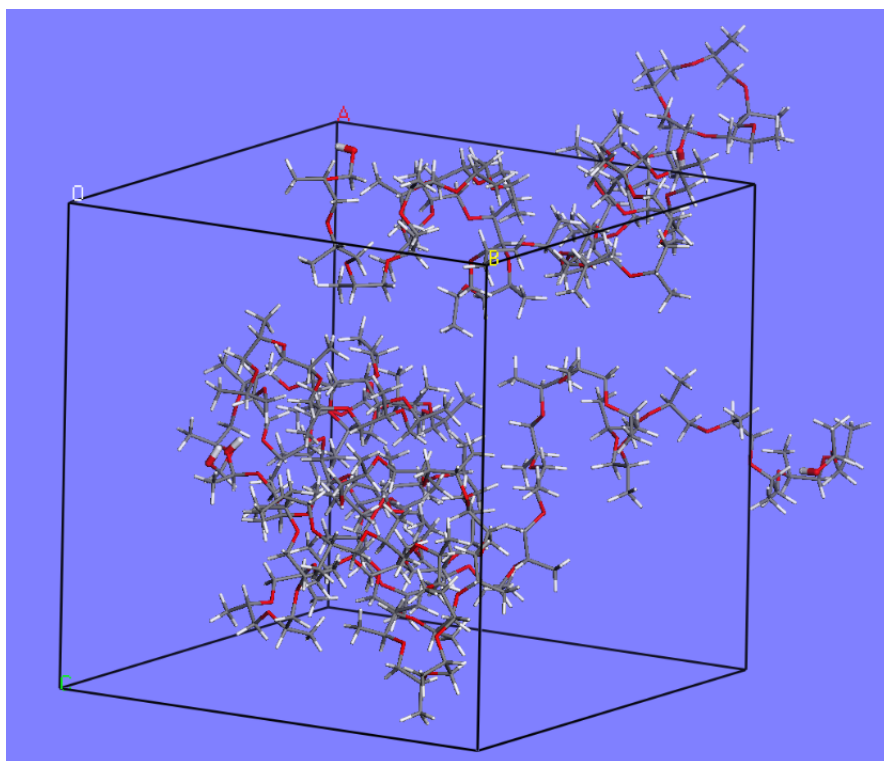


Figure 14.10: Polypropylene oxide with three chains in the cubic simulation cell.

The glass liquid transition temperature for PPO is reported to be at about $-75\text{ }^{\circ}\text{C}$, determined with dipole relaxation spectroscopy.[7] Tengroth *et al.* also obtained a similar value.[8] Because of the method used by Williams [7] probably the small segment rotational motions as the side CH_3 group has been seen. According to other literature sources, also glass liquid transition temperature in the higher range of $-60\text{ }^{\circ}\text{C}$ have been observed.[9]

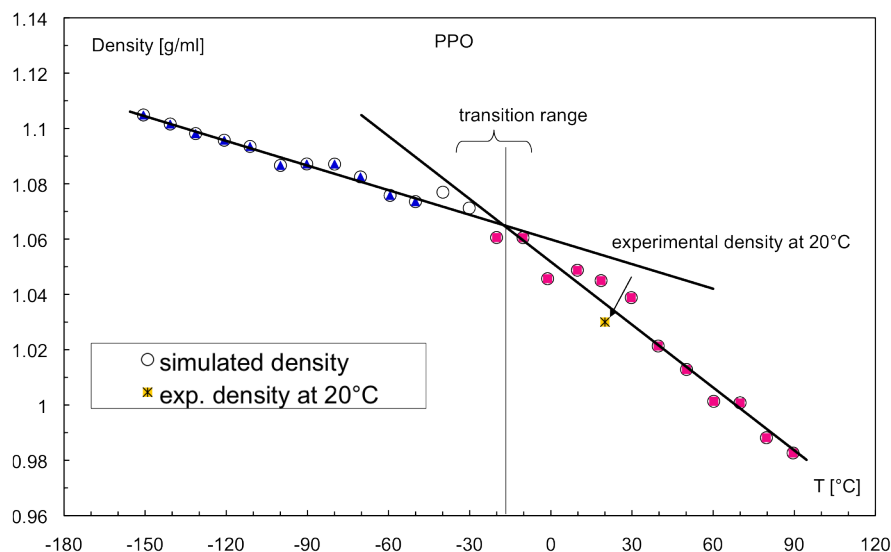


Figure 14.11: Density as function of temperature of polypropylene oxide (PPO).

In Figure 14.11 the results of the density calculations as a function of temperature are shown. The density decreases linear up to $0\text{ }^{\circ}\text{C}$. Between $-10\text{ }^{\circ}\text{C}$ and $-30\text{ }^{\circ}\text{C}$ a transition range occurs, then the density starts a linear decrease again. A reasonable explanation for this phenomena was not found, one supposition is phase change that occurs in the polymer at lower temperatures.

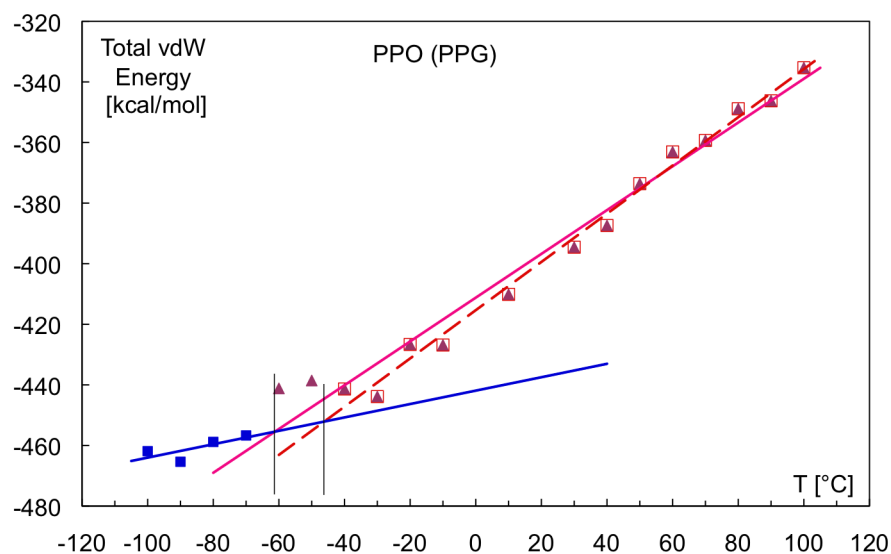


Figure 14.12: Total (intra+inter) van-der-Waals energy as function of temperature for not cured PPO.

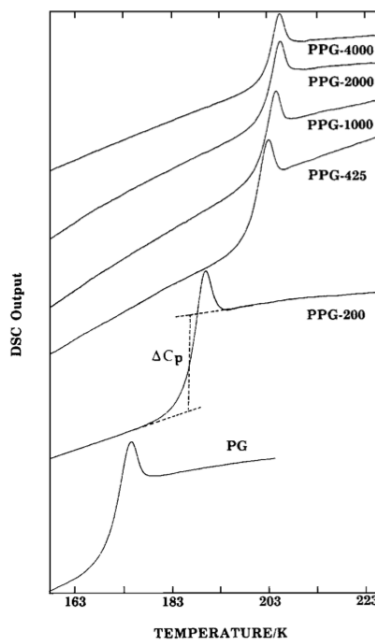


Figure 14.13: DSC scans for PPO (PPG) of various molecular weights.

In Figure 14.13 DSC measurements of PPO are reported.[10] Different PPO molecules were measured, whereas PPG-2000 is comparable with the simulated PPO. PPG-2000 means an oligomer with 2000 g/mol mean molar mass. The T_g from the measurement is -73°C , exactly in the temperature range of the simulated PPO.

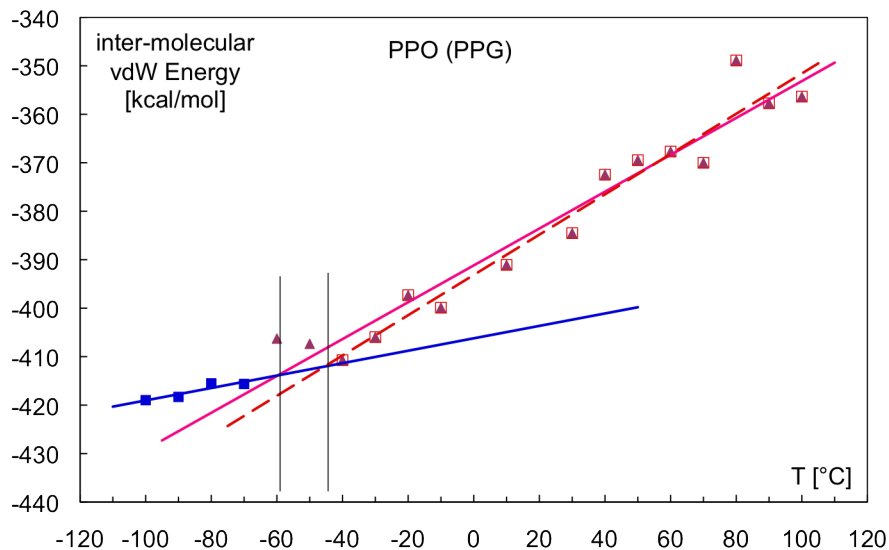


Figure 14.14: Inter-molecular van-der-Waals energy versus temperature for not cured PPO.

The Figures 14.12, 14.14, 14.15, 14.16 and 14.17 show five energy types as function of temperature: the total vdW energy, the inter-molecular vdW energy, the intra-molecular vdW energy, the intra-molecular electrostatic energy and the inter-molecular electrostatic energy, respectively.

The total vdW energy shows a transition range between $-60\text{ }^{\circ}\text{C}$ to $-45\text{ }^{\circ}\text{C}$, also with the inter-molecular and intra-molecular energies. The intra-molecular energies are already negative or more negative in contrast to HTPB, which means a quite different situation in PPO, because of its polar groups. Interesting is the course of the inter-molecular electrostatic energy (see Figure 14.17).

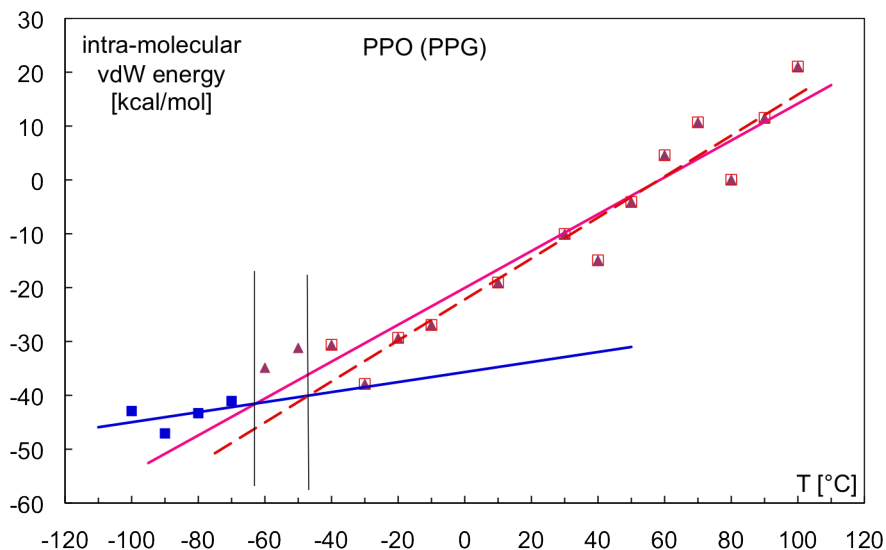


Figure 14.15: Intra-molecular van-der-Waals energy versus temperature for not cured PPO.

The course is in a wider range similar to the one of HTPB, but the values are much higher and even positive, a result of the C-O dipoles in PPO. This means, in PPO are the distances between the dipoles already in such a magnitude that already repulsive forces are acting. A qualitative explanation are the more or less fixed orientations of the two dipoles C-O-C in the main chain. The energy increases first with decreasing temperature because with increasing hindrance of the rotational motions the two dipoles in average get more and more oriented and this increases the energy in such a configuration.[9] At the transition range the tendency to decrease the electrostatic energy is observable. Whereas the molecular motions are considerably reduced and the material must be in the energy-elastic state. The decrease is explainable by the orientation of the dipoles in order to increase the intermolecular interaction more than the intramolecular, which in sum leads to a more favorable energetic state. This behavior is reflected in Figure 14.17 showing the inter-molecular electrostatic energy as function of temperature.

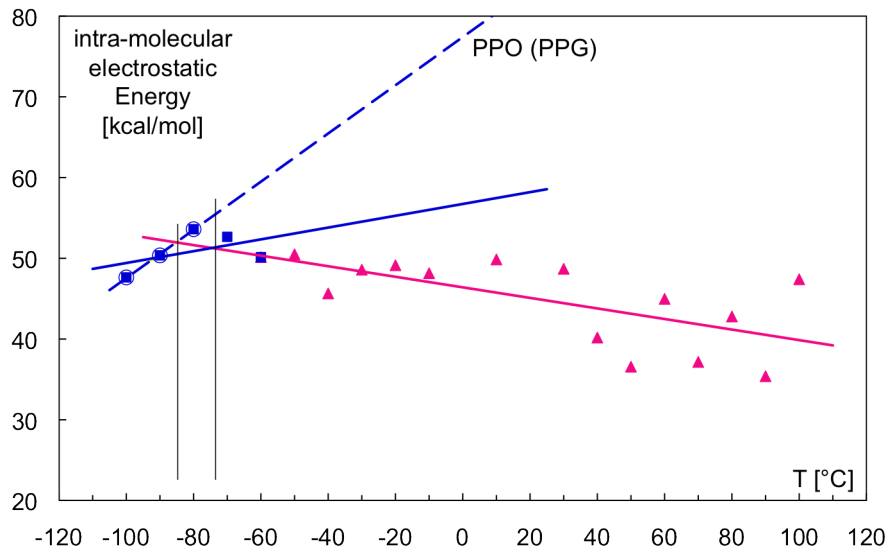


Figure 14.16: Intra-molecular electrostatic energy versus temperature for not cured PPO.

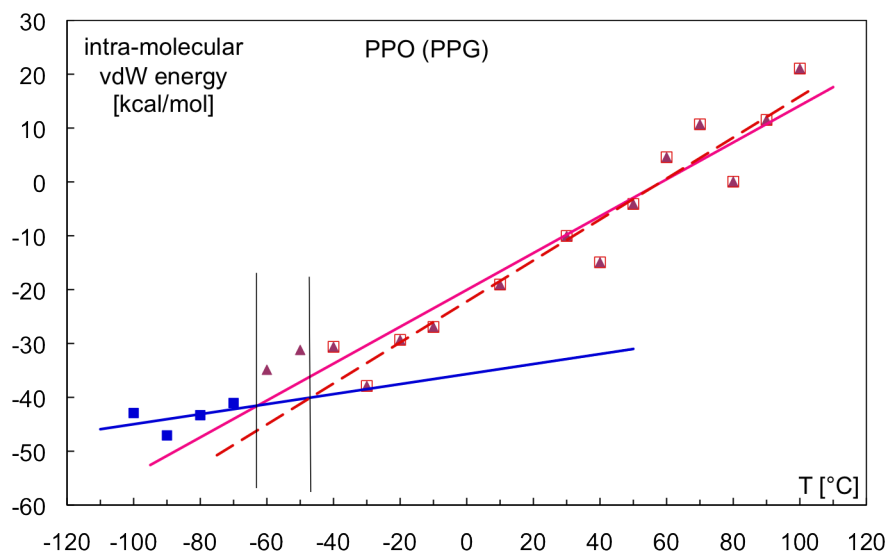


Figure 14.17: Inter-molecular electrostatic energy versus temperature for not cured PPO.

In this case, in contrast to HTPB, the CED_{Coul} is higher with a value of 14.9 J/cm^3 . That results from the C-O dipoles in the central chain. But most of the contribution to CED is still by vdW interaction at room temperature with a value of 237.7 J/cm^3 . For the solubility parameters, the Coulomb contributions are as strong as in the case of HTPB ($2.9 (\text{J/cm}^3)^{0.5}$), a tendency is recognizable with a bigger value of δ_{Coul} ($3.8 (\text{J/cm}^3)^{0.5}$). [11]

Table 14.2: Cohesive energy density (CED) at 25 °C values for polypropylene oxide (PPO).

$CED_{Tot} [J/cm^3]$	$CED_{vdW} [J/cm^3]$	$CED_{Coul} [J/cm^3]$	$\delta_{Tot} [J/cm^3]^{0.5}$	$\delta_{vdW} [J/cm^3]^{0.5}$	$\delta_{Coul} [J/cm^3]^{0.5}$
251.8	237.7	14.9	15.9	15.4	3.8

14.3 DesmophenTM

DesmophenTM D-2200 (Desmo) is a condensation product of adipic acid and diethylene glycol. The compound is used for the production of glues, foam and as binder for solid rocket propellants. It is a polyol and cured with a polyisocyanate to a polyurethane elastomer.

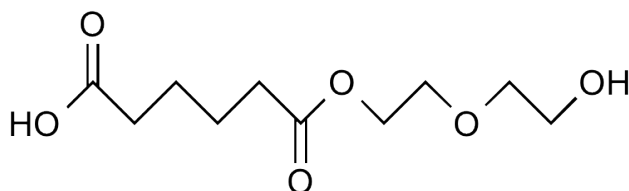


Figure 14.18: Structure of DesmophenTM D-2200.

For the calculation four units were used in simulation cell (see Figure 14.19) with approximately 1000 atoms.

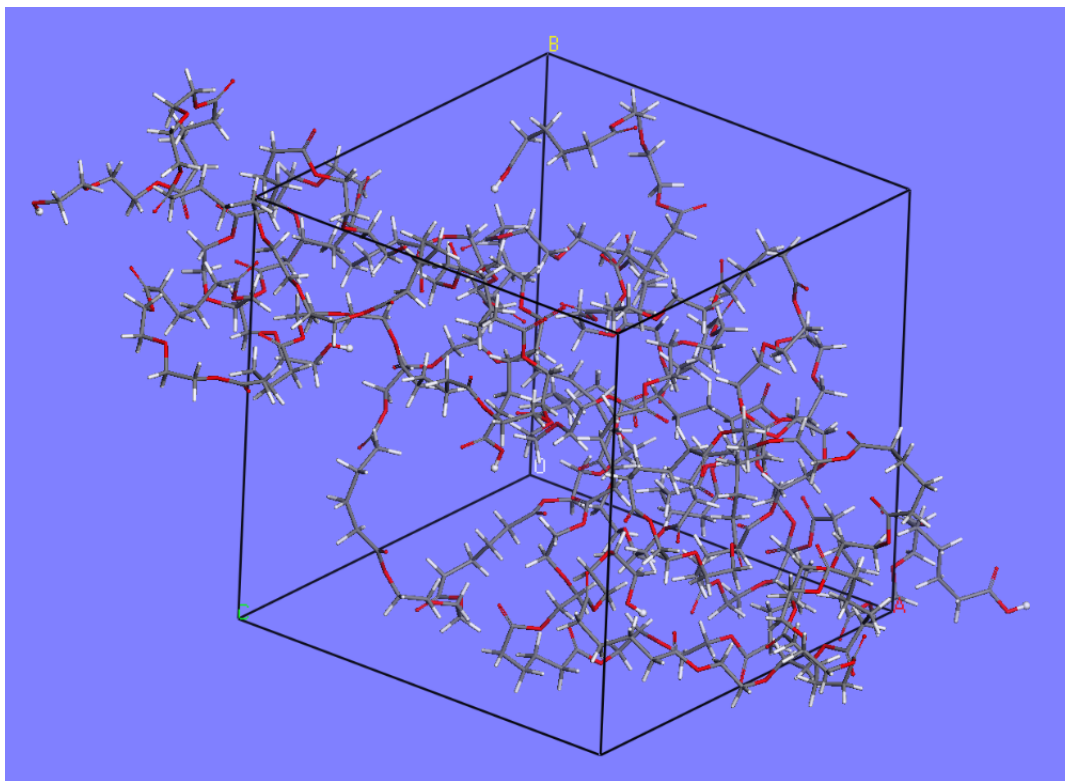


Figure 14.19: Four units of DesmophenTM in the cubic simulation cell.

For this compound only few calculations were performed, because of the time consuming calculation of HTPB and PPO, and also because of the straight-forward comparison with literature values. The first calculation to investigate the density values yields a value of 1.149 g/cm^{-3} . By a comparison with the experimental value of 1.18 g/cm^{-3} , a small deviation was observed.

The second calculation was the CED calculation (see Table 14.3).

Table 14.3: Cohesive energy density (CED) at 25 °C values for DesmophenTM.

$\text{CED}_{Tot}[\text{J/cm}^3]$	$\text{CED}_{vdW}[\text{J/cm}^3]$	$\text{CED}_{Coul}[\text{J/cm}^3]$	$\delta_{Tot}[\text{J/cm}^3]^{0.5}$	$\delta_{vdW}[\text{J/cm}^3]^{0.5}$	$\delta_{Coul}[\text{J/cm}^3]^{0.5}$
373.5	319.5	53.9	19.3	17.9	7.3

DesmophenTM has polar groups of ester and ether, but the vdW part is still the highest. Comparing DesmophenTM and HTPB, the quite low value of CED for HTPB is evident. But this low CED has another interesting consequence: the transition region from energy elastic to entropy elastic state and vice versa (shortly glass-to-rubber transition) is with HTPB PUR pre-polymer exceptional low in the range of -75 °C in comparison to -35 °C with DesmopheneTM, both without plasticizers and determined by DMA (dynamic mechanical analysis) at 0.01 Hz.[3][4]

Chapter 15

Plasticizers

15.1 Dioctyl adipate

Dioctyl adipate (DOA) is used as plasticizer in HTPB-systems. It is a typical, cold-resistant plasticizer for polyvinyl chloride, chloroethylene copolymer, polystyrene, ethyl cellulose and synthetic rubber. Its application is often in combination with main plasticizers such as dioctyl phthalate (DOP), dibutyl phthalate (DBP) etc. for making cold-resistant agricultural plastic thin film, packing membrane for freezing food, cable, coating, leatherette, sheet materials and water pipes in the open air etc. Compounds made with it have low viscosity at the beginning and a good stability of viscosity. DOA is used in solid propellants mixtures.[12]

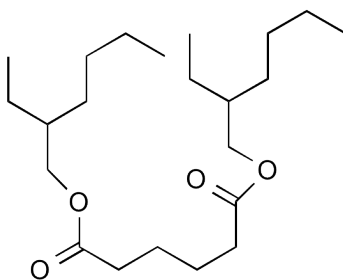


Figure 15.1: Structure of dioctyl adipate (DOA).

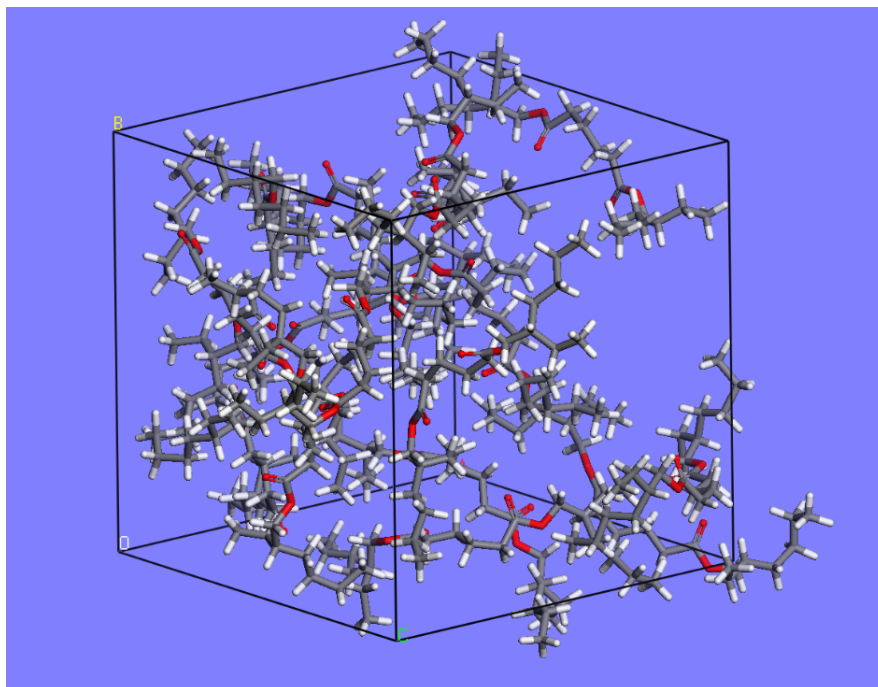


Figure 15.2: Eight molecules of dioctyl adipate (DOA) in the cubic NPT simulation cell.

In the cell eight molecules of DOA are included as shown in Figure 15.2. The density as function of temperature was calculated by molecular dynamics simulation as shown in Figure 15.3. The range was from +100 °C (density of 0.86 g/cm³) to -160 °C (density of 1.01 g/cm³) and the density increases with decreasing temperature as to be expected. The experimental density is indicated by a star dot, at +20 °C. A transition point in density was observed around -50 °C, that can be connected with the freezing point of the compound around -67.8 °C.

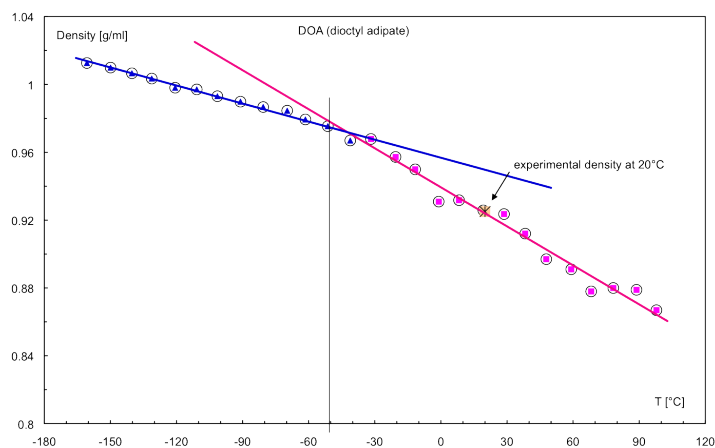


Figure 15.3: Density as function of temperature of the the DOA.

As in the case for the binder HTPB and PPO, different energy contributions in the system were

analyzed. In Figure 15.4, 15.5, 15.6, 15.7 and 15.8 the total vdW, electrostatic and potential energy contributions as functions of temperature are presented. The total vdW energy in Figure 15.4, shows a transition point around -65°C .

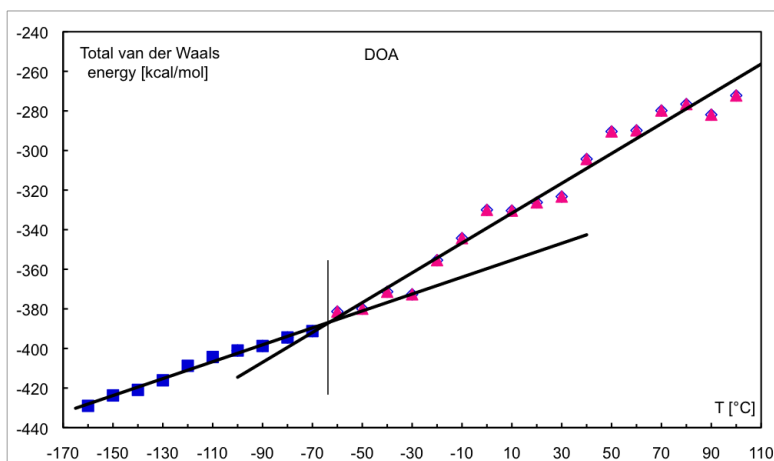


Figure 15.4: Total (intra+inter) van-der-Waals energy as function of temperature for DOA.

For the intra- and inter-molecular vdW components, shown in Figure 15.5 and 15.6, similar trend as for the total vdW energy are observable with transition point around -60°C .

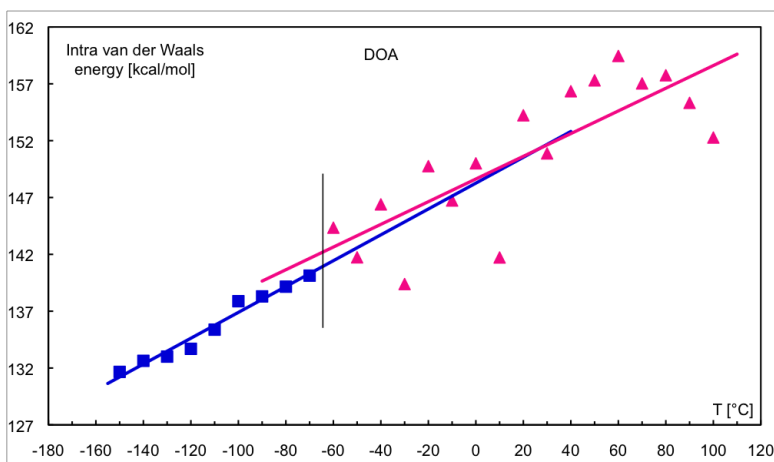


Figure 15.5: Intra-molecular van der Waals energy versus temperature for DOA.

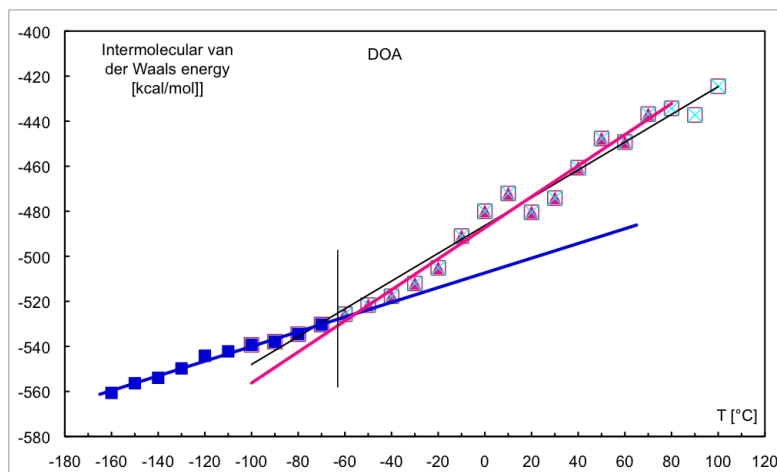


Figure 15.6: Inter-molecular van der Waals energy versus temperature for DOA.

Concerning the potential energies (intra and inter-molecular, in Figure 15.7 and 15.8 respectively), the situation is different. For the intra-molecular potential energy only a linear decrease is found, but for the inter-molecular part a change in slope is recognizable around -50°C .

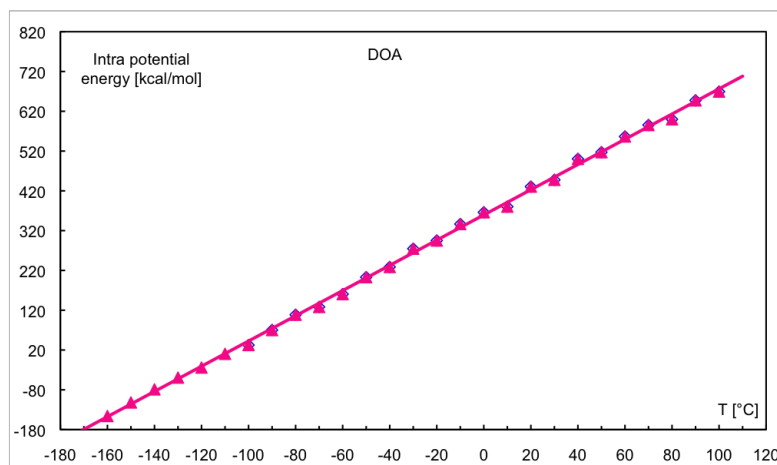


Figure 15.7: Intra-molecular potential energy versus temperature for DOA.

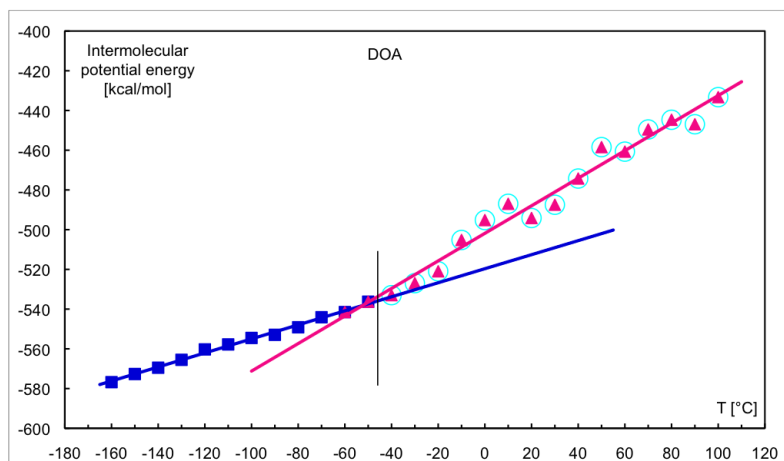


Figure 15.8: Inter-molecular potential energy versus temperature for DOA.

Further investigations were performed with CED calculation and in Table 15.1 the resulting values are shown. Analyzing the absolute contribution in Table 15.1, the CED_{vdW} with a value of 310.3 J/cm^3 shows the main contribution comparing to the CED_{Coul} by a values of 8.6 J/cm^3 . That is not surprising and confirmed the trend as in the Figure 15.4, 15.5 and 15.6 with a distinct influences of the van der Waals forces. The reason is to attribute to the low polar interactions in DOA.

Table 15.1: Cohesive energy density (CED) at 25°C values for dioctyl adipate (DOA).

$CED_{Tot} [\text{J/cm}^3]$	$CED_{vdW} [\text{J/cm}^3]$	$CED_{Coul} [\text{J/cm}^3]$	$\delta_{Tot} [\text{J/cm}^3]^{0.5}$	$\delta_{vdW} [\text{J/cm}^3]^{0.5}$	$\delta_{Coul} [\text{J/cm}^3]^{0.5}$
318.9	310.3	8.6	17.9	17.6	2.9

15.2 1,2,4-Butanetriol trinitrate

1,2,4-Butanetriol trinitrate (BTTN, see Figure 15.9) is an important military energetic plasticizer. It is a colorless to brown explosive liquid. It is less volatile, less sensitive to shock, and more thermally stable than nitroglycerine, for which it is a replacement. BTTN is often used in a mixture with nitroglycerin. BTTN is also used as a plasticizer in some nitrocellulose based propellants.

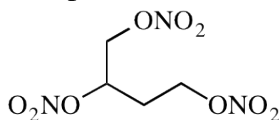


Figure 15.9: Structure of 1,2,4-butanetriol trinitrate (BTTN).

For the calculation 45 molecules of BTTN were used, with a cell containing about 100 atoms, as shown in Figure 15.10.

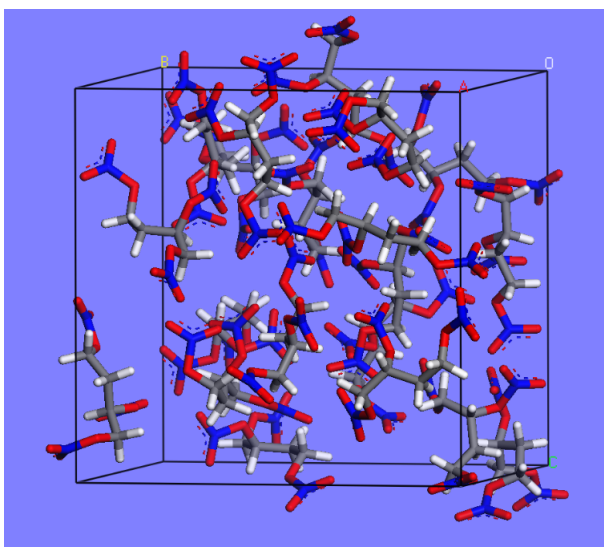


Figure 15.10: 1,2,4-Butanetriol trinitrate (BTTN) in the cubic simulation cell.

For this molecule only few calculations were performed, because DOA was preferred for the simulations. Anyway the density was calculated and a value of 1.56 g/cm^{-3} resulted. The value is slightly different from the experimental one of 1.52 g/cm^{-3} .

Table 15.2: Cohesive energy density (CED) at 25 °C values for 1,2,4-butanetriol trinitrate (BTTN)

$\text{CED}_{\text{Tot}}[\text{J/cm}^3]$	$\text{CED}_{\text{vdW}}[\text{J/cm}^3]$	$\text{CED}_{\text{Coul}}[\text{J/cm}^3]$	$\delta_{\text{Tot}}[\text{J/cm}^3]^{0.5}$	$\delta_{\text{vdW}}[\text{J/cm}^3]^{0.5}$	$\delta_{\text{Coul}}[\text{J/cm}^3]^{0.5}$
709.4	403.1	306.3	26.6	20.1	17.5

The energetic plasticizer BTTN has the highest CED value of all substances investigated here. But nevertheless, at room temperature (25 °C) the vdW-interaction part is still somewhat higher than the polar part.

Chapter 16

Mixtures of Binder Pre-polymers with Plasticizers

16.1 HTPB and DOA Mixture

The first investigated and often used mixture is HTPB and DOA. As shown in the simulation cell in Figure 16.1, two units of HTPB and five molecules of DOA were mixed together, which means 29.7 mass % of DOA is in the mix.

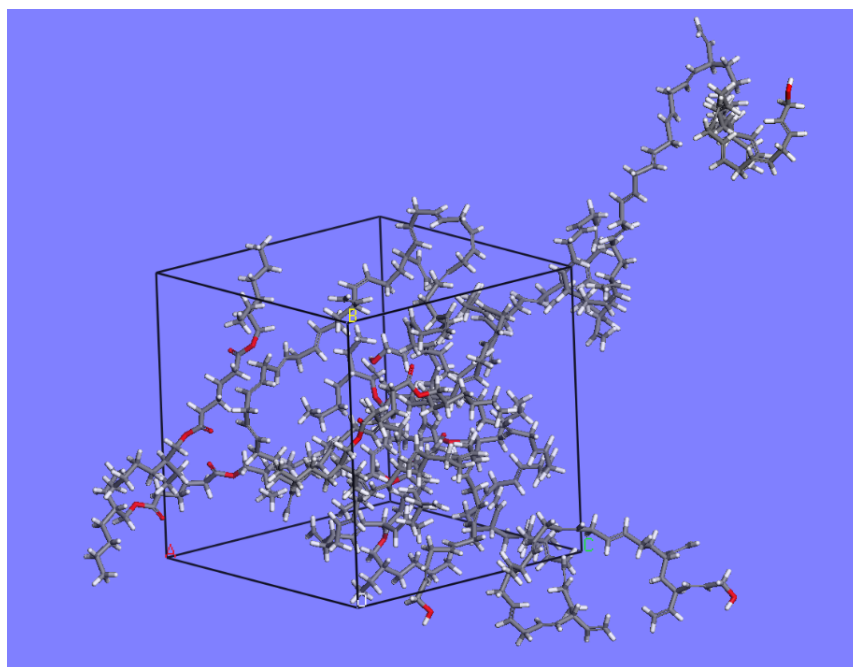


Figure 16.1: Two HTPB units and five DOA molecules in the simulation box.

The first data set of interest for this mixture was the calculation of the density as a function of temperature (see Figure 16.2). The scale was from +160 °C to –160 °C, and the density increases

from 0.84 g/cm^3 with decreasing temperature to 0.98 g/cm^3 . The time period of evolution was 250 ps. The experimental density is indicated in Figure 16.2 and a transition range is observed at -60° where the mixture freezes in mobility.

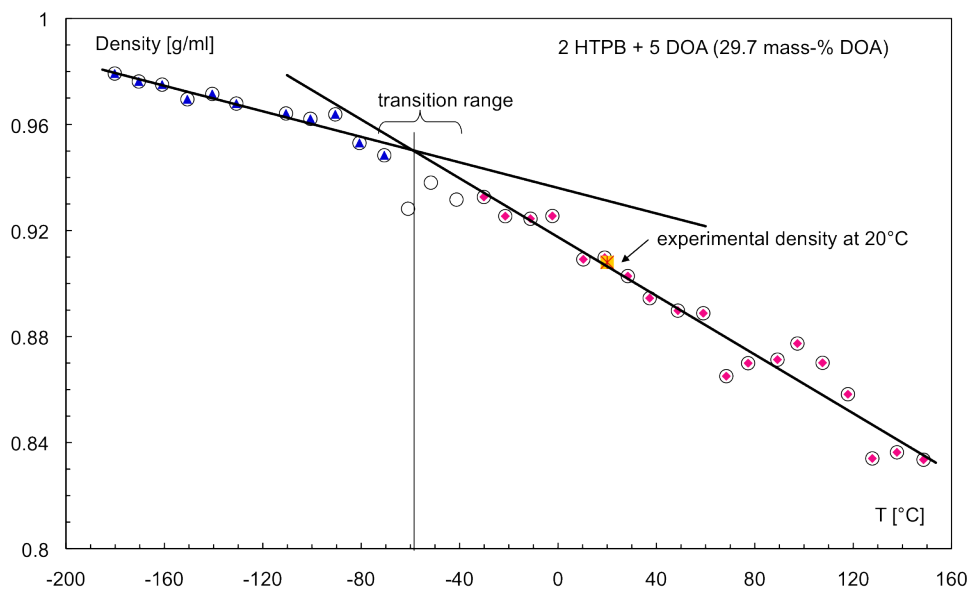


Figure 16.2: Density as function of temperature of HTPB and DOA mixture.

Further investigation, confirm the transition point as shown in Figure 16.3. With the total van der Waals energy a change was observed by -85°C . Analysing the data in Section 14.1 for HTPB and in Section 15.1 for DOA, the transition points for the compound calculated alone appeared around -50°C in both case. As expected, in the mixture of them the transition point is at a lower temperature.

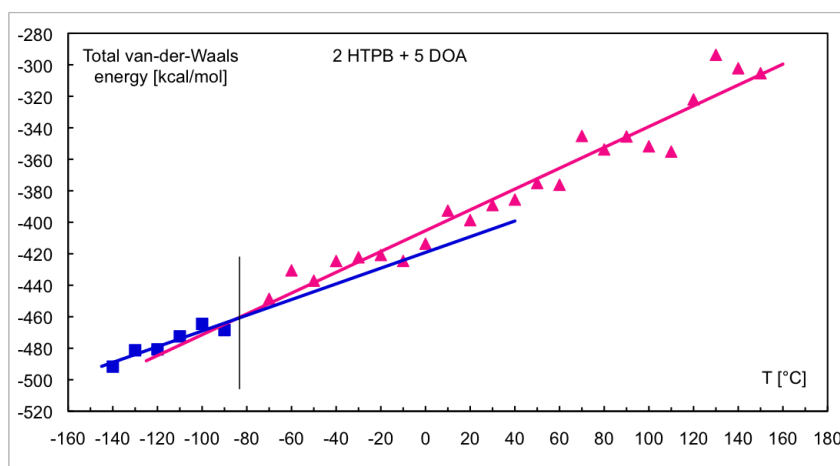


Figure 16.3: Total (intra+inter) van-der-Waals energy as function of temperature for HTPB and DOA mixture.

The intra-molecular potential energy in Figure 16.4 has the same transition range ($-85\text{ }^{\circ}\text{C}$), whereas the intra-molecular vdW energy has a transition at $-95\text{ }^{\circ}\text{C}$ (see Figure 16.5). Some internal movements in the HTPB or in the plasticizer DOA may cause this phenomenon.

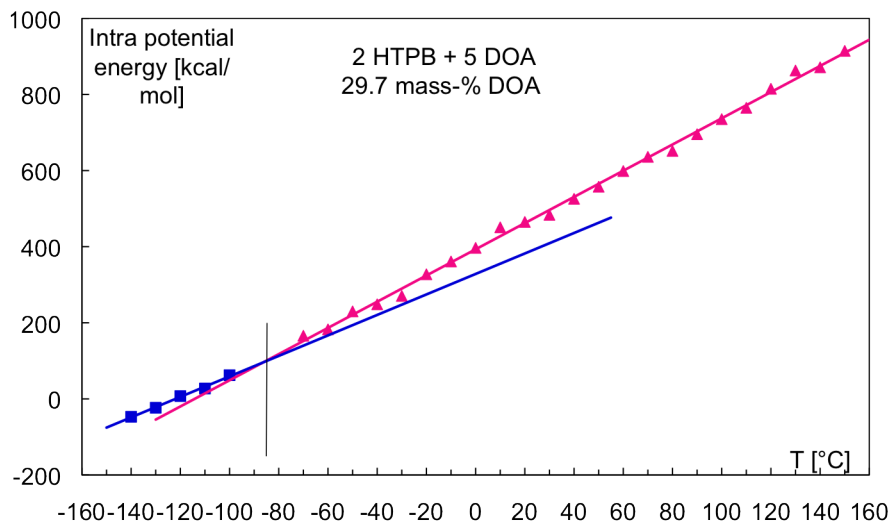


Figure 16.4: Intra-molecular potential energy versus temperature for HTPB and DOA mixture.

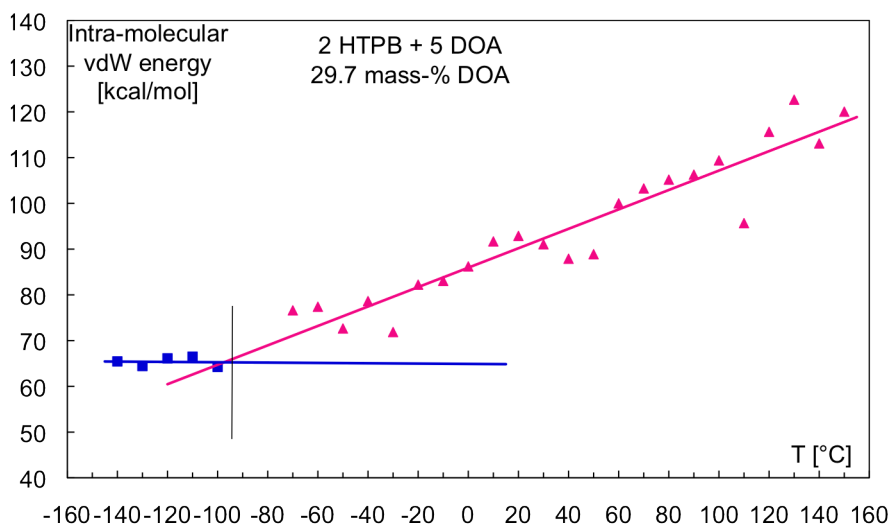


Figure 16.5: Intra-molecular van der Waals energy versus temperature for HTPB and DOA mixture.

The intra-molecular electrostatic energy (see Figure 16.6) should be dominated by DOA. The transition is again in accordance with the others.

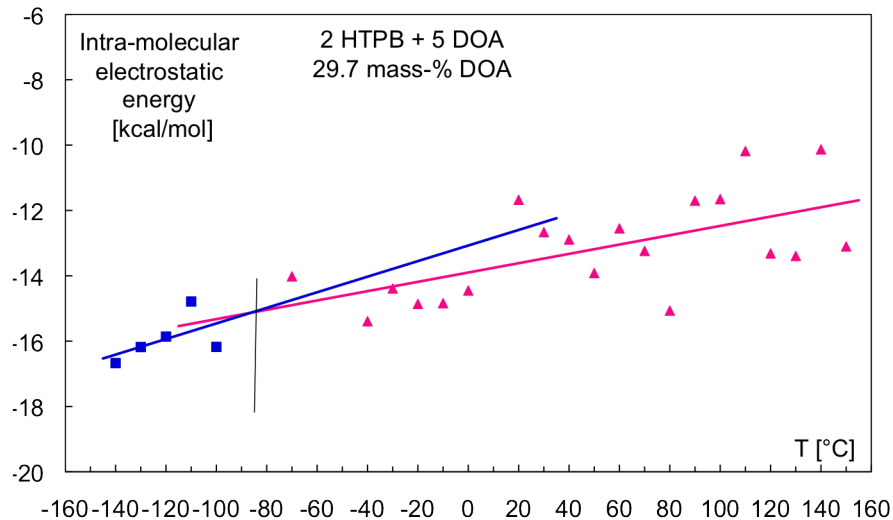


Figure 16.6: Intra-molecular electrostatic energy versus temperature for HTPB and DOA mixture.

In Figure 16.7 the inter-molecular vdW energy as function of temperature can be seen. The transition is at about -80°C to -85°C . This is quite well what is found experimentally for such a mixture.

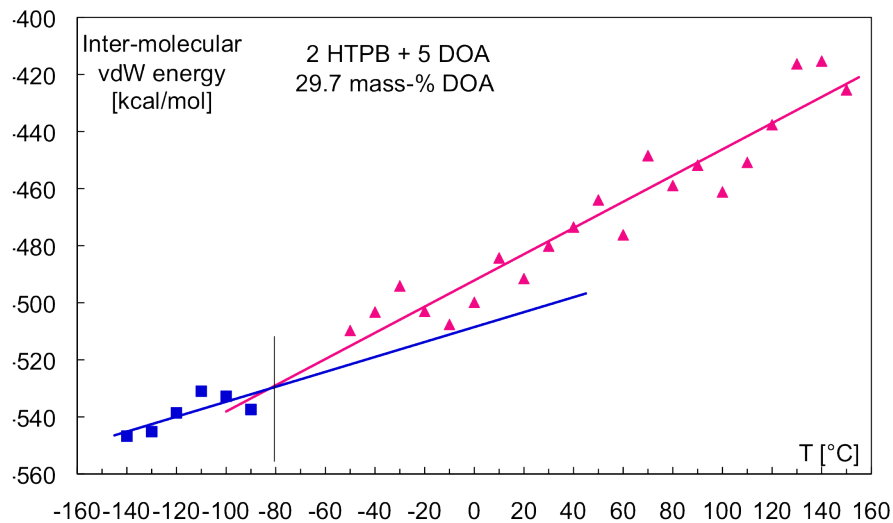


Figure 16.7: Inter-molecular van der Waals energy versus temperature for HTPB and DOA mixture.

Figure 16.8 shows the inter-molecular potential energy with a transition in the same range as the inter-molecular vdW energy. This potential energy is completely dominated by the intermolecular vdW interaction.

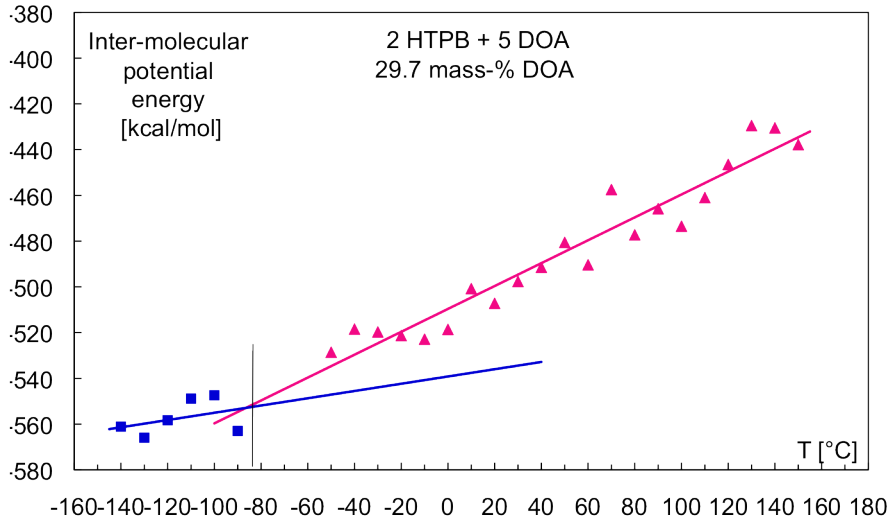


Figure 16.8: Inter-molecular potential energy versus temperature for HTPB and DOA mixture. The calculation of CED (see Table 16.1) show a predominance of the vdW-terms. It is not surprising, considering the low polar character of HTPB and DOA.

Table 16.1: Cohesive energy density (CED) at 25 °C values for HTPB and DOA mixture.

$\mathbf{CED}_{Tot}[\mathbf{J}/\mathbf{cm}^3]$	$\mathbf{CED}_{vdW}[\mathbf{J}/\mathbf{cm}^3]$	$\mathbf{CED}_{Coul}[\mathbf{J}/\mathbf{cm}^3]$	$\mathbf{\delta}_{Tot}[\mathbf{J}/\mathbf{cm}^3]^{0.5}$	$\mathbf{\delta}_{vdW}[\mathbf{J}/\mathbf{cm}^3]^{0.5}$	$\mathbf{\delta}_{Coul}[\mathbf{J}/\mathbf{cm}^3]^{0.5}$
310.50	300.91	9.58	17.62	17.34	3.08

16.2 PPO and DOA Mixture

The second investigated mixture is with PPO and DOA molecules, as show in the simulation cell in Figure 16.9. Two units of PPO and ten molecules of DOA were mixed, which gives a content of DOA of 46.6 mass %. Unfortunately also in this case no experimental values for a comparison were found in literatures.

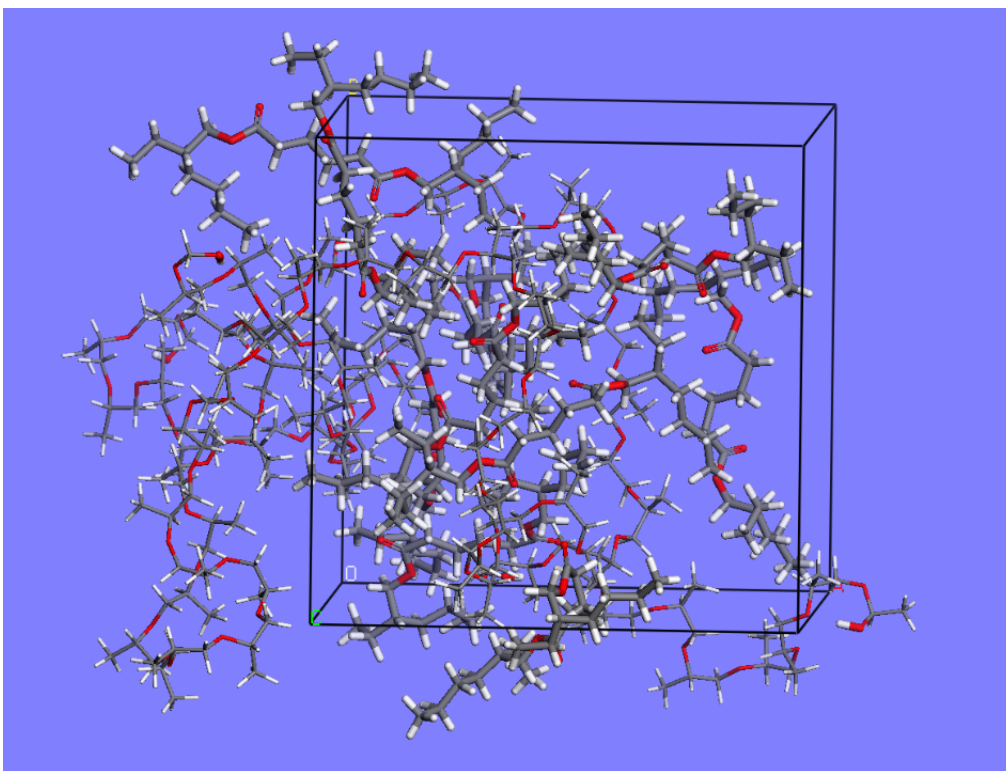


Figure 16.9: Two PPO units and ten DOA molecules in the simulation box.

The density as function of temperature was calculated as shown in Figure 16.10. The range was from +160 °C (density of 0.92 g/cm³) to -160 °C (density of 1.04 g/cm³) and the density increases with decreasing temperature as to be expected. The time period of evolution was 250 ps. The experimental density is indicated by a star dot, at +20 °C is 0.96 g/cm³. A transition point in density was observed around -70 °C, similar as for the mixture HTPB and DOA.

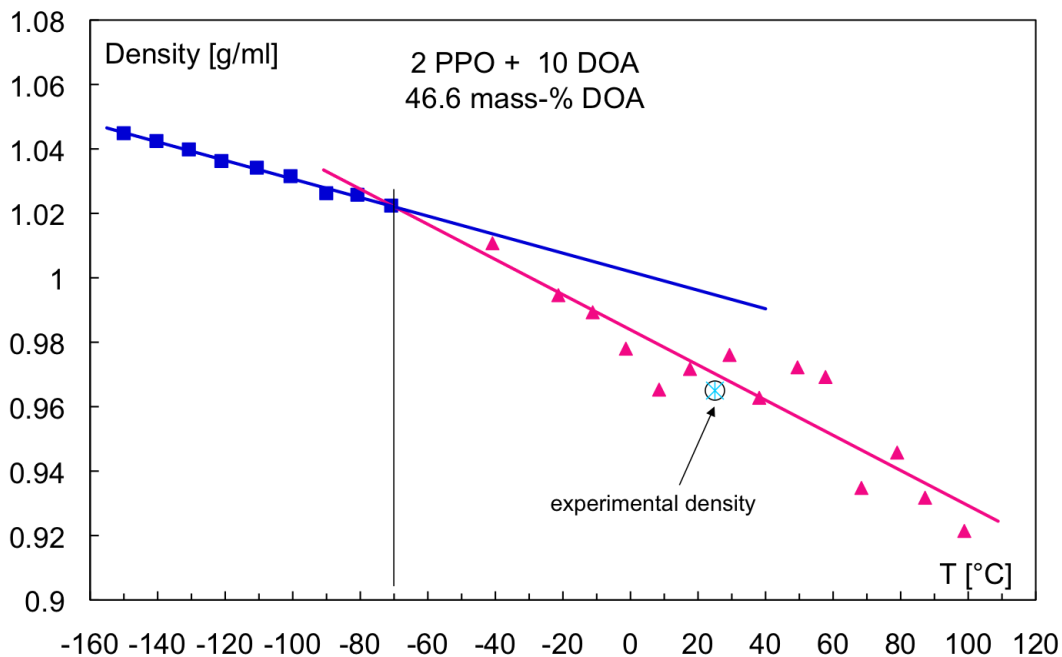


Figure 16.10: Density as function of temperature of the mixture PPO and DOA.

As shown in Figures 16.11 and 16.2, the transition point of the mixture PPO and DOA is in a lower transition range between -70°C and -100°C , compared to the two compounds calculated alone (-50°C for DOA and -60°C for PPO). Also in this case, like for HTPB and DOA mixture, the transition shifts to lower temperature range.

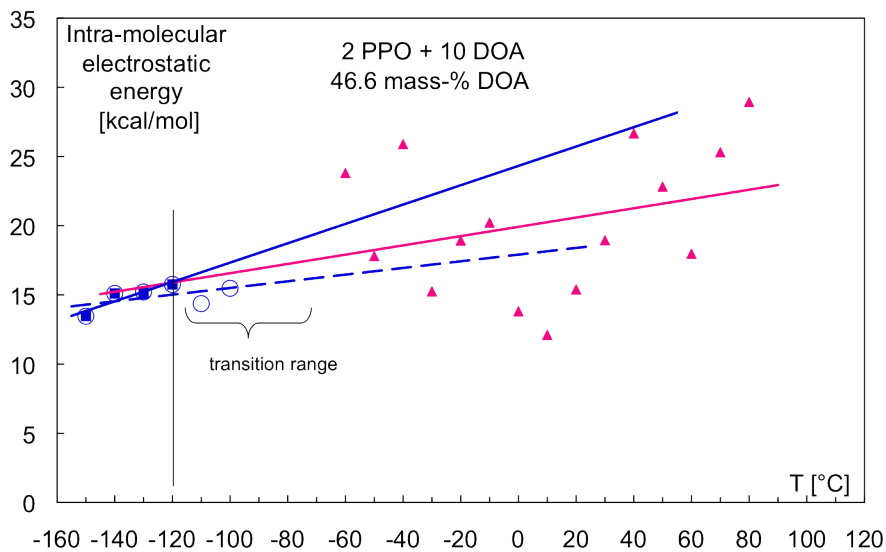


Figure 16.11: Intra-molecular electrostatic energy versus temperature for PPO and DOA mixture.

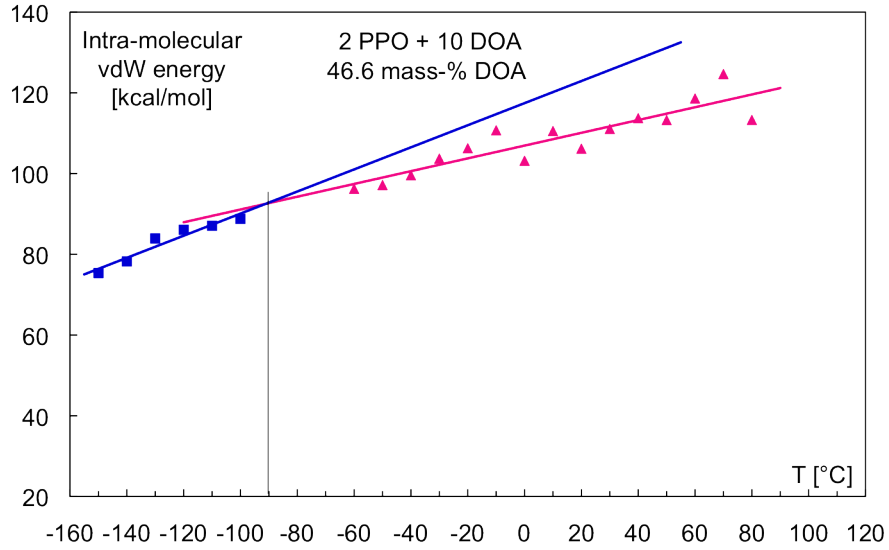


Figure 16.12: Intra-molecular van der Waals energy versus temperature for PPO and DOA mixture.

The evaluation of the inter-molecular electrostatic energy (see Figure 16.13) is quite difficult, because an unexpected quasi-linear behavior of the values is shown.

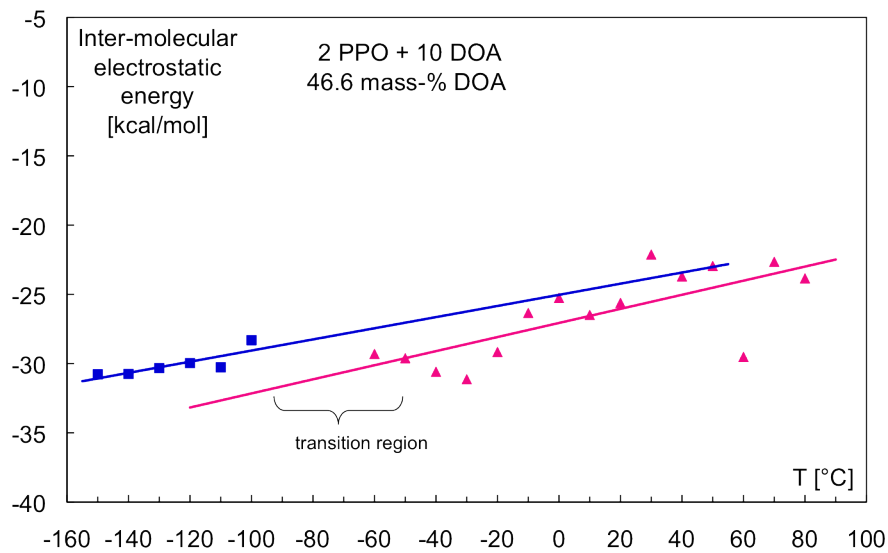


Figure 16.13: Inter-molecular electrostatic energy versus temperature for PPO and DOA mixture.

But in the case of the inter-molecular van der Waals (Figure 16.14) and inter-molecular potential energy (Figure 16.15) a clearly change in slope is recognizable.

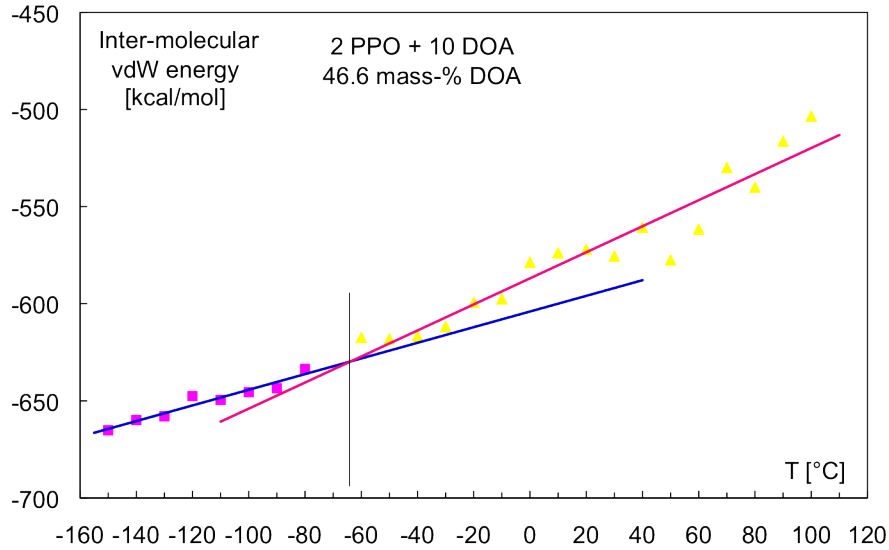


Figure 16.14: Inter-molecular van der Waals energy versus temperature for PPO and DOA mixture.

In both cases a transition region between $-60\text{ }^{\circ}\text{C}$ and $-80\text{ }^{\circ}\text{C}$ is available.

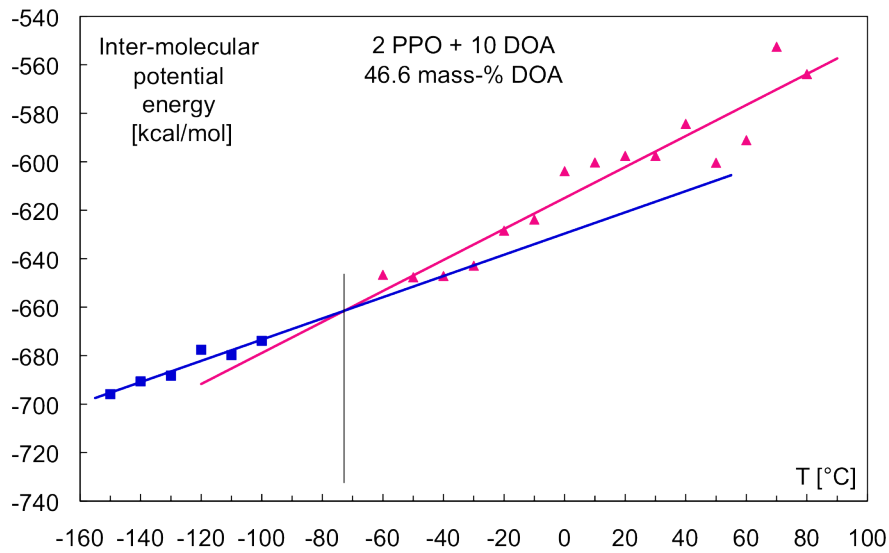


Figure 16.15: Inter-molecular potential energy versus temperature for PPO and DOA mixture.

Comparing the CED values from the mixture PPO/DOA and HTPB/DOA (see ??), the coulomb components (CED_{Coul} and δ_{Coul}) are higher for the PPO/DOA mixture (CED_{Coul} : 9.58 and 13.9 J/cm^3 ; δ_{Coul} : 3.08 and 3.61 J/cm^3 respectively). The reason is the strong polar character of the O-C bond in the PPO unit. Whereas similar values result from the vdW components (CED_{vdW} and δ_{vdW}), probably due to the dioctyl adipate molecules.

Table 16.2: Cohesive energy density (CED) values at 25 °C for PPO and DOA mixture.

$\mathbf{CED}_{Tot}[\text{J}/\text{cm}^3]$	$\mathbf{CED}_{vdW}[\text{J}/\text{cm}^3]$	$\mathbf{CED}_{Coul}[\text{J}/\text{cm}^3]$	$\mathbf{\delta}_{Tot}[\text{J}/\text{cm}^3]^{0.5}$	$\mathbf{\delta}_{vdW}[\text{J}/\text{cm}^3]^{0.5}$	$\mathbf{\delta}_{Coul}[\text{J}/\text{cm}^3]^{0.5}$
305.26	292.17	13.9	17.47	17.09	3.61

16.3 HTPB and BTTN Mixture

The last investigated mixture was HTPB and BTTN. Different mass content for the plasticizer and the binder were investigated as shown in Table 16.3. Figure 16.16 shows the simulation cell for a mixture of medium size (two HTPB and eight BTTN).

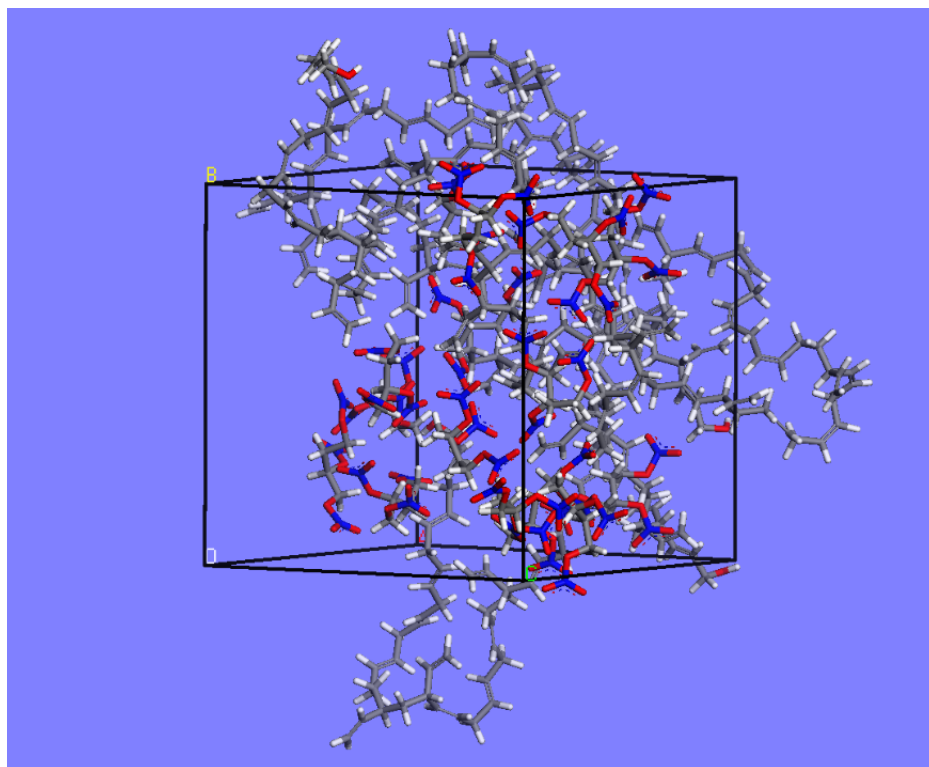


Figure 16.16: Two HTPB units and eight BTTN molecules in the simulation box.

Anyway in the Table 16.3, a couple of performed calculations for this system were compared with experimental values.

Table 16.3: Comparison between experimental density and calculated density obtained with a simulated cell with different content of HTPB and BTTN.

HTPB	BTTN	Mass BTTN [%]	Exp density [g/cm³]	Calc density [g/cm³]
3	5	15.5	0.962	0.960
2	8	30.5	1.029	1.044
2	15	45.2	1.104	1.116

All the values show only a low deviation from the experimental data.

Bibliography

- [1] A. K. Mahanta, D. D. Pathak, *HTPB-Polyurethane: A Versatile Fuel Binder for Composite Solid Propellants*, InTech, Rijeka, Croatia, **2012**.
- [2] S. Cerri, M. A. Bohn, K. Mente, L. Gafetti, *Propell Explos Pyrot* **2010**, 38, 190-198.
- [3] M. A. Bohn, *Energetic Science & Technology in Central Europe*, CALCE EPSC Press, **2012**.
- [4] M. A. Bohn, G. Mußbach, S. Cerri, *Influences on the loss factor of elastomer binders and its modeling*, From International Annual Conference of ICT, 43th, **2012**, 60/1-60/43
- [5] J. H. Hildebrand, J. M. Prausnitz, R. L. Scott, *Regular and Related Solution*, van Nostrand, New York, **1970**.
- [6] S. Wang, S. Hou, P. Kuo, H. Teng, *Appl. Mat. Inter.* **2013**, 17, 8477-8485.
- [7] G. Williams, *Trans. Faraday Soc.* **1965**, 61, 1564-1577.
- [8] C. Tengroth, D. Engberg, G. Wahnstrom, L. Borjesson, P. Carlsson, P. Ahlstrom, W. S. Howells, *Soft Mater.* **2005**, 3, 1-20.
- [9] M. J. O' Sickey, *Characterization of structure property relationship of poly(urethane-urea)s for fiber applications*, Dissertation, Virginia, U.S.A, **2002**.
- [10] G. P. Johari, A. Hallbrucker, E. Mayer, *J. Polym. Scie. Part B* **1988**, 26, 1923-1930.
- [11] M. A. Bohn, C. Evangelisti, T. M. Klapötke, *Atomistic simulation of temperature dependence of density and van-der-Waals interactions of binders, plasticizers and mixture of them*, International Annual Conference of ICT, 45th (Energetic Materials: Particles, Processing, Applications), 1-7, **2014**.
- [12] A. I. Atwood, K. P. Ford, C. J. Wheeler, *Progress in Propulsion Physics* **2013**, 4, 3-14.

Chapter 17

Molecular Dynamic Simulations of the Interactions between with HTPB and the Organic Oxidizers TNC-NO₂ and TNE-NAP-NC

It is of interest to investigate, for composite rocket propellants mixture, the interaction between an elastomeric matrix, a solid crystalline oxidizers a metallic fuel as Aluminum. In this chapter two oxidizers were examined. One oxidizer, the 2,2,2-trinitroethyl nitrocarbamate (TNC-NO₂), was already characterized in this work using bomb calorimetric measurements (see section 9.1) and the other is 2,2,2-trinitroethyl(2-nitro-2-azapropyl) nitrocarbamate (TNE-NAP-NC) (see Figure 17.1). These two compounds were synthesized in the research group of Prof. Klapötke and fully characterized. [1] [2] They were chosen here to investigate them because of the promising properties: green oxidizer, good performance and temperature stability. At first the interaction with HTPB is investigated.

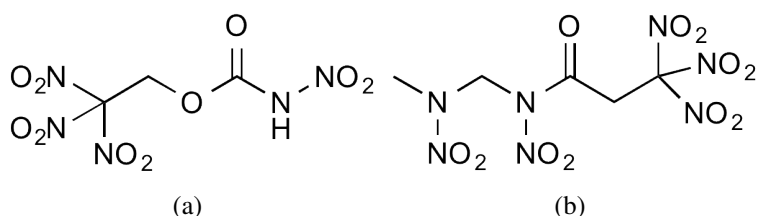


Figure 17.1: 2,2,2-trinitroethyl nitrocarbamate (TNC-NO₂)(a) and 2,2,2-trinitroethyl(2-nitro-2-azapropyl)nitrocarbamate (TNE-NAP-NC)(b).

For the simulations, starting from the crystallographic file, four Miller index surfaces for TNC-NO₂ and three for TNE-NAP-NC respectively, were taken per compound. The used surfaces are shown in Figure 17.2 and 17.3. The other surfaces, which appear, are the symmetric equivalent.

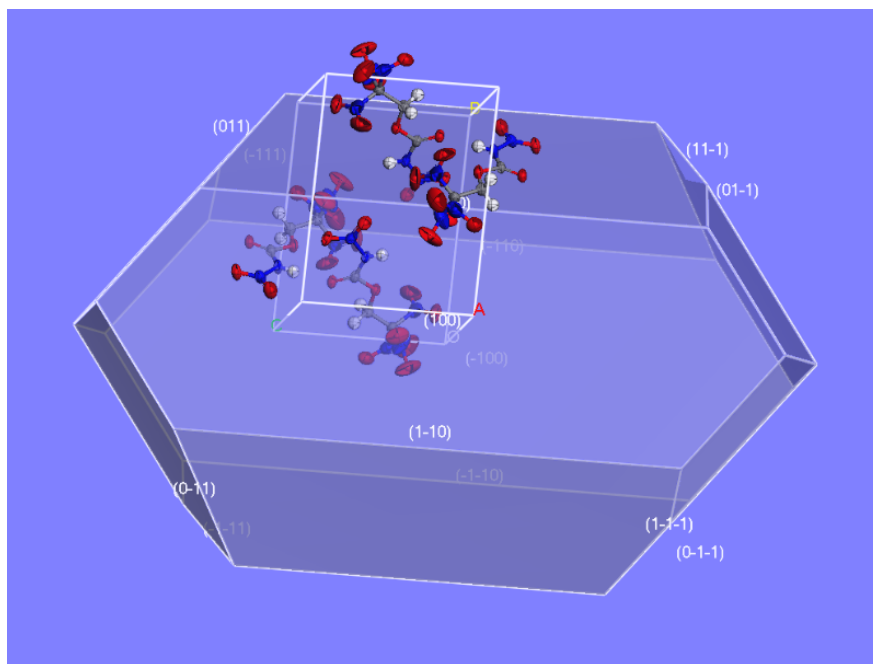


Figure 17.2: Crystal shape of 2,2,2-trinitroethyl nitrocarbamate (TNC-NO₂) with Miller index surfaces.

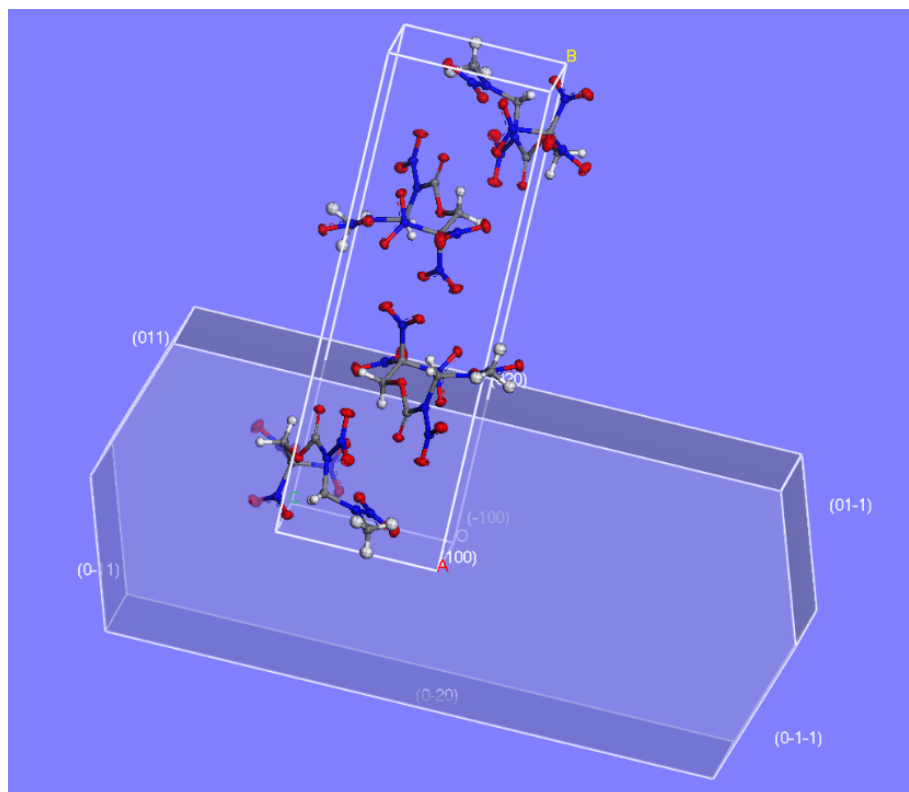


Figure 17.3: Crystal shape of 2,2,2-trinitroethyl(2-nitro-2-azapropyl)nitrocarbamate (TNE-NAP-NC) with Miller index surfaces.

Four different periodic simulation cells, each per Miller index, were built for TNC-NO₂ and analogously three periodic cells for TNE-NAP-NC. In Table 17.1 the cell dimensions for the TNC-NO₂ surface are listed. A vacuum slab along the c-axis, above the crystal packing of the oxidizers surface as shown in Figure 17.4 (a), was prepared and in a second step six units of HTPB were inserted (see Figure 17.4 (b)).

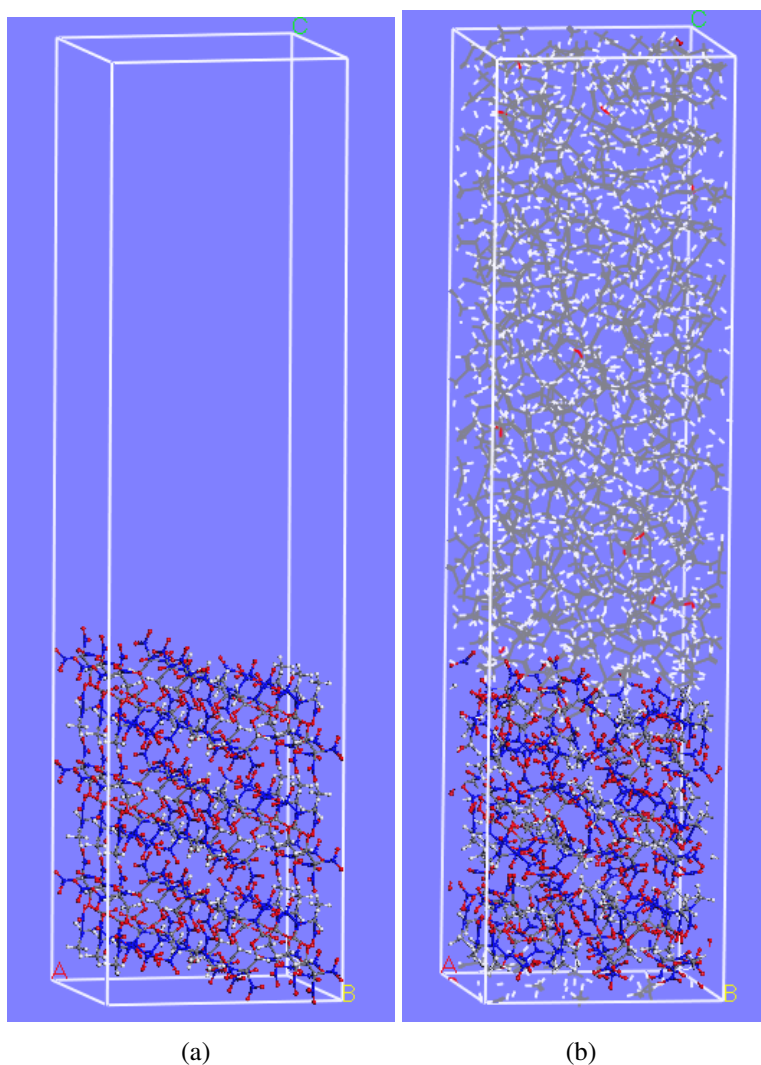


Figure 17.4: 2,2,2-trinitroethyl(2-nitro-2-azapropyl)nitrocarbamate (TNE-NAP-NC) crystal surface with Miller index (100), with vacuum (a) and with six HTPB units (b) in the simulation cells.

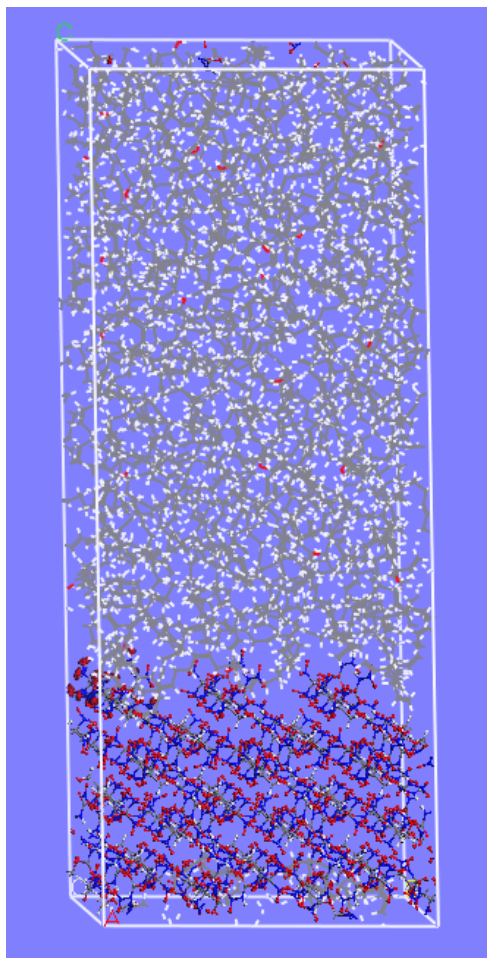


Figure 17.5: 2,2,2-trinitroethyl nitrocarbamate (TNC-NO₂) with the Miller index surface (11-1) and filled above with six HTPB units in the simulation cell.

All the systems were geometry optimized. Then NVT dynamic simulations [3], 250 ps long, were performed at +25 °C, −30 °C and −100 °C for each surface. In Figure 17.6 and 17.7 the four surface structures of the TNC-NO₂ are represented.

Table 17.1: List of the surfaces and simulation cell dimensions used with 2,2,2-trinitroethyl nitrocarbamate (TNC-NO₂).

Surface	Lenght a [Å]	Lenght b [Å]	Lenght c [Å]
011	32.3520	28.9457	79.2996
110	26.2551	31.5700	82.1523
100	34.5810	35.0068	79.5203
11-1	28.9457	34.7186	88.2118

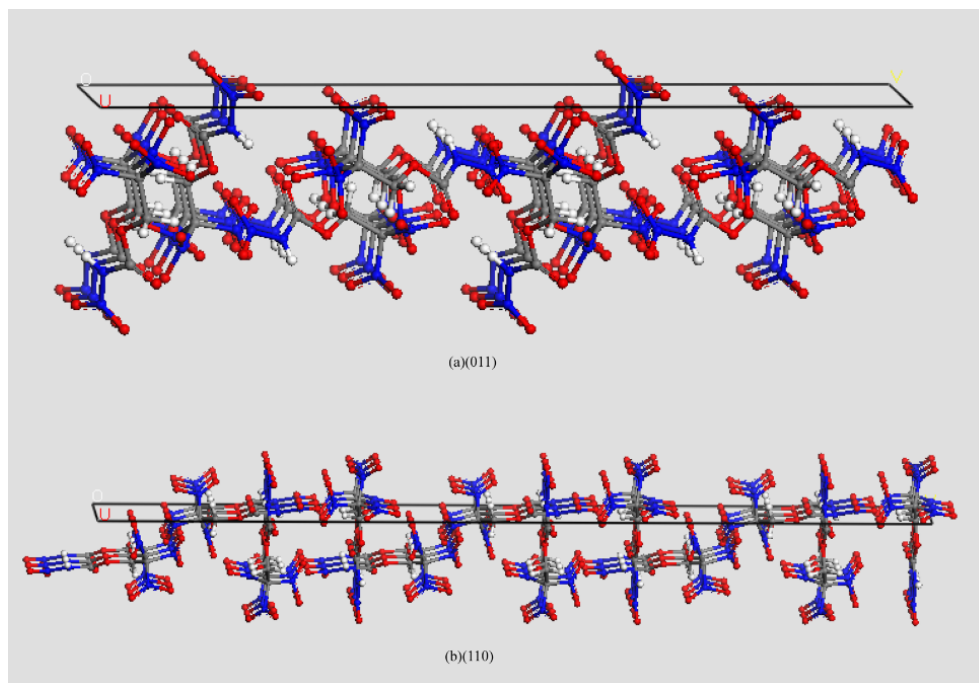


Figure 17.6: 2,2,2-trinitroethyl nitrocarbamate (TNC-NO₂) with the Miller index surface: (011)(a); (110)(b).

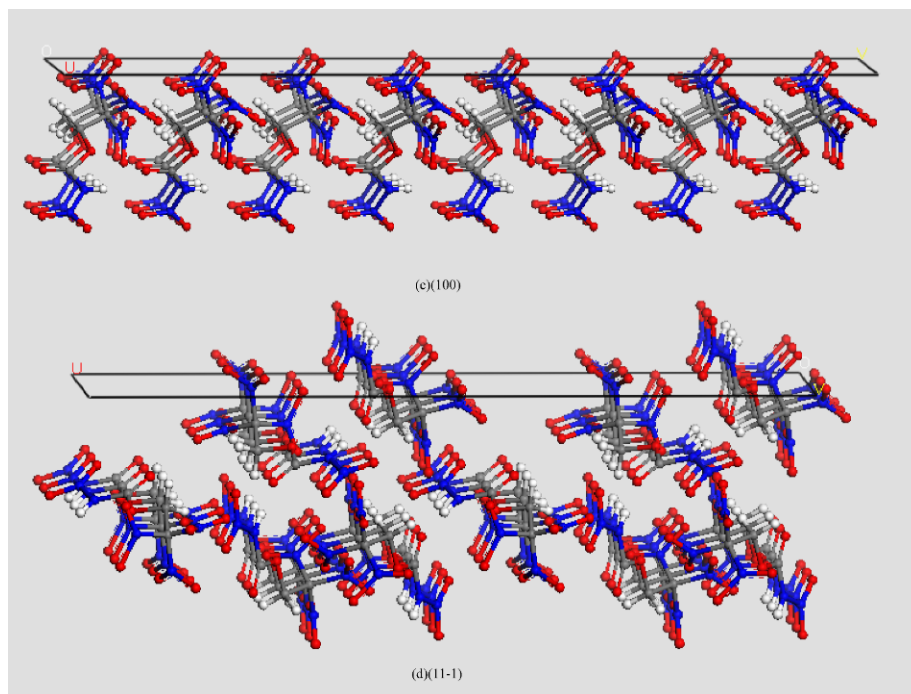


Figure 17.7: 2,2,2-trinitroethyl nitrocarbamate (TNC-NO₂) with the Miller index surface: (100)(c); (11-1)(d).

In Tables 17.2 the results for potential (E_{pot}), vdW (E_{vdW}) and electrostatic (E_{Coul}) energies of TNC-NO₂, at three different temperature are summarized. For the evaluation the last 150 ps of the MD runs were taken and the values averaged. The values listed are calculated by the subtracting from the energy of the complete system, the energy contributions HTPB and from the oxidizer. From the simulations the energy values per mol simulation cells are obtained. To get the energy values for the surface interaction, the values obtained from the subtraction method are divided by the avogadro number and by the geometric surfaces considered in the simulation cells. This methods was used for all the three presented energies (E_{pot} , E_{vdW} and E_{Coul}).

Table 17.2: Energy values at +25 °C, −30 °C and −100 °C for the four chosen surfaces of 2,2,2-trinitroethyl nitrocarbamate (TNC-NO₂).

Surface and temperatures	E_{pot} [J/m ²]	E_{vdW} [J/m ²]	E_{Coul} [J/m ²]
+25 °C			
011	−0.0532	−0.0651	−0.0133
110	−0.1777	−0.07649	−0.0819
100	−0.1078	−0.0976	−0.0102
11-1	−0.2224	−0.0897	−0.1227
−30 °C			
011	−0.0935	−0.0642	−0.0665
110	−0.1344	−0.0616	−0.0265
100	−0.1103	−0.1034	−0.0023
11-1	−0.1266	−0.0884	−0.0598
−100 °C			
011	−0.1312	−0.0582	−0.0702
110	−0.1038	−0.0714	−0.0215
100	−0.1564	−0.0960	−0.0141
11-1	−0.1133	−0.0917	−0.0147

The most negative values of the potential energies E_{pot} for (11-1) and (110) surfaces were obtained at +25 °C. Especially the surface (11-1) shows the most negative value with −0.2224 J/m², that results from a strong interaction between the surface group of the TNC-NO₂ and HTPB. The (11-1) surface in Figure 17.7 shows additionally to the NO₂-group, also the NH-group and the CH₂ at the surface. This characteristic appears only for this surface, for (100) the three NO₂-moieties and the NO₂/NH-groups alternated are pointed out to the surface. The surface (011) three NO₂-moiety are alternated with the other NO₂-end-group. Finally for (110) surface, the entire groups of the TNC-NO₂ molecule can interact with the HTPB units, due to linear arrangement (parallel to the surface) of the molecules. At −30 °C the values shrink together, and are all around −0.100 J/m². At this temperature a experimental crystal phase transition is observed as described in [1]. Whereas at −100 °C the surface (110) and (11-1) show slightly higher E_{pot} values (−0.1038 and −0.1133, respectively).

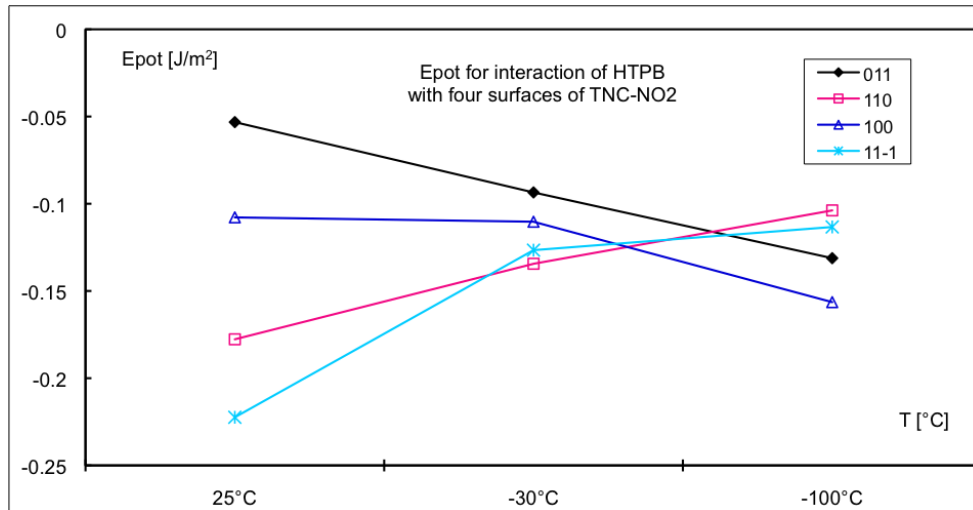


Figure 17.8: Potential energy difference values at +25 °C, -30 °C and -100 °C for the four Miller indices surfaces (011; 110; 100 and 11-1) of 2,2,2-trinitroethyl nitrocarbamate (TNC-NO₂).

For the vdW-energy E_{vdW} , the values at +25 °C are in the range between -0.1564 and -0.0935 J/m². At -30 °C for the surface (011) the vdW-energy increases and for surface (100) decreases, both slightly. The surface (11-1) remains constant at all three different temperatures. For the electrostatic energy E_{Coul} the (11-1) surface and (011) shown at +25 °C the most positive values (-0.0102 and -0.0133 J/m², respectively). The most negative value is shown for (11-1) surface by -0.1227 J/m².

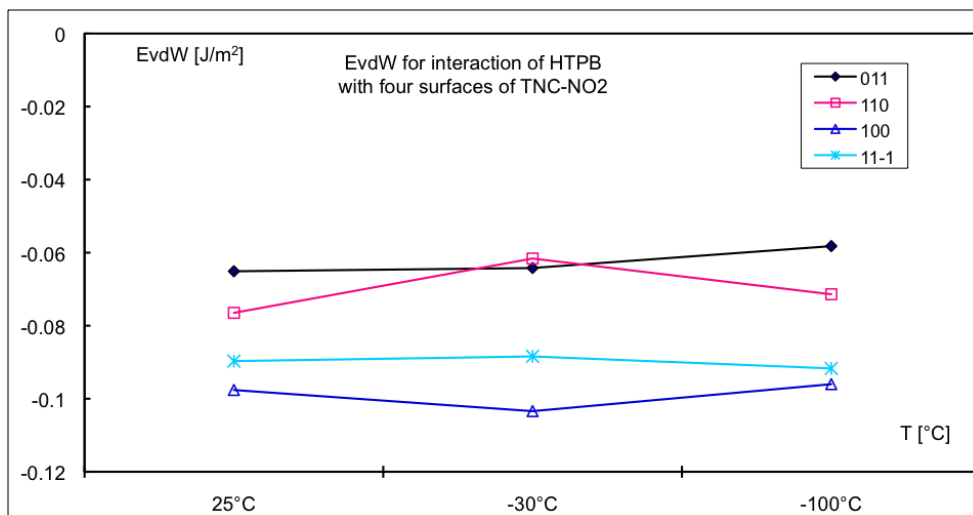


Figure 17.9: Van der Waals energy values at +25 °C, -30 °C and -100 °C for the four Miller indices surfaces of 2,2,2-trinitroethyl nitrocarbamate (TNC-NO₂).

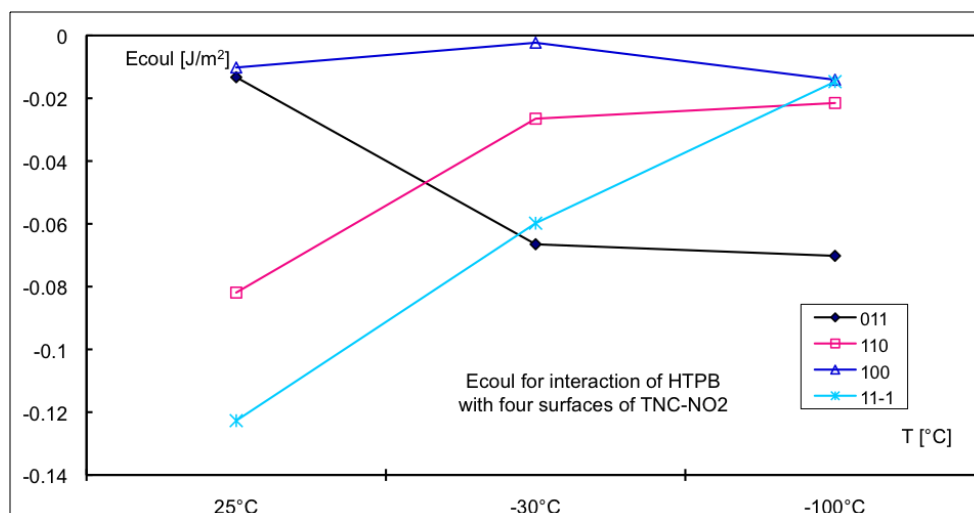


Figure 17.10: Electrostatic energy values at +25 °C, −30 °C and −100 °C for the four Miller indices surfaces of 2,2,2-trinitroethyl nitrocarbamate (TNC-NO₂).

In a previous work [4], the interaction energy (E_{vdW} and E_{Coul}) at the surface was estimated between several polymers (*e.g.* polyethylene, polystyrene, nylon) and liquid materials. The obtained values were in the same range as the results (10^{-2}) given here. Expected are the slightly lower values of the E_{Coul} compared to the E_{vdW} , because the molecular structure of HTPB, does not show polar groups.

For the second simulated oxidizers, 2,2,2-trinitroethyl(2-nitro-2-azapropyl) nitrocarbamate (TNE-NAP-NC), three simulation cell for three Miller index surfaces were built (see Table 17.3).

Table 17.3: List of the surfaces and simulation cell dimensions used with 2,2,2-trinitroethyl(2-nitro-2-azapropyl) nitrocarbamate (TNE-NAP-NC).

Surface	Lenght a [Å]	Lenght b [Å]	Lenght c [Å]
110	20.4195	22.3155	88.3056
100	20.2565	20.4195	79.6441
020	20.4195	18.7250	84.6636

The three Miller index surfaces are shown in Figure 17.11.

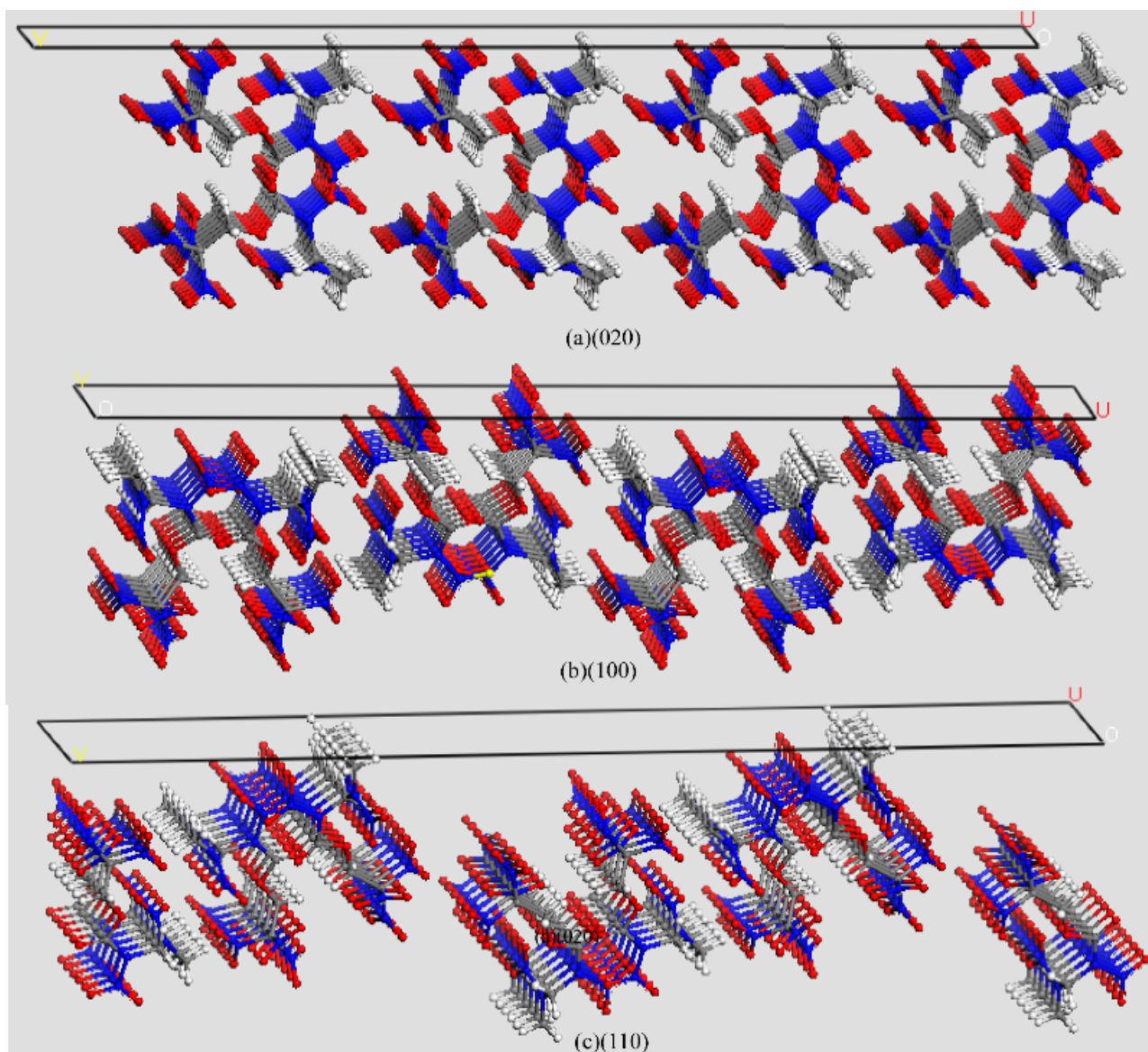


Figure 17.11: 2,2,2-trinitroethyl(2-nitro-2-azapropyl) nitrocarbamate (TNE-NAP-NC) with the Miller index surface (020)(a), (100)(b) and (110)(c).

In Table 17.4 the energies resulting from the interaction between HTPB and TNE-NAP-NC at +25 °C, -30 °C and -100 °C for the chosen surfaces are listed.

Table 17.4: Energy values at +25 °C, −30 °C and −100 °C for the three chosen surfaces of 2,2,2-trinitroethyl(2-nitro-2-azapropyl) nitrocarbamate (TNE-NAP-NC).

Surface and temperatures	E_{pot} [J/m ²]	E_{vdW} [J/m ²]	E_{Coul} [J/m ²]
+25 °C			
020	−0.6053	−0.2030	−0.3751
110	−0.4050	−0.1944	−0.2166
100	−0.3039	−0.1769	−0.0920
−30 °C			
020	−0.4054	−0.1483	−0.2389
110	−0.4088	−0.1640	−0.2271
100	−0.3362	−0.1705	−0.1468
−100 °C			
020	−0.2835	−0.1471	−0.1199
110	−0.3652	−0.1765	−0.1748
100	−0.3187	−0.1743	−0.1245

Evaluating the potential energies E_{pot} for the three surfaces at the three different temperatures, clearly increasing values (from −0.6053 to −0.2835 J/m²) are observed for the surface (020), whereas the ones of the surfaces (110) and (100) changed only slightly. Analyzing the group at the surface, it was recognized that for the surface (020) and (110) the CH₂-group is strongly available additionally to the NO₂-group. Whereas the (100) surface shows the NO₂-group predominantly. These arrangements can explain the most positive values of the (100) surface, due to less interactions at the surface with HTPB.

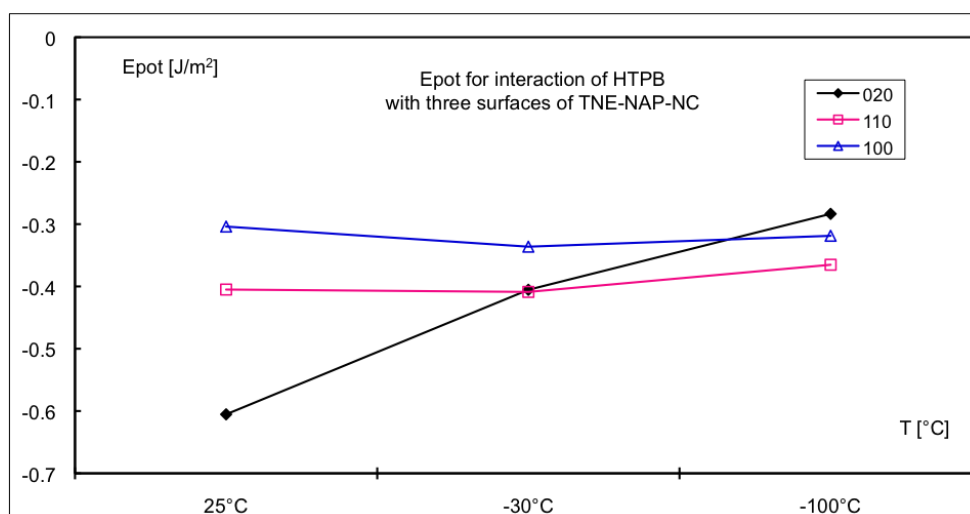


Figure 17.12: Potential energy values at +25 °C, −30 °C and −100 °C for the four Miller indices surfaces of 2,2,2-trinitroethyl(2-nitro-2-azapropyl) nitrocarbamate (TNE-NAP-NC).

Differently the E_{vdW} increased for all the three surfaces by decreasing the temperatures. The surface (020) show the highest values -0.2030 J/m^2 at $+25^\circ\text{C}$, -0.1483 J/m^2 at -30°C and -0.1471 J/m^2 at -100°C .

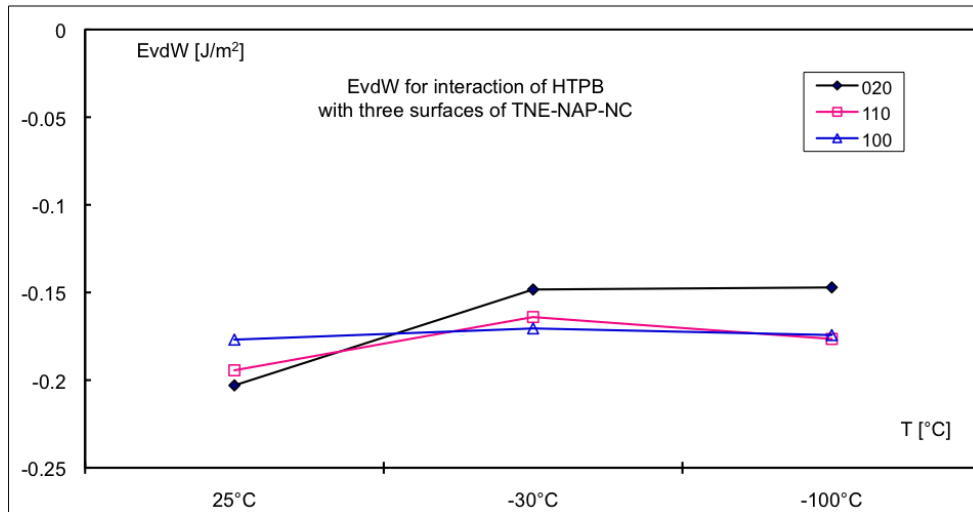


Figure 17.13: Van der Waals energy values at $+25^\circ\text{C}$, -30°C and -100°C for the four Miller indices surfaces of 2,2,2-trinitroethyl(2-nitro-2-azapropyl) nitrocarbamate (TNE-NAP-NC).

Finally the E_{Coul} values show a strong a linear increase by decreasing the temperatures for the (020) surface, a slightly decreasing for (100) surface and first a decrease then an increase for the (110) surface.

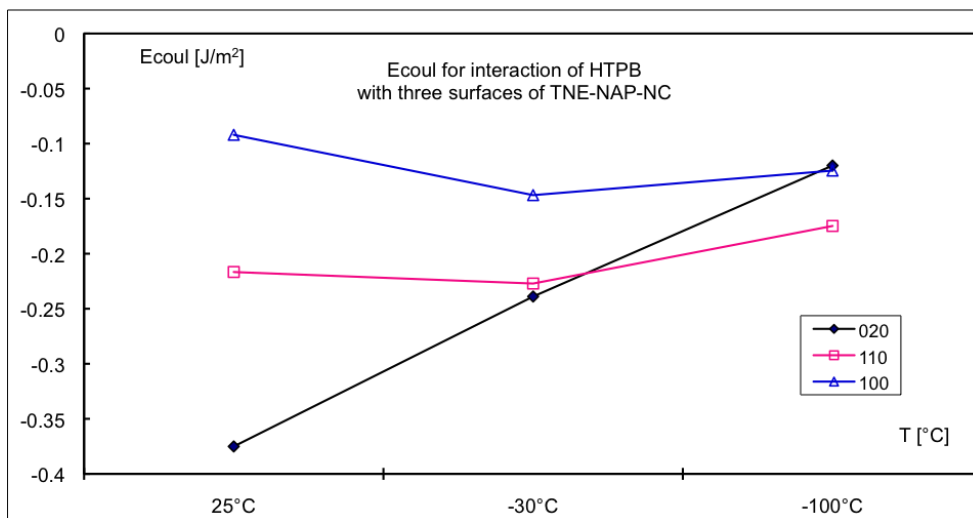


Figure 17.14: Electrostatic energy values at $+25^\circ\text{C}$, -30°C and -100°C for the four Miller indices surfaces of 2,2,2-trinitroethyl(2-nitro-2-azapropyl) nitrocarbamate (TNE-NAP-NC).

The energy difference between the two oxidizers is remarkable. The interaction energies are stronger for TNE-NAP-NC. Additionally for TNE-NAP-NC the values between all energies (E_{pot} , E_{vdW} and E_{Coul}) are in the same decimal range (10^{-1}), whereas for TNC-NO₂ show higher deviations (from 10^{-1} to 10^{-2}). Regard to the application in composite propellants the interaction energy between binder and oxidizer should be as high as possible in order to improve the mechanical properties, especially strain capability. From this point of view the oxidizer TNE-NAP-NC is the better one.

Bibliography

- [1] Q. J. Axthammer, T. M. Klapötke, B. Krumm, R. Moll, S. F. Rest, *Z. Anorg. Allg. Chem.* **2014**, *640*, 76-83.
- [2] B. Aas, M. A. Kettner, T. M. Klapötke, M. Sucéska, C. Zoller, *Eur. J. Inorg. Chem.* **2013**, *36*, 6028-6036.
- [3] T. A. Andrea, W. C. Swope, H. C. Andersen, *J. Chem. Phys.* **1983**, *79*, 4576-4584.
- [4] D. K. Owens, R. C. Wendt, *J. Appl. Polym. Sci.* **1969**, *13*, 1741-1747.

Chapter 18

Summary Molecular Dynamics Simulations of Composite Propellants Ingredients

The objective of this work was an accurate study of the dynamic behavior of some composite propellant ingredients. Molecular dynamic simulations at different conditions (*e.g.* temperature change, cell dimensions, number of molecules in the simulated cell) of several compounds (pre-binders, plasticizers and oxidizers) were performed. At first three pre-binders were calculated: HTPB, PPO and DesmophenTM. Due to the wide usage in composite propellant formulations, HTPB was the most interesting compound. The obtained results confirmed the experimental measurements, for example in the case of T_g and of the density. For the density a linear increasing was observed by decreasing the temperature. Concerning T_g , a temperature range between $-70\text{ }^\circ\text{C}$ and $-50\text{ }^\circ\text{C}$ was observed, quite similar to the experimental values. Further molecules, the plasticizers, were of interest. Especially the plasticizer DOA was investigated. DOA shows also density and T_g in agreement with experimental data. The next step, was to mix the two systems (pre-binder and plasticizers) together. Unfortunately in the literature it was not possible to find experimental results. Whereas analyzing the results, some expected behavior was pointed out. For example, by mixing of the two components the T_g should turn to a lower temperature range, and this was the case. Also interesting were the CED values, that changed by adding a more or less polar component in the system. By PPO and DOA mixture the electrostatic part increase, due to the strong polar character of PPO. Whereas by HTPB and DOA mixture, the vdW part dominates.

The investigated oxidizers are the linkage with the first part of this thesis. A couple of new designed oxidizers were analyzed for the first time, using molecular dynamic simulations. Because of the cost from a synthetic route and the time invested in the experimental tests, a theoretical analysis could be helpful. The molecules (TNC-NO₂ and TNE-NAP-NC), starting from the crystallographic file, were simulated in cells with several surfaces. In these cells a vacuum slab filled with HTPB was prepared and the dynamic simulations then performed. The results show a mainly potential energetic components between the oxidizers and the HTPB. The coulomb and vdW energies are smaller. The simulations were performed at three temperatures: $+25\text{ }^\circ\text{C}$, $-30\text{ }^\circ\text{C}$ and $-100\text{ }^\circ\text{C}$. The molecule TNE-NAP-NC shows the higher interaction energies with HTPB, and seems to be the most appropriate ingredient for a composite propellant mixture.

Chapter 19

Curriculum Vitae

Camilla Evangelisti

Aberlestr. 29
81371 München
Deutschland

Phone: +49 89 76776095
Cell: +49 176 21320289
email: camilla.evangelisti@gmx.de



Personal Data

Place and Date of birth: Sondalo, (Sondrio) Italy, December 27th , 1984
Nationality: Italian

Languages

Italian- mother language
German- fluently written and spoken
English- fluently written and spoken
French- basic knowledge
Spanish- basic knowledge

Academics

September 2011 - today: **Ph.D student** in Prof. Klapötke's group , Inorganic and theoretic chemistry

March 2009 - August 2011: **Graduate student** in chemistry at Ludwig-Maximilians University Munich, Germany

April 2006 - February 2009: **Undergraduate student** in chemistry at Ludwig-Maximilians University Munich, Germany

October 2004 - March 2006: **Undergraduate student** in the Erasmus Program (student exchange program) in chemistry at Technical University Munich, Germany

September 2003 - September 2004: **Undergraduate student** in chemistry at University of Milan, Italy

Camilla Evangelisti - Aberlestr. 29 - 81371 München - Deutschland
P: +49 89 76776095 - C: +49 176 21 320289 - @: camilla.evangelisti@gmx.de

Personal experience

August 2012 – today: **Research associate** Force field calculation with Accelrys®, Fraunhofer Institute for chemical technology, ICT, Pfinztal-Karlsruhe

April 2009 – November 2013: **Research associate**, Quantum chemical Calculation in Prof. Klapoetke's group, Ludwig-Maximilians University Munich, Germany

Formation courses

"Executive manager", Ludwig-Maximilians University Munich, Germany, 2014

"Human resources management", Ludwig-Maximilians University Munich, Germany, 2013

"People management", Ludwig-Maximilians University Munich, Germany, 2013

International experiences

April 2010: **Research project** with Prof. Politzer and Jane Murray, New Orleans, U.S.A.

May 2011: **Workshop** at University of California, UCLA, Los Angeles, U.S.A.

November 2009 - January 2010: **Research internship** at the Massey University Auckland, New Zealand, in Prof. Schwerdtfeger's Group

Scientific cooperations

April 2014 – today: **Research project** with Prof. M. Gozin, Tel Aviv University, Israel

May 2010 - August 2011: **Research project** with Prof. Frank, University Hannover, Germany

November 2009 - April 2011: **Research project** with M. Perruzzini, ICCOM CNR, Sesto Fiorentino, Italy

May 2008 - November 2010: **Research project**, Dr. Bohn, Fraunhofer-Institut, Pfinztal-Berghausen, Germany

19.1 Papers and Conferences

19.1.1 Papers

- (i) C. Rotter, C. Evangelisti, S. Schenberger, T. M. Klapötke, K. Karaghiosoff, *py2P2S7*: a bis(pyridine)adduct stabilized phosphorus sulfide, *Chemical Communications* 46 (27), 2011
- (ii) C. Evangelisti, T. M. Klapötke, B. Krumm, A. Nieder, R. J. F. Berger, S. A. Hayes, N. W. Mitzel, D. Troegel, R. Tacke, Sila-substitution of alkyl nitrates: synthesis, structural characterization, and sensitivity studies of highly explosive (nitratomethyl)-, bis(nitratomethyl)-, and tris(nitratomethyl)silanes and their corresponding carbon analogues; *Inorganic Chemistry*, 49 (11), 2010
- (iii) E. Goekinar, K. Karaghiosoff, T. M. Klapötke, C. Rotter, C. Evangelisti, Structure and Bonding in the Trichalcogenometaphosphate-Pyridine Anion [PX₃-Py]-(X= O, S, Se, Te), *Phosphorous, Sulfur, and Silicon and the Related Elements*, Volume 185 Issue 12, 2527, 2010
- (iv) C. Evangelisti, T. M. Klapötke, A. Nieder, *Bis(Nitratomethyl)dimethylsilane and 2,2-dimethyl-1-nitratopropane*, *New Trends in Research of Energetic Materials*, Proceedings of the Seminar, 13th, Pardubice, Czech Republic, Apr. 21-23, 2010
- (v) C. Evangelisti, T. M. Klapötke, K. Karaghiosoff, M. Bohn, 2-Nitro and 4-nitro-N-nitroso-N-ethylaniline: crystal structure and quantum chemical calculations, *New Trends in Research of Energetic Materials*, Proceedings of the Seminar, 14th, Pardubice, Czech Republic, Apr. 13-15, 2011
- (vi) C. Evangelisti, Daniel Izsk, T. M. Klapötke, J. Stierstorfer, *Preparation and characterization of 5-azido-3-nitro-1H-1,2,4-triazole and selected metal salts*, *New Trends in Research of Energetic Materials*, Proceedings of the Seminar, 14th, Pardubice, Czech Republic, Apr. 13-15, 2011
- (vii) C. Evangelisti, T. M. Klapötke, K. Karaghiosoff, M. Bohn, 2-Nitro and 4-nitro-N-nitroso-N-ethylaniline: NMR spectroscopy, crystal structure and quantum chemical calculations, *From International Annual Conference of ICT*, Karlsruhe, Germany, 43th, 88/1-88/15, 2011
- (viii) Q. J. Axthammer, C. Evangelisti, T. M. Klapötke, *Characterization, bomb calorimetric measurements and quantum chemical calculations of high energetic dense oxidizers (HEDO)*, *From International Annual Conference of ICT*, Karlsruhe, Germany, 44th, 88/1-88/15, 2013
- (ix) L. Ascherl, C. Evangelisti, T. M. Klapötke, B. Krumm, J. Nafe, A. Nieder, S. Rest, C. Schuetz, M. Sucasca, M. Trunk, *Chemistry and structures of hexakis(halogenomethyl)-, hexakis(azidomethyl)-, and hexakis(nitratomethyl)disiloxanes*, *Chemistry- An European Journal*, 19(28), 921-936, 2013
- (x) Q. J. Axthammer, C. Evangelisti, T. M. Klapötke, *Synthesis and characterization of 2,2,2-trinitroethyl carbamate and 2,2,2-trinitroethyl nitrocarbamate*, *New Trends in Research of Energetic Materials*, Proceedings of the Seminar, 16th, Pardubice, Czech Republic, Apr. 10-13, 2013
- (xi) M. A. Bohn, C. Evangelisti, T. M. Klapötke, *Atomistic simulation study of intermolecular interactions between binders and plasticizers used in propellants and high explosive charges*, *International Annual Conference of ICT*, Karlsruhe, Germany, 44th, 2013

- (xii) A. Baumann, A. Erbacher, C. Evangelisti, T. M. Klapötke, B. Krumm, S. F. Rest, M. Reyn-
ders, V. Sproll, *Multiplied nitrated high-energy dense oxidizers derived from the simple amino
acid glycine*, *Chemistry European Journal*, 19, 2013
- (xiii) S. Schnberger, C. Jagdhuber, L. Ascherl, C. Evangelisti, T. M. Klapötke, K. Karaghiosoff,
New acyclic neutral phosphorous sulfides and sulfide oxides, *Zeitschrift für Anorganische und
Allgemeine Chemie*, 52(1), 214-227, 2014
- (xiv) M. A. Bohn, C. Evangelisti, T. M. Klapötke, *Atomistic simulation of temperature dependence
of density and van-der-Waals interactions of binders, plasticizers and mixture of them*, *New
Trends in Research of Energetic Materials, Proceedings of the Seminar, 17th, Pardubice,
Czech Republic, Apr. 9-11, 2014*
- (xv) Q. J. Axthammer, C. Evangelisti, T. M. Klapötke, *Michael addition of nitroform as a source
of energetic materials, synthesis and characterization*, *New Trends in Research of Energetic
Materials, Proceedings of the Seminar, 17th, Pardubice, Czech Republic, Apr. 9-11, 2014*

19.1.2 Conference/Workshop

- (i) 6th European Workshop on Phosphorous Chemistry, Florence, Italy, March 2009
- (ii) 13th International Seminar New Trends in Research of Energetic Materials, Pardubice, Czech
Republic, April 2010 (Poster-presentation)
- (iii) Inaugural CleveTheoComp Workshop in New Orleans, U.S.A., April 2010 (Oral-presentation)
- (iv) 8th European Workshop on Phosphorous Chemistry, Münster, Deutschland, March 2011 (Poster
-presentation)
- (v) 14th International Seminar New Trends in Research of Energetic Materials, Pardubice, Czech
Republic, April 2011 (Poster-presentation)
- (vi) Workshop at UCLA, Los Angeles, U.S.A. (Physical Frameworks for Sampling Chemical
Compound Space), May 2011
- (vii) IUCr 2011 Satellite Workshop, Sigüenza, Spain, August 2011 (Poster-presentation)
- (viii) 8th International Conference on Inorganic Chemistry, Heidelberg, Germany, September 2011
(Poster-presentation)
- (ix) 9th European Workshop on Phosphorous Chemistry, Rennes, France, March 2012 (Poster pre-
sentation)
- (x) 43th International Annual Conference of the Fraunhofer ICT, Karlsruhe, Germany, June 2012
(Poster presentation)
- (xi) 15th International Seminar New Trends in Research of Energetic Materials, Pardubice, Czech
Republic, April 2013 (Poster-presentation)
- (xii) 44th International Annual Conference of the Fraunhofer ICT, Karlsruhe, Germany, June 2013
(Oral presentation+Poster Presentation)
- (xiii) 6th International Seminar New Trends in Research of Energetic Materials, Pardubice, Czech
Republic, April 2014 (Poster-presentation)
- (xiv) 45th International Annual Conference of the Fraunhofer ICT, Karlsruhe, Germany, June 2014
(Oral presentation+Poster Presentation)

